Aus dem Bereich Anatomie und Zellbiologie
Theoretische Medizin und Biowissenschaften
der Medizinischen Fakultät
der Universität des Saarlandes, Homburg/Saar

Die Expression von Pannexin1

in der Mausentwicklung

Dissertation zur Erlangung des Grades eines Doktors der
Naturwissenschaften

der Medizinischen Fakultät

der UNIVERSITÄT DES SAARLANDES

2015

Vorgelegt von: Abdulrahman Raslan

geb. am: 06.01.1976 in Aleppo, Syrien

Table of Contents

Zusammenfassung

Pannexine (Panx) sind eine Proteinfamilie mit drei Mitgliedern, i.e. Panx1, Panx2 und Panx3. Auf Gen-Ebene zeigen die Pannexine Sequenzhomologie zu den Invertebraten Gap Junction Proteinen, den Innexinen. Im Gegensatz dazu weisen die Proteine eine vergleichbare Struktur- und Membran-Topologie wie die Vertebraten Gap Junction Proteine, die Connexine, auf. Funktionell vermitteln Pannexin-Kanäle den Transport kleiner Moleküle (bis zu 1.5 kDa) zwischen Zytoplasma und Extrazellulärraum. Panx1 ist mit purinergen Rezeptoren assoziiert und hat besondere Bedeutung als Kanal für den Second Messenger ATP.

Für den Zeitraum der postnatalen Neurogenese wurde festgestellt, dass Panx1 eine Rolle in der Proliferation und Migration der Zellen spielt und die Extension von Neuriten fördert. Dieses führte zu der Hypothese dieser Arbeit, dass Panx1 auch in früheren Stadien der Neurogenese (Embryonaltag (E) 9.5 – E12.5) von Bedeutung sein könnte. Voraussetzung für funktionelle Analysen war jedoch die Darstellung der zeitlichen und räumlichen Expression von Panx1.

Das erste Ziel dieser Arbeit war somit die Untersuchung der Expression von Panx1 in den Embryonalstadien E9.5 bis E12.5 der Maus. Die zeitliche Expression von Panx1 mRNA und Protein wurde mittels RT-PCR und Western Blot Analysen untersucht. Die Lokalisation der Panx1 Expression wurde ebenfalls auf mRNA und Protein Ebene analysiert und mittels Whole-Mount *in situ* Hybridisierung und Immunfluoreszenz dargestellt. Zudem wurde in Panx1-transgenen Mäusen die Expression des Reportergens ß-Gal analysiert.

Während der frühen Entwicklungsstadien (E9.5, E10.5, E11.5, und E12.5) wurden Panx1 mRNA und Protein in Kopf und Körper der Embryonen nachgewiesen. Insbesondere das Nervensystem zeigte sehr früh die Expression von Panx1. Erstmalig konnten die Expression von Panx1 zu diesem Zeitpunkt der Entwicklung in Organen nachgewiesen werden, in denen die Expression erst in späteren Entwicklungsstufen beschrieben war. Zudem konnten neue Expressionsorte beschrieben werden: Die Expression von Panx1 im Rückenmark und in sensiblen Ganglien der Hirnnerven und des Rückenmarks war bis dato noch nicht bekannt. Für Panx1-positive Zellen konnte die Lokalisation in post-mitotischen Neuronen des Rückenmarks und sensiblen Ganglien beschrieben werden.

Das zweite Ziel dieser Arbeit lag somit in der detaillierten Analyse des Rückenmarks und der sensiblen Ganglien in der Embryonalentwicklung sowie in postnatalen und adulten Stadien. Mögliche strukturelle Defizite aufgrund einer Panx1 Deletion wurden in Panx1-transgenen Tieren untersucht,

konnten im Rückenmark jedoch nicht identifiziert werden. Die Panx1 Expression wurde in den Stadien E18,5 und an Postnataltag (P) 9 und P12 sowie in adulten Tieren untersucht. Zu allen Stadien wurde Panx1 Expression im Rückenmark detektiert. Interessant war die Verteilung Panx1-positiver Zellen innerhalb der grauen Substanz des Rückenmarks: In embryonalen Stadien nahm die Anzahl Panx1-positiver Zellen von dorsal nach ventral ab; postnatal war dieser Unterschied ebenfalls vorhanden und an P12 signifikant. Auf mRNA Ebene konnte eine vergleichbare Expression von Panx1 und der purinergen Rezeptoren P2X3 und P2X7 beobachtet werden, während Panx2 gegenläufig exprimiert war. Die Analyse der Expression von Panx1 in Spinalganglien zeigte eine differentielle Expression abhängig von der Segmenthöhe. In Spinalganglien war die Expression der Panx1 mRNA mit der des purinergen Rezeptors P2X3 vergleichbar, nicht jedoch mit P2X7.

Zusammenfassend konnte in dieser Arbeit erstmalig gezeigt werden, dass Panx1 bereits zu frühen Entwicklungsstadien im zentralen und peripheren Nervensystem exprimiert ist. Panx1 mRNA und Protein konnten in post-mitotischen Neuronen identifiziert werden. Insbesondere die sehr spezifische Verteilung von Panx1 im Rückenmark lässt eine funktionelle Bedeutung dieses Proteins vermuten, wie z.B. eine Rolle von Panx1 in der Entstehung des neuropathischen Schmerzes.

Summary

Pannexins (Panx) are a protein family with three members, Panx1, Panx2 and Panx3. At gene level, these pannexins display sequential homology with invertebrate gap junction proteins, innexins. On the other hand, the proteins possess a structural and membrane topology similar to vertebrate gap junction proteins, connexins. Pannexin channels function as a mechanism for the transport of smaller molecules (up to 1.5 kDa) between cytoplasm and extracellular space. Panx1 is associated with purinergic receptors and is of particular importance as a channel for second messenger ATP.

With regard to the period of postnatal neurogenesis, it has been determined that Panx1 plays a role in the proliferation and migration of cells and enhances neurite extension. This led to the hypothesis of this study that Panx1 may also be of importance in early stages of neurogenesis (embryonic day (E) 9.5-E12.5). Functional analysis required, however, demonstration of the expression of Panx1 over time and its localization.

The main aim of this study was thus the examination of the expression of Panx1 in the embryonic stages E9.5 to E12.5 in mice. Expression over time of Panx1 mRNA and protein was examined by means of RT-PCR and Western Blot analysis. Localization of Panx1 expression was also analyzed using whole mount *in situ* hybridization and immunofluorescence. Furthermore, the expression of reporter gene ß-Gal was analyzed.

Panx1 mRNA and protein were detected in the heads and bodies of the embryos in the early stages of development (E9.5, E10.5, E11.5, E12.5). The nervous system in particular displayed expression of Panx1 at a very early stage. This was the first time that expression of Panx1 had been demonstrated in organs at this early point and not only at later stages of development. In addition, new expression locations were described: expression of Panx1 in the spinal cord and in afferent ganglia of brain nerves and spinal cord was hitherto unknown. Panx1-positive cells were also located in post-mitotic neurons of the spinal cord and in sensory ganglia.

The second part of this study was thus directed at the detailed analysis of the spinal cord and of the sensory ganglia both in embryonic development as well as at post natal and adult stages. Possible structural deficits as a result of Panx1 deletion were examined in Panx1 transgenic animals but could not be identified in the spinal cord. Expression of Panx1 was examined on E18.5 and on postnatal days (P)9 and P12 as well as in adult animals. Panx1 expression was detected at all stages in the spinal cord. The distribution of Panx1-positive cells within the grey matter of the spinal cord was interesting: in

studied stages, the number of Panx1-positive cells decreased from dorsal to ventral, this reduction was significant at P12. At mRNA level a similar expression of Panx1 and the purinergic receptors P2X3 and P2X7 was detected, while in Panx2 it was diametrically opposed. Analysis of the expression of Panx1 in spinal ganglia showed a differential expression, dependent on segment height. In spinal ganglia expression of Panx1 mRNA was comparable to that of purinergic receptor P2X3, however not with P2X7.

In summary this study shows, for the first time, that Panx1 is already expressed in early developmental stages in the central and peripheral nervous system. Panx1 mRNA and protein were identified in post-mitotic neurons. The highly specific distribution of Panx1 in spinal cord in particular suggests that this protein is of functional importance; that it, for example, might play a role in the generation of neuropathic pain.

Abbreviations

°C	degree Celsius
µg	microgram
µl	micro liter
aa	amino acid
ADP	adenosine diphosphate
AMP	adenosine monophosphate
AP	alkaline phosphatase
APS	ammonium peroxydisulfate
ATP	adenosine triphosphate
BCA	bicinchoninic acid
bp	base pairs
BSA	bovine serum albumin
C	cervical
cDNA	complementary DNA
CHAPS	3-[(3-cholamidopropyl)dimethylammonio]-1-propansulfonat
CNS	central nervous system
cRNA	complementary RNA
Ct	threshold cycle
Cx	connexin
DAPI	4',6-diamidino-2-phenylindole
ddH$_2$O	double-distilled water
DEPC	diethyl pyrocarbonate
dH$_2$O	distilled water
DIG	digoxigenin
DMSO	dimethyl sulfoxide
DNA	deoxyribonucleic acid
dNTP	deoxynucleotide triphosphate
DRG	dorsal root ganglion
E	embryonic day
EDTA	ethylenediaminetetraacetic acid
EGTA	ethylene glycol-bis-(2-aminoethylether)-N,N,N',N'-tetraacetic acid
ELISA	enzyme-linked immune-sorbent assay
g	gravitation force
IB	immunoblotting
IF	immunofluorescence
Inx	innexin
ISH	*in situ* hybridization

kDa	kilo Dalton
KTBT	sodium potassium buffer
L	lumbar
LFB	luxol fast blue
M	mol
m	meter
mA	milliampere
mAb.	monoclonal antibody
mg	milligram
min	minute
ml	milliliter
mM	millimolar
mp.	melting point
mRNA	messenger ribonucleic acid
NAD$^+$	nicotinamide adenine dinucleotide
NBT/BCIP	nitro blue tetrazolium chlorid / 5-bromo-4-chloro-3-indolyl phosphate
ng	nanogram
NGS	normal goat serum
NR	no reverse transcriptase
NT	no template
p	probability
P	postnatal
pAb	polyclonal antibody
PAGE	polyacrylamide gel electrophoresis
PANX	human pannexin gene
PANX	human pannexin protein
Panx	mouse pannexin gene
Panx	mouse pannexin protein
Panx1 Ct	carboxy- terminus of Panx1
PB	phosphate buffer
PBS	phosphate buffered saline
PCR	polymerase chain reaction
PFA	paraformaldehyde
pH	negative of the logarithm to the base 10 of the hydrogen ion concentration
PIS	pre-immune serum
PNS	peripheral nervous system
RNA	ribonucleic acid
rpm	revolutions per minute
RT-PCR	reverse transcriptase-polymerase chain reaction
s	second

SDS	sodium dodecyl sulfate
SEM	standard error of the mean
SGC	satellite glial cell
SSC	saline sodium citrate
T	thoracic
TAE	tris-acetate-EDTA
TEMED	N,N,N',N'-tetramethylethylenediamine
tg	transgenic
U	unit
UTP	uridine triphosphate
v/v	the ratio of volume to volume
w/v	the ratio of weight to volume
w/w	the ratio of weight to weight
WM-ISH	whole-mount *in situ* hybridization
wt	wildtype
X-Gal	5-bromo-4-chloro-3-indolyl-β-d-galactopyranoside
β-Gal	β-galactosidase

Figures

Tables

1 Introduction

1.1 Gap junction

Cell communication in multicellular organisms is an essential process, where cells communicate with their environment and other cells. Via cell communication, cells exchange water, signal molecules, or metabolic molecules to be used in complex processes like development, differentiation, and function of whole organs. Cells contact with each other directly via specialized regions of membrane junctions e.g. tight junctions and gap junctions.

Gap junctions are formed by linking two hemichannels at adjacent cells, resulting in a separation of junctional membranes with a gap of 3.5 nm (Perkins et al., 1997). These channels connect cells directly and allow the passage of cytoplasmic molecules between adjacent cells including ions (Na^+, K^+, Ca^+, H^+, Cl^-), amino acids (glycine, glutamate), metabolites (glucose, glutathione, adenosine, adenosine monophosphate (AMP), adenosine diphosphate (ADP), adenosine triphosphate (ATP)), and short interfering RNA (Wong et al., 2008). The intercellular communication of gap junction is involved in various cellular mechanisms e.g. in electrical synchronization (Bennett and Zukin, 2004), cell growth and differentiation (Wei et al., 2004), in cell survival and cell death (Krysko et al., 2005), and in carcinogenesis (Mesnil et al., 2005).

Gap junctions are very important intercellular channels even during the embryonic development (Houghton, 2005). They occur in all multicellular organisms, both in invertebrates and vertebrates. They consist of two species-specific types of integral membrane proteins named connexins (Cx) and innexins (Inx) (Phelan et al., 1998). Recently, a new family of vertebrates gap junctions has been discovered and was called pannexin (Panx) (Panchin et al., 2000).

1.1.1 Connexins

Vertebrate gap junctions are composed of proteins termed Connexins. The connexin family consists of 20-21 members, 20 members in the mouse and 21 members in the human genome, 19 members of them are grouped as orthologous pairs (Sohl and Willecke, 2004). Most connexin genes contain two exons; the coding region is mostly located on the second exon as an uninterrupted reading frame

(Figure 1). A phylogenetic classification of connexins genes reveals six subfamily (α β γ δ ζ and ε). Subfamilies α and β are described as sister groups (Abascal and Zardoya, 2013).
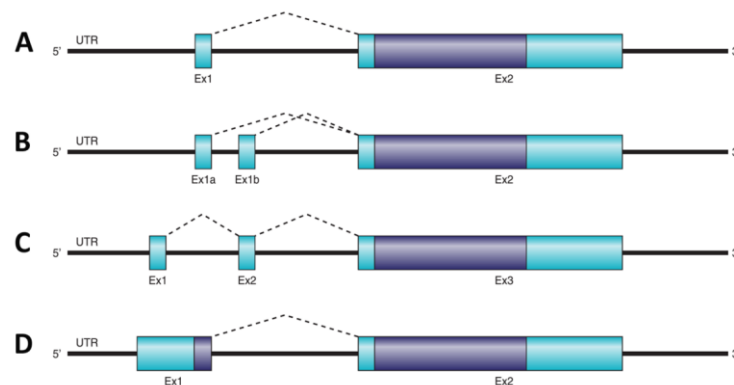
Figure 1. An alignment of different connexin genes
(A) Most connexin genes consist of two exons; the coding region (dark blue) is mostly located on the second exon as an uninterrupted reading frame. (B) Some connexin genes can be transcribed through different promoters in different tissues. (C) Other connexin genes (e.g. Cx45) contain different exons that can be present in the mature mRNA to generate alternatively spliced mRNA. (D) In some connexin genes (e.g. Cx36), the coding region is interrupted by an intron. Taken from Bosco et al. (2011).

Individual proteins are different in size, they are named on the basis of the family name connexin (Cx) followed by the molecular mass (e.g. the connexin protein with a molecular mass of 43 kDa is named Cx43) (Bosco et al., 2011). All connexin proteins show similar membrane topology. The protein monomer integrates into the cell membrane forming four transmembrane domains, two extracellular loops, and one cytoplasmic loop. The N- and C- termini have a cytoplasmic localization (Bruzzone et al., 1996) (Figure 2). The amino acid sequence of extracellular loops is highly conserved between different connexins. There are three cysteine residues in each loop (except for Cx31) (Sohl and Willecke, 2004). In contrast, the intercellular loop is variable between connexin isoforms (Bosco et al., 2011). Whereas the N-terminus is constant in length, the C-terminus is very variable in length and sequence between connexin isoforms (Bosco et al., 2011). Thus, the C-terminus part of the protein causes the difference in molecular weight between isoforms, is highly specific for each connexin protein and also leads to a specific interaction of individual connexins with other proteins (Herve et al., 2004).
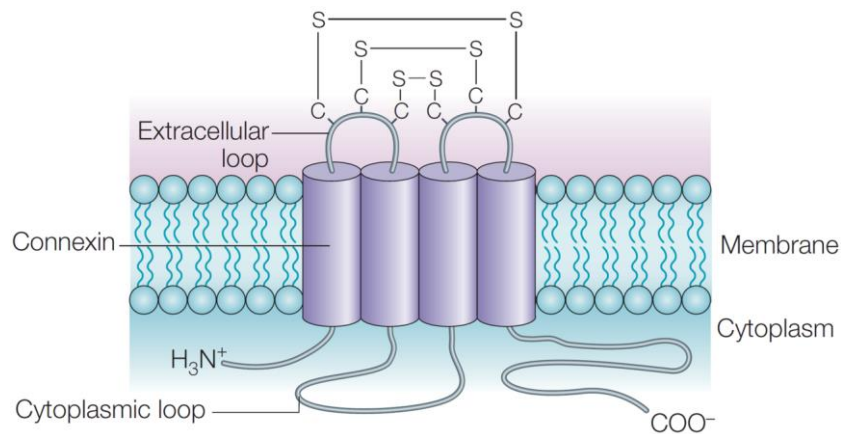
Figure 2. Membrane topology of a vertebrate gap junction protein, connexin.
Four transmembrane domains integrate into the cell membrane, forming two extracellular loops and one cytoplasmic loop. N- (H_3N^+) and C- (COO^-) termini have a cytoplasmic localization. Three cysteine residues (C) are present in each extracellular loop and connected by disulfide bridges. Taken from Sohl et al. (2005).

Six connexin monomers oligomerize to form one hemichannel named connexon. Connexons can be composed of one connexin isoform (homomeric) or by different isoforms (heteromeric). Two connexons of closely apposed cells link to each other and form a hydrophilic pore of 2.5-3 nm in diameter called gap junction (Bosco et al., 2011). Gap junctions are either of homotypic or of heterotypic form (Figure 3). Homotypic channels are composed of two homomeric connexons or of two identical heteromeric connexons. On the other hand, heterotypic channels are composed of two different homomeric connexons or of heteromeric connexons (Kumar and Gilula, 1996).
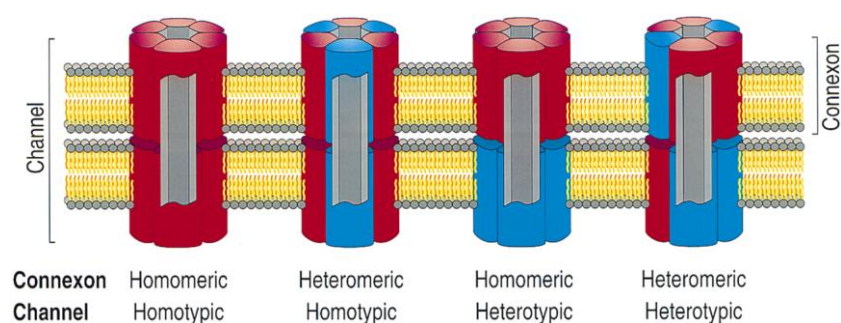
Figure 3. Schematic representation of connexon types forming different gap junction channels
The oligomerization of six connexin subunits forms either homomeric connexons (consisting of identical subunits) or heteromeric connexons (consisting of different subunits). Two connexons compose either homotypic channels (formed by two identical connexons) or heterotypic channels (formed by two different connexons). Taken from Kumar and Gilula (1996)**.**

Connexins can also form non-junctional channels, when connexons do not link to each other, but form hemichannels between the cytoplasm and the extracellular space. Hemichannel formation has been reported for several connexin isoforms, particularly Cx43, with the possibility to release small molecules (e.g. ATP, glutamate and nicotinamide adenine dinucleotide (NAD^+)) into the extracellular space (Evans et al., 2006, Lohman and Isakson, 2014).

Connexins are expressed in all tissues of the vertebrate, for instance in the nervous system, liver, and heart. Connexin expression is highly specific, however, more than one connexin can be expressed in one cell. In the liver, hepatocytes communicate with each other through Cx32 and Cx26, whereas non-parenchymal liver cells express Cx43. On the other hand, Cx37 and Cx40 are expressed in vascular cells in the liver (Maes et al., 2014). In the nervous system, connexins are expressed in neuronal and non-neuronal cells. Cx29, Cx32, and Cx43 are expressed in myelinating Schwann cells (Li et al., 2007). In neurons, Cx36 is strongly expressed in different regions of the brain i.e. olfactory bulb, hippocampus and nuclei of brainstem (Condorelli et al., 1998). Many mutations in connexins are associated with diseases. Exemplarily, two diseases of the nervous system are highlighted here: mutations in Cx32 cause a demyelination in the peripheral nervous system called X-linked Charcot-Marie-Tooth disease (CMTX) (Bergoffen et al., 1993). Mutations in Cx47 are associated with a dysmyelinating disease called Pelizaeus–Merzbacher-like disease (PMLD) (Orthmann-Murphy et al., 2007).

1.1.2   Innexins

Gap junctions are also present in invertebrates and formed by membrane proteins. Since they form functional junctions and are analogous to vertebrate connexins, they were given the functional name innexin (<u>in</u>vertebrate analogues of the con<u>nexin</u>) (Phelan et al., 1998). Innexins do not have any sequence homology to connexins (Bauer et al., 2005) but are similar to them in structure and function. The coding region of many innexins is located on multiple exons, which provides the possibility to encode more than one protein by differential splicing (Phelan, 2005). Innexins are named on the basis of the family name innexin (inx) which is prefixed two letters denoting the organism (Phelan and Starich, 2001). Innexins within an organism are numbered, but numbers do not imply any genetic relationship, e.g. Ce-inx-3 of C. elegans is not orthologous to Dm-inx3 of Drosophila melanogaster (Phelan and Starich, 2001). There are 25 innexin genes in C. elegans (Phelan and Starich, 2001). On the other hand, only 8 innexin genes have been identified in Drosophila melanogaster (Stebbings et al., 2002).

The membrane topology of innexins is similar to that of connexins. Innexin protein also forms four transmembrane domains, two extracellular loops, and one intracellular loop in addition to the cytoplasmic localization of C- and N-termini (Figure 4) (Phelan et al., 1998). In contrast to connexins, in which three extracellular cysteine residues are conserved, innexins have only two cysteine residues in each of the extracellular loops. Like connexins, innexin monomers oligomerize into a hexameric structure of a hemichannel named innexon; two innexons of adjacent cells link to each other and form the invertebrate gap junction (Liu et al., 2013). Some innexins are able to form functional hemichannels as demonstrated by exogenous expression in Xenopus oocytes (Bao et al., 2007). These hemichannels are mechanosensitive (Bao et al., 2007); the activity of channels increases after applying mechanical stress using the membrane patch technique. Furthermore, innexin hemichannels can be activated by intracellular application of calcium in a micromolar range (Bao et al., 2007). The depolarization of these hemichannels with potassium solution induces channel opening and increases ATP release (Bao et al., 2007).
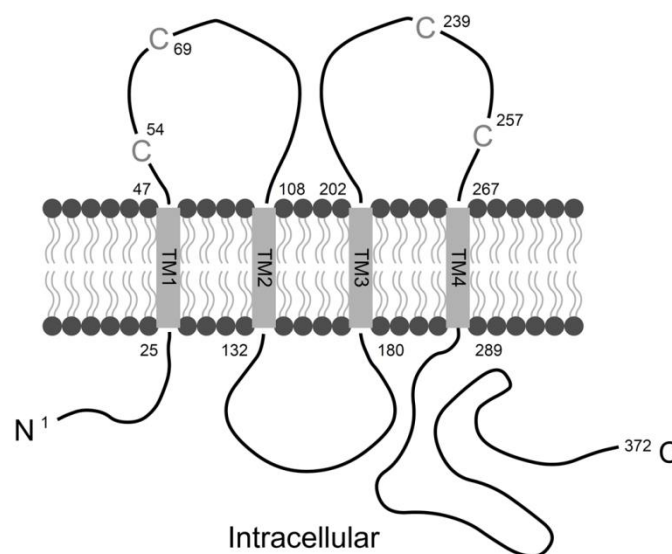
Figure 4. Membrane topology of an invertebrate gap junction protein, innexin.
Four transmembrane domains (TM 1-4) integrate into the cell membrane, forming two extracellular loops and one cytoplasmic loop. N- and C- termini have an intracellular localization. Two cysteine residues (C) are present in each extracellular loop. Taken from Phelan et al. (1998).

1.1.3   Pannexins

1.1.3.1 Pannexin discovery

Connexins are specific vertebrate proteins; no sequence homolog of connexins was found in invertebrates (Phelan et al., 1998, Panchin et al., 2000). Fourteen years ago, Panchin et al. (2000) analyzed the genome of vertebrates for innexin homologs using innexin degenerate primers (Panchin et al., 2000). The similarity of these newly described sequences to innexins sequences was analyzed using PSI-BLAST database. Sequences homolog to innexins were found in different taxonomic groups including vertebrates, for instance in human and mouse genomes. This newly discovered gene was called pannexin (from the Latin pan; all, nexus; connection) (Panchin et al., 2000, Panchin, 2005). Sequence homology of the mammalian protein (pannexin) to invertebrate innexins was confirmed in other studies (Baranova et al., 2004). Genes encoding innexins were significantly similar to that of the putative mammalian protein MRS1 (Baranova et al., 2004). Sequence analysis of the newly discovered pannexin gene revealed two additional isoforms in mouse and human genomes. The three pannexin mouse genes were named Panx1, Panx2, and Panx3 (Bruzzone et al., 2003, Baranova et al., 2004). In this study, pannexin genes were abbreviated with italicized letters of PANX or Panx for human and mouse, respectively, whereas pannexin proteins were abbreviated with not italicized letters of PANX or Panx for human and mouse, respectively.

1.1.3.2 Pannexin genes

Pannexin-encoding genes are highly conserved in the vertebrate genome. They are orthologs to invertebrate innexins but do not have any sequence similarity to vertebrate connexins. *Panx1* and *Panx3* genes are located on the same chromosome in human and mouse genomes. This is similar to innexins, in which genes are often located in cluster of two or three, and can be related to evolution by local duplication (Baranova et al., 2004). Compared to connexin genes (see Chapter 1.1.1), pannexin genes have a higher number of exons (3, 4 or 5 exons), and the coding region is not restricted to one exon but located on all exons of the gene (Bruzzone et al., 2003). *Panx1* and *Panx3* genes are located on chromosome 9 of the mouse genome. The *Panx1* gene includes five exons, whereas the *Panx3* gene includes four exons (Figure 5). Unlike *Panx1* and *Panx3*, the *Panx2* gene is located on another chromosome (chromosome 15 of the mouse genome) and includes only three exons.
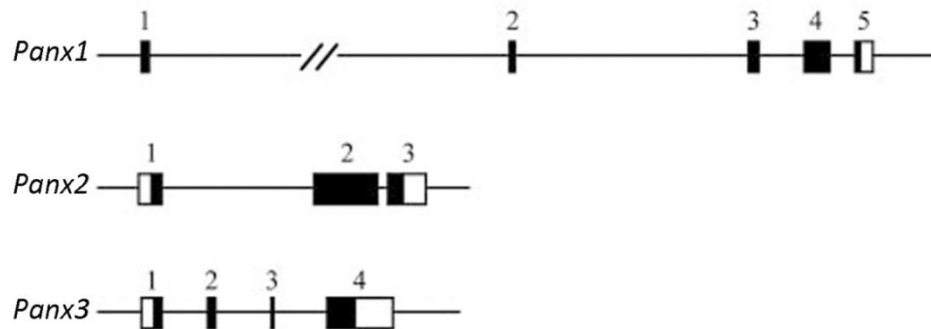
Figure 5. Mouse Pannexin genes
Genomic regions of mouse Panx1, Panx2, and Panx3 are represented. Exons are presented by numbered boxes. Black regions point to coding regions. Taken from Bruzzone et al. (2003).

1.1.3.3 Pannexin proteins

Pannexin proteins have a similar topology as the gap junction proteins connexins and innexins (Ambrosi et al., 2010). Thus, the secondary structure of pannexin proteins also exhibits four transmembrane domains, two extracellular loops (EL), one intracellular loop (IL), and the cytoplasmic localization of N- and C-termini (Bruzzone et al., 2003) (Figure 6). Like innexins, pannexins display two conserved cysteine residues in extracellular loops, but there are also additional intracellular and transmembrane cysteine residues in Panx1 (Bunse et al., 2010). Panx1 and Panx3 proteins are homolog in sequence and size, they exhibit 41 % identity at the amino-acid level (Penuela et al., 2007). The Panx1 mRNA encodes a protein of 448 aminoacids (aa) with a molecular mass of 48.07 kDa. Panx3 encodes a slightly shorter protein of 392 aa of with a molecular mass of 44.98 kDa. In contrast, Panx2 is different in size and sequence. The Panx2 protein consists of 607 aa and has a molecular weight of 73.27 kDa, which is higher than that of Panx1 and Panx3 (Bruzzone et al., 2003).
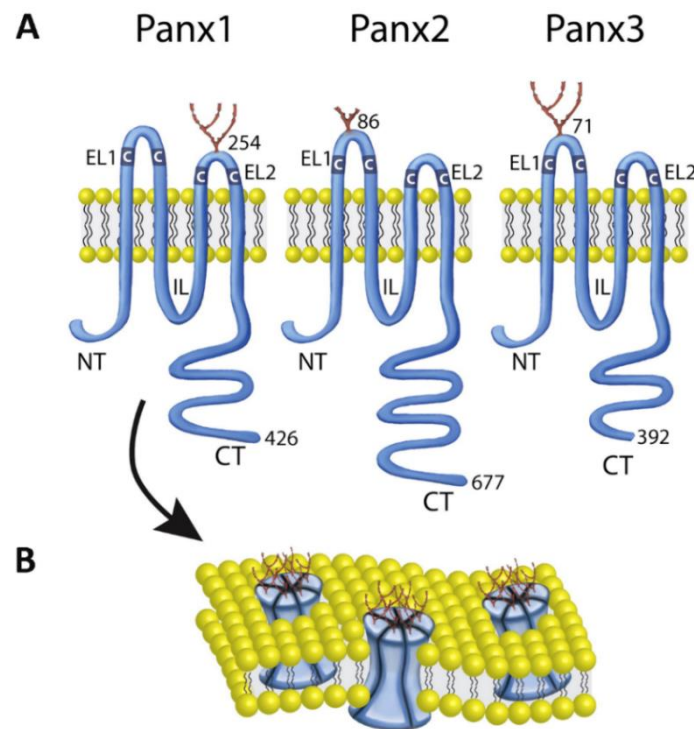
Figure 6. The membrane topology of pannexin family members
(A) Secondary structures of Panx1, Panx2 and Panx3 proteins show four transmembrane domains, two extracellular loops (EL), one intracellular loop (IL), and the cytoplasmic localization of the amino terminus (NT) and carboxy terminus (CT). Extracellular loops are conserved and contain two cysteine residues (C). N-glycosylation sites (in red) locate at the first (Panx2, Panx3) or second (Panx1) extracellular loop. (B) The predicted hexameric structure of Panx1 forming membrane channels. Taken from Penuela et al. (2013).

Pannexins differ from connexins and innexins by possessing N-glycosylation sites (Boassa et al., 2007, Penuela et al., 2007), which are located at the first (Panx2, Panx3) or second (Panx1) extracellular loop (Penuela et al., 2007, Penuela et al., 2014b). Pannexin proteins possess various glycosylation levels: Panx1 and Panx3 have a high-mannose and complex carbohydrate glycosylation. In contrast, glycosylation of Panx2 has a high-mannose content only (Penuela et al., 2009, Penuela et al., 2014b). The N-glycosylation of Panx1 and Panx3 at the extracellular loop probably prevents the formation of intercellular channels (Boassa et al., 2007). The de-glycosylation at the cell surface produces a higher junctional conductance in oocyte pairs, which express Panx1 (Boassa et al., 2008). On the other hand, glycosylation is required for trafficking of the protein from the endoplasmic reticulum into the plasma membrane in many cell types (Boassa et al., 2007, Penuela et al., 2007). Additional glycosylation sites were predicted in the intracellular loop and in the carboxy terminus of Panx1 and Panx3 (Penuela et al., 2007). These results were obtained using sequence analysis, since it is possible to predict post-

translational glycosylation and phosphorylation sites of a protein from its amino acid sequences (Blom et al., 2004).

Sequence analyses of pannexin proteins showed the presence of consensus sequences for several phosphorylation sites (Barbe et al., 2006, Penuela et al., 2007). Thus, pannexins might be phosphorylated at these sites via protein kinases in a post-translational event. Immunoprecipitation analysis of muscles fiber lysates confirmed that Panx1 is a phosphoprotein: Threonine and serine residues are phosphorylated in resting muscles fibers and the phosphorylation was enhanced in electrically stimulated fibers (Riquelme et al., 2013). In contrast, de-phosphorylation analysis of protein lysates did not support the finding of Panx1 and Panx3 phosphorylation as immunoblotting analysis did not exhibit fewer sizes of immunoreactive proteins after de-phosphorylation (Boassa et al., 2007, Penuela et al., 2007, Swayne et al., 2010).

Further post-translational modification was observed in Panx2, which can be found in a palmitoylated or unpalmitoylated form. In neural stem and progenitor cell development, palmitoylated forms of Panx2 were cell type-specific and post-translational modification was associated with the subcellular localization of Panx2 (Swayne et al., 2010).

As outlined above, pannexin monomers oligomerize to form a hemichannel named pannexon (Figure 6). Pannexons, however, are differently composed within the family. Cross-linking analyses showed that Panx1 oligomerizes into a dimeric or hexameric pannexon (Boassa et al., 2007), whereas Panx2 oligomerizes into an octameric pannexon (Ambrosi et al., 2010). However, most pannexins seem to form homomeric channels. The exogenous overexpression of Panx1 or Panx2 in mammalian cells showed the formation of homomeric channels, which were observed electron microscopically (Ambrosi et al., 2010). It was reported that homomeric pannexin channels appear similar to homomeric channels of the gap junction protein Cx26 (Ambrosi et al., 2010). Unlike connexins, heteromeric pannexons are unstable: exogenously overexpressed Panx1 and Panx2 form unstable heteromeric pannexons that disappear in a few hours. One hypothesis is that heteromeric pannexons disintegrate because of the different molecular weight of their protein components (Ambrosi et al., 2010).

1.1.3.4 Pannexin expression

The three pannexin isoforms show different distribution in the vertebrate body. The first Northern blot analysis of pannexin expression (Bruzzone et al., 2003) revealed that Panx1 was expressed in a variety of tissues e.g. in brain, spinal cord, liver, bladder, thyroid gland, and eye, whereas Panx2 was more

restricted to the nervous system. Using the expressed sequence tags database (dbEST), Panx3 had been found in libraries of osteoblasts, synovial fibroblasts, cartilage, and the inner ear (Baranova et al., 2004).

In the adult mouse and rat, Panx1 was expressed in different regions of the brain, e.g. in neurons of the hippocampus, thalamus, olfactory bulb, cortex, and in the cerebellum (Bruzzone et al., 2003). Within the central nervous system (CNS), the hippocampus was shown to have higher expression levels than cortex and cerebellum (Hanstein et al., 2013). Many nuclei of the midbrain and hindbrain also expressed Panx1. Panx1 mRNA and protein were observed in motor nuclei of oculomotor, facial, vagus and hypoglossal nerves as well as in spinal trigeminal nucleus (Ray et al., 2005, Zappala et al., 2006). On the other hand, Panx1 mRNA and protein were absent in the mesencephalic trigeminal nucleus and motor trigeminal nucleus (Ray et al., 2005, Zappala et al., 2006). In spinal cord of adult mice, Panx1 protein was detected in the ventral spinal cord in laminae VII, VIII, and IX, whereas in the dorsal region (laminae I-VI) no expression was observed. The protein showed a cytoplasmic localization in motor neurons (Zappala et al., 2006).

On the other hand, conflicting observations have been reported for Panx1 expression in glia cells. Whereas Panx1 mRNA was absent in glial-like cells RT4-B5 (Ray et al., 2005) and in astrocytes of rat brain (Vogt et al., 2005), Panx1 mRNA was observed in the white matter of rat cerebellum and corpus callosum (Bruzzone et al., 2003). Furthermore, Panx1 protein was also observed in Bergmann glial cells of the cerebellar cortex (Zappala et al., 2006) and in cultured astrocytes (Iglesias et al., 2009) as well as in immature oligodendrocytes (Huang et al., 2007b).

In the peripheral nervous system (PNS), Panx1 was detectable not only in the trigeminal ganglion but also in neurons of the nodose-petrosal-jugular complex (NPJc). In the trigeminal ganglion, Panx1 expression was present in sensory neurons and in some satellite glial cells (SGCs) (Hanstein et al., 2013). In contrast, Panx1 was present in the soma of NPJc neurons but not in SGCs (Retamal et al., 2014). The protein showed a cytoplasmic localization and different expression levels within the neuronal soma.

Recently, a quantitative analysis compared Panx1 expression between several tissues (Hanstein et al., 2013). The highest expression level of Panx1 was found in the trigeminal ganglion followed by bladder and spleen. A lower expression was detected in the brain, calvaria, and heart. On the other hand, kidney and liver were shown to contain very low levels of Panx1.

In sensory organs, Panx1 mRNA and protein were also detected (Huang et al., 2007a, Romanov et al., 2007). In taste buds, Panx1 showed a more abundant expression than connexin proteins Cx30 and Cx43. Expression sites included all taste receptor cells (type II) and only 50 % of other cell types as glial-like (type I) and presynaptic cells (type III) (Huang et al., 2007a). In the retina, Panx1 mRNA was detectable in nearly all retinal layers (Ray et al., 2005). In the outer plexiform layer, immunolabeling and electron microscopy analyses revealed that Panx1 was mostly localized in dendritic and axonal terminals of horizontal cells (Kranz et al., 2013).

Panx2 mRNA showed a similar distribution as Panx1 in many regions of rat CNS, for instance in olfactory bulb, hippocampus, dentate gyrus, and Purkinje cells of cerebellum (Vogt et al., 2005). In the PNS, Panx2 was also reported to be expressed in spiral ganglion neurons of the mammalian cochlea (Wang et al., 2009). In the retina, Panx2 was detectable in nearly all retinal layers of postnatal mice (Dvoriantchikova et al., 2006). Panx2 had higher expression levels than Panx1 in the whole retina and particularly in isolated retinal ganglion cells (Dvoriantchikova et al., 2006).

Panx3 mRNA was detectable in human fetal hippocampal neurons and in adult rat brain (Baranova et al., 2004, Wang et al., 2009). In contrast, Panx3 was very weakly detectable in mouse brain (Penuela et al., 2007, Wang et al., 2009).

On the other hand, Panx3 was predominantly expressed in the skin and cartilage, and was also detectable in other organs like liver, lung, and kidney (Penuela et al., 2007).

In the skin, Panx1 and Panx3 exhibited coexpression, as shown in the epidermis of an E13.5 mouse embryo (Celetti et al., 2010). In the epidermis Panx3 displayed unchanged expression levels in embryonic and newborn mice. In the developing cartilage, Panx3 regulated chondrocyte proliferation and differentiation by promoting ATP release into the extracellular space (Iwamoto et al., 2010).

1.1.3.5 Pannexin function

The structural similarity of pannexins to the channel forming proteins connexins and innexins led to test the possibility whether pannexins form intercellular gap junctions. On way to investigate gap junction function of a protein is the paired oocyte assay (Dahl et al., 1987). In this experiment, no junctional currents were observed for Panx1 compared to the positive control using Cx43 mRNA (Dahl and Keane, 2012) when recording the transjunctional current 30 min after pairing and 48 hours after injection. Other studies observed a transjunctional current with Panx1 alone or with both Panx1 and Panx2 after pairing the oocytes for a longer time (24 - 48 hours) (Bruzzone et al., 2003). Panx2 alone

did not produce any current (Bruzzone et al., 2003). On the other hand, only Panx1, but not Panx2, formed functional hemichannels in the non-junctional membrane of single Xenopus oocytes (Bruzzone et al., 2003). These results and others supported the idea of a non-junctional function of Panx1. Lack of pairing might be due to the protein glycosylation at the extracellular loop, which might hinder the docking of two hemichannels (Boassa et al., 2007). Therefore, the functional pannexin oligomer was named `channel` to distinguish it from gap junction hemichannels (Sosinsky et al., 2011).

Pannexin1 is the most studied and characterized member of the pannexin family (Ohbuchi et al., 2013). Panx1 channels transit ions and second messenger molecules up to a molecular weight of 1.5 kDa. These include positively and negatively charged molecules (e.g. ATP, UTP and Ca^{2+}) (Dahl and Keane, 2012). Furthermore, Panx1 channels mediate dye-take up, for instance of monomeric cyanine (Yo-PRO) (Chekeni et al., 2010) or carboxyfluorescein (Dahl and Locovei, 2006), from the extracellular space to the cytoplasm. On the other hand, no uptake of high-molecular-weight dyes (dextran rhodamine, 10 kDa) was observed (Penuela et al., 2007).

Panx1 is implicated in ATP release from the cytoplasm to the extracellular space. Cells release ATP as a signaling molecule into the extracellular space by two ways, either by vesicular release or through membrane channels. The first description of ATP release through Panx1 has been given by Bao et al. (2004) using luminometry analysis. Exogenously expressed Panx1 in Xenopus oocytes caused an efflux of ATP under depolarization conditions (high K^+) (Bao et al., 2004). Erythrocytes express also Panx1, they show significant carboxyfluorescein uptake in the presence of high K^+ concentration or upon ATP release under low oxygen conditions (Locovei et al., 2006a).

In Xenopus oocytes, exogenously expressed Panx1 channels are closed at the resting membrane potential, and can be activated by a positive membrane potential (Bruzzone et al., 2003). Extracellular ATP also activates Panx1 channels via purinergic P2Y or P2X receptors (Locovei et al., 2006b). The extracellular application of ATP induced currents in Xenopus oocytes, which co-express Panx1 and P2Y1 or P2Y2 (Locovei et al., 2006b). Furthermore, after ATP stimulation, Panx1 induces also the pore formation and dye uptake in oocytes, which co-express Panx1 and P2X7R (Locovei et al., 2007). ATP-receptor activation (P2Y or P2X) increases the cytoplasmic concentration of calcium, which induces ATP release via Panx1 channels (Figure 7). This process is achieved in several steps: By activation of G-protein-linked receptors, the phospholipase C becomes active and produces IP3 protein, which leads to Ca^{2+} release from the endoplasmic reticulum (Scemes and Giaume, 2006).
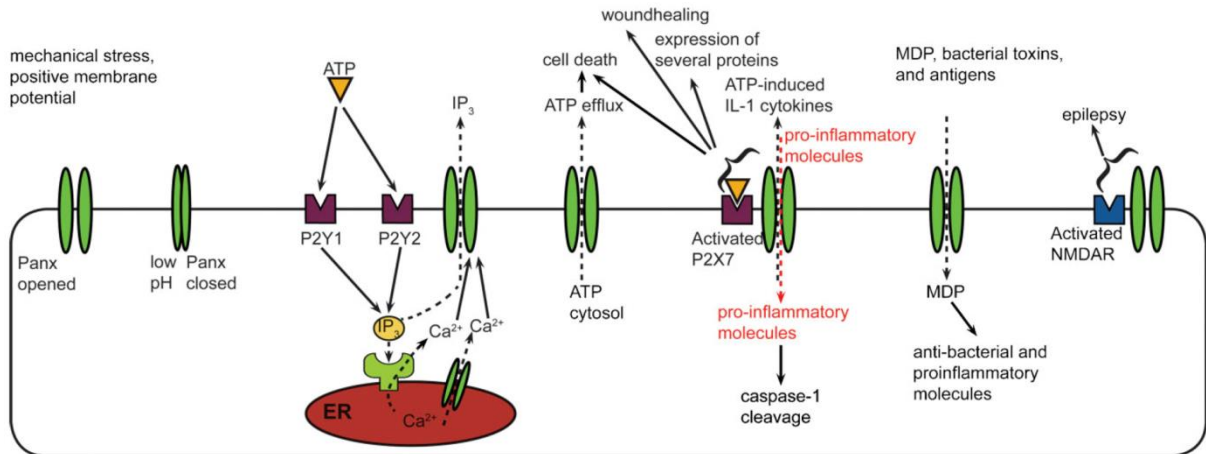
Figure 7. Functions of Panx1 channels

Panx1 channels (green) are closed at low intracellular pH (resting membrane potential). They become active by a positive membrane potential, stimulation of P2Y and P2X receptors, and an increase of cytoplasmic Ca^{2+}. ATP stimulation via P2Y and P2X receptors leads to production of IP3 protein via phospholipase C. IP3, in turn, leads to the release of Ca^{2+} from the endoplasmic reticulum (ER). The cytoplasmic Ca^{2+} induces Panx1 channel activation and ATP release. Opened Panx1 channels allow the transit of small molecules including pro-inflamatory molecules, muramyl dipeptide (MDP), bacterial toxin and antigens. Panx1 is involved in several cellular mechanisms e.g. inflammasome activation, apoptosis, and wound healing. Taken from D'Hondt et al. (2009).

ATP release via Panx1 channels is involved in different cellular mechanisms e.g. inflammasome activation and apoptosis. In macrophages, Panx1 induces caspase-1 activation (Figure 7) to convert the inactive interleukin-1β (pro-IL-1β) into the active form of mature IL-1β, in addition to the interaction between Panx1 and the inflammasome protein NLRP3 (Pelegrin and Surprenant, 2006, Wang et al., 2013). Furthermore, in apoptotic cells (jurkat cells), Panx1 mediates "find-me" signals by releasing ATP from apoptotic cells (Chekeni et al., 2010). This signal is required to recruit phagocytes for quick removal of dying cells (Elliott et al., 2009). Panx1 is also permeable for specific dyes during apoptosis; the uptake of the apoptotic cell-indicator-dye YO-PRO-1 (monomeric cyanine) is Panx1-dependent (Chekeni et al., 2010).

On the other hand, co-immuneprecipitation analysis revealed that Panx1 interacts with different proteins e.g. cytoskeletal proteins. Actin microfilaments regulate the distribution and the mobility of Panx1 on the cell surface (Bhalla-Gehi et al., 2010). The C-terminus of Panx1 interacts preferentially with actin and this might be a direct interaction (Bhalla-Gehi et al., 2010). Endogenous expression of Panx1 in Neuro-2a cells confirms the interaction of Panx1 with β-actin and with the actin-related protein3 (arp3) (Wicki-Stordeur and Swayne, 2013).

1.2 Gap junctions in development

1.2.1 Connexins in development

Gap junctions have been described in early phases of the embryogenesis. Cx32 mRNA is expressed in the zygote and remains present as an oogenetic protein product until the late morula stage (Barron et al., 1989). Nine connexin members are expressed in pre-implantation embryos (Wong et al., 2008). The expression of Cx43 begins at least at the 4-cells stage and was detected in gap junction-like plaques at the 8-cells stage (De Sousa et al., 1993). However, gap junctions in early stages can be required for intercellular communication after cell compaction (Barron et al., 1989).

Studies on connexin knockout mice revealed that gap junction are very important in mammalian development. For example, there is no fertilization possible in Cx37$^{-/-}$ mice, as oocytes require Cx37 gap junctions for signal transport between the oocyte and surrounding follicular cells (Simon et al., 1997). Cx45 is also important for heart development in early embryonic stages. Cx45$^{-/-}$ mice die at E9 (Kruger et al., 2000, Kumai et al., 2000, Alexander and Goldberg, 2003). Cx43$^{-/-}$ mice show heart defects in the development; they die shortly after the birth (Reaume et al., 1995).

Gap junctions are present not only in embryonic stem cells but also in various somatic stem cells. They are involved in the proliferation, differentiation, and apoptosis of stem cells (Wong et al., 2008). In nervous system development, connexin gap junction proteins are present in neuronal and glial cells, they mediate cell communication and regulate neural progenitor cells proliferation and differentiation (Hartfield et al., 2011). During the proliferation in the cortical ventricular zone, radial glial cells require gap junction hemichannels for the propagation of calcium waves, which play a role in the regulation of neuronal proliferation (Weissman et al., 2004). In neurons, gap junctions are commonly regarded as electrical synapses and occur even during neurogenesis, whereas chemical synapses appear in the postnatal phase (Winterhager, 2005).

1.2.2 Pannexins in development

The expression of Panx1 was described in late stages of mouse and rat development. In the mouse embryo, Panx1 mRNA was detected by real time qPCR in embryonic (E14, E16, and E18) and postnatal development (P0, P3, P7 and P14) in the cortex, cerebellum and eye (Ray et al., 2005). The expression level of Panx1 peaks in late embryonic development at E18, is reduced thereafter in postnatal stages and shows further down-regulation in the adult mouse (Ray et al., 2005). *In situ* hybridization analysis

showed a high level of Panx1 in the cortical plate and subplate of an E18 embryo, in addition to a high expression levels in hippocampus (Ray et al., 2005). In rat embryos at E14 and E17, a high expression level of Panx1 was found in the brain and spinal cord, as observed using radioactive *in situ* hybridization (Vogt et al., 2005).

In vitro, endogenous expression of Panx1 has also been reported during differentiation of many neural stem cell lines. In cell culture of RT4 cells, which are derived from a rat peripheral neurotumour and consist of multipotent stem cells, Panx1 mRNA was found in stem cells RT4-AC and neuron-like cells RT4-E5 and RT4-D8, but was absent in glial-like cells RT4-B5 (Ray et al., 2005). These results led the authors to suggest that Panx1 expression is restricted to neurons in the peripheral nervous system as well as in the CNS. Others reported Panx1 expression in Neuro-2a cells (N2a), a cell line which is derived from murine neuroblastoma and capable to differentiate into neuron-like cells (Wicki-Stordeur et al., 2012, Wicki-Stordeur and Swayne, 2013).

The expression of Panx1 in neural stem cells provides hints that Panx1 might play a role in the development of nervous system. The postnatal neurogenesis (Ming and Song, 2011) and N2a cells are ideal to investigate Panx1 function. *In vivo,* Panx1 is expressed in defined populations during postnatal neurogenesis, in neural stem and progenitor cells (NSC/NPCs) as well as in immature neurons. Whereas Panx1 was absent in neuroblasts (doublecortin-positive cells; Dcx) of immature mice (P15) (Wicki-Stordeur et al., 2012), Panx1 was present in these cells of the adult mouse brain (Wicki-Stordeur and Swayne, 2013). Neuroblasts of the adult mouse brain exhibited lower expression level of Panx1 than NSC/NPCs, revealing that Panx1 expression decreases during differentiation of neural stem cells (Wicki-Stordeur and Swayne, 2013).

During postnatal neurogenesis, Panx1 is involved in the regulation of NSC/NPC proliferation by mediating ATP release (Wicki-Stordeur et al., 2012). Furthermore, Panx1 influences cell migration and neurite extension; inhibition or knockdown of Panx1 induces the extension of neurites, while Panx1 overexpression inhibits the outgrowth of neurites (Wicki-Stordeur and Swayne, 2013).

During spinal cord development, Panx1 mRNA and protein expression were detected in isolated microglia cells, which were obtained from spinal cord of an E13.5 mouse embryo (Rigato et al., 2012). In contrast to P2X7R, Panx1 expression did not influence the proliferation of embryonic microglia cells (Rigato et al., 2012).

Panx2 is also expressed at late stages of mouse and rat development. In contrast to Panx1, Panx2 mRNA shows an extremely low expression in late embryonic stages during cerebellar development.

This expression level increases during postnatal development and the adult (Ray et al., 2006). Using radioactive *in situ* hybridization, Panx2 shows also low expression in the brain and spinal cord of rat embryos at E14 and E17 (Vogt et al., 2005).

During the postnatal neurogenesis, Panx2 is expressed in early stem-like hippocampal neural progenitors, but it is absent in intermediate progenitor cells (doublecortin-positive cells) or in immature neurons. Interestingly, Panx2 is re-expressed in mature neurons of the hippocampus (Swayne et al., 2010).

In vitro, Panx2 is endogenously expressed in N2a cells (Swayne et al., 2010). In these cells, the reduction of Panx2 expression to about 50 % accelerates morphological differentiation. Thereby, the expression of the marker of mature neuronal cells (NeuN) is increased, whereas the expression of the immature neuronal marker β-III-tubulin (Tuj1) in neurons was decreased (Swayne et al., 2010). Thus, investigation of neurogenesis suggests that Panx1 and Panx2 might have a specific function during the development. On the other hand, only limited data is available on both the embryonic expression and function in very early stages of embryogenesis.

1.3   Development of the nervous system

As this study focuses on the developmental and spatial expression of Panx1 in the nervous system, crucial steps of CNS and PNS development, particularly the development of spinal cord and sensory ganglia, are described.

1.3.1   Cranial sensory ganglia development

Cranial sensory ganglia develop from two cell structures: neural crest and sensory placodes (Lleras-Forero and Streit, 2012). Placodes are ectodermal epithelium, outside the central nervous system, and originate from a pre-placodal region (PPR), a horseshoe-shaped ectodermal region surrounding the anterior part of the neural plate (Sato et al., 2010). In sensory cranial ganglia, neurons are derived from both neural crest cells and ectodermal placodes (Figure 8), whereas all satellite glial cells are derived from neural crest only.

1.3.1.1 Trigeminal ganglion

In trigeminal ganglion development, mesenchymal cells begin to migrate from the trigeminal placode at E8.5 and this process ends at E10.5 (Nichols, 1986). At E9.5, the trigeminal placode appear as a thickened region of the ectodermal epithelium along the side of the embryonic head. Neurogenesis in the trigeminal ganglion occurs between E9.5 and E13.5 (Huang et al., 1999).

The trigeminal ganglion complex itself develops by the fusion of two ganglia: the ophthalmic trigeminal ganglion in the anterior portion of the ganglion complex and maxillomandibular trigeminal ganglion (Figure 8). Neurons of ophthalmic branch innervate the head, including the nose and eyeballs. Neurons of maxillomandibular branch innervate the lower face, jaws, tongue and teeth. Trigeminal neurons transmit cutaneous information (touch, pain and temperature) from the skin and proprioceptive information from the muscles. Proprioceptive neurons seem to be derived from the neural crest (Rao and Jacobson, 2005).
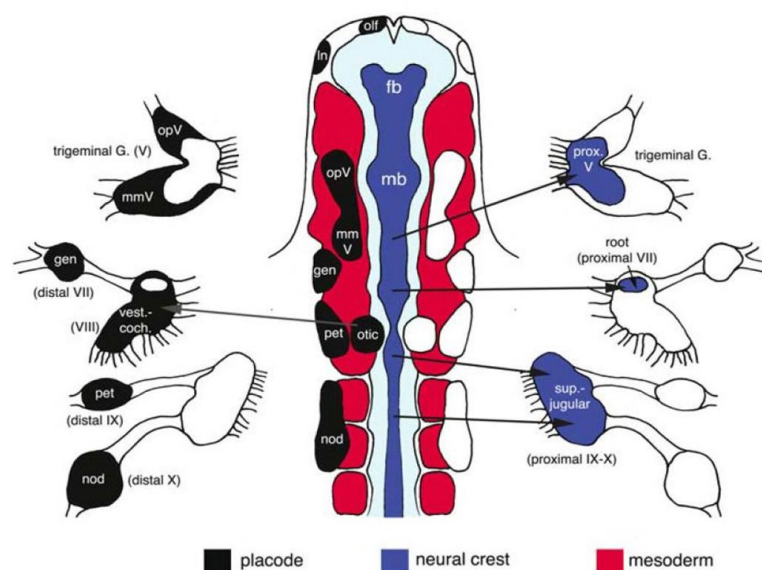
Figure 8. Illustration of placodes and neural crest forming cranial sensory ganglia in the head of chicken embryo
Neurons in cranial sensory ganglia contribute to placode cells or neural crest cells. All satellite cells are derived from the neural crest. Fb, forebrain; G, ganglion; gen, geniculate; ln, lens; mb, midbrain; mmV, maxillomandibular trigeminal; nod, nodose; olf, olfactory; opV, ophtalamic trigeminal; pet, petrosal; prox, proximal; sup, superior; vest-coch, vestibulocochlear. Taken from Rao and Jacobson (2005).

1.3.1.2 Geniculate, vestibular and spiral ganglia

The geniculate ganglion of cranial nerve VII, i.e the facial nerve, arises from the first epibranchial placode and neural crest, whereas the spiral and vestibular ganglia are derived from the otic placode and neural crest. At E9, neural progenitor cells of all of these ganglia migrate and coalesce into a single ganglion complex (facio-acoustic ganglion complex), which differentiates at E12.5 into the geniculate ganglion and the vestibulocochlear ganglion. The vestibulocochlear ganglion divides at E13.5-E14.5 into a vestibular and a spiral ganglion primordial, whereas their physical separation occurs at E17.5 (Wikstrom and Anniko, 1987, Huang et al., 2001, Rao and Jacobson, 2005).

Neurons in the geniculate ganglion provide dendrites to innervate taste buds of the tongue, taste buds of the palate, and the skin of the external ear (Patel and Krimm, 2010). Neurons in the spiral ganglion locate inside the otic capsule, innervate the cochlea and transmit the information to the brain. The vestibular ganglion locates outside the otic capsule, innervates the vestibular organs and transmits information into the vestibular nuclei in the medulla oblongata.

1.3.2   Spinal cord development

At the dorsal site of an E9.5 mouse embryo appears the structure of the neural tube after closing of the neural plate along the anterior-posterior axis. The neural plate contains initially only one ectodermal cell layer, which via cell division becomes later a ticker tube consisting of three layers: the ependymal layer (ventricular zone), the mantle layer and the marginal layer. The ventricular zone surrounds the lumen of the neural tube and the central canal. This zone contains progenitor cells, which give rise to neurons during neurogenesis (~E9-E14) and oligodendrocytes during gliogenesis (~E13 to postnatal) (Battiste et al., 2007). Cells in the midline of the ventral part differentiate into epithelial-like cells called the "floor plate". At the dorsal part, a tissue known as the "roof plate", develops. Between dorsal and ventral parts appears a fissure called the sulcus limitans.

Spinal progenitor cells are arrayed at dorsoventral positions along the midline and proliferate to give rise to post-mitotic neurons during temporally restricted periods (Arber, 2012). Generation of neurons is induced by signaling activity of the floor plate and the roof plate. The gradational expression of Sonic Hedgehog (SHH) protein from the notochord and the floor plate establishes five ventral progenitor domains (Jessell, 2000), while gradational expression of Wingless/Int (WNT) and bone morphogenic protein (BMP) from the roof plate establishes six dorsal progenitor domains (Luu et al., 2011). Neurons derived from different progenitor cells migrate radially to the target destination in the mantle layer

(gray matter) to form neuronal subpopulations, which are organized in laminae known as Rexed´s laminae (Rexed, 1952). Laminae I-VI form the dorsal horn. The lamina VI is present in cervical and lumbosacral segments, but not in thoracic segments. Lamina VII forms the intermediate gray matter, and laminae VIII and IX form the ventral horn, whereas the lamina X surrounds the central canal (Figure 9) (Watson et al., 2012).

Finally, the gray matter consists of motor neurons, interneurons, axons of neurons and glia cells. The marginal layer (white matter) contains axons of neurons and glia cells (astrocytes and oligodendrocytes). Microglia cells, which originated form mesoderm, begin to invade the spinal cord at early stages E11.5 of mouse development (Rigato et al., 2011).
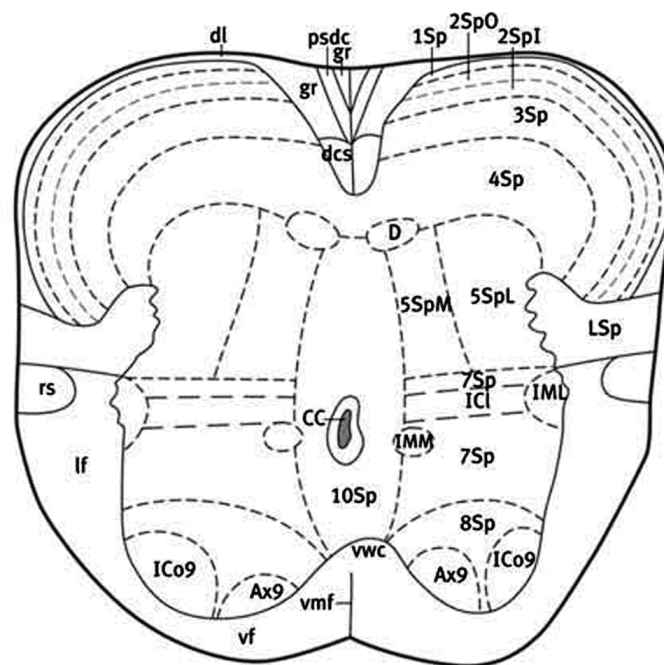
Figure 9. Laminar organization of the thoracic segment T7 from P4 mouse spinal cord
The dorsal horn contains laminae (I-V). Lamina VII forms the intermediate gray matter. Laminae VIII and IX form the ventral horn, and lamina X surrounds the central canal. Lamina VI is absent in the thoracic region. Axial muscle motor neurons of lamina 9 (Ax9), central canal (cc), dorsal corticospinal tract (dcs), dorsal nucleus (D), dorsolateral fasciculus (dl), gracile fasciculus (gr), intercalated nucleus (ICl), intercostal muscle motor neurons of lamina 9 (ICo9), intermediolateral column (IML), intermediomedial column (IMM), lamina 1 (1Sp), inner part of lamina 2 (2SpI), outer part of lamina 2 (2SpO), lamina 3 (3Sp), lamina 4 (4Sp), lamina 5 (5Sp), lateral part of lamina 5 (5SpL), lateral spinal nucleus in the white matter (LSp), medial part of lamina 5 (5SpM), lamina 7 (7Sp), lamina 8 (8Sp), lamina 9(9Sp), lamina 10 (10Sp), lateral funiculus (lf), postsynaptic dorsal column pathway (psdc), rubrospinal tract (rs), ventral funiculus (vf), ventral median fissure (vmf), ventral white commissure (vwc). Taken from Sengul et al. (2012).

1.3.3 Dorsal root ganglion development

After closure of the neural plate, neural crest progenitor cells leave the neuroepithelium and migrate between the mesenchymal cells lateral of the neural tube. Neural crest cells (NCCs) are progenitors of different cell types, e.g. peripheral neurons, peripheral glia (Schwann cells) and melanocytes. Two types of NCCs are present during the development of DRG neurons, which occurs in three waves of neurogenesis (Figure 10). The first wave occurs between E9.5 and E11.5, generating large neurons from the first type of NCCs. In the second wave between E10.5 and E13.5, the second type of NCCs generates large and small neurons of DRG neurons. In the third wave, boundary cap cells, neural crest derivatives at the spinal cord entry points, generate small neurons that largely consist of nociceptive neurons. All types of NCCs and boundary cap cells are involved in generating glia cells of DRGs (Maro et al., 2004, Marmigere and Ernfors, 2007).
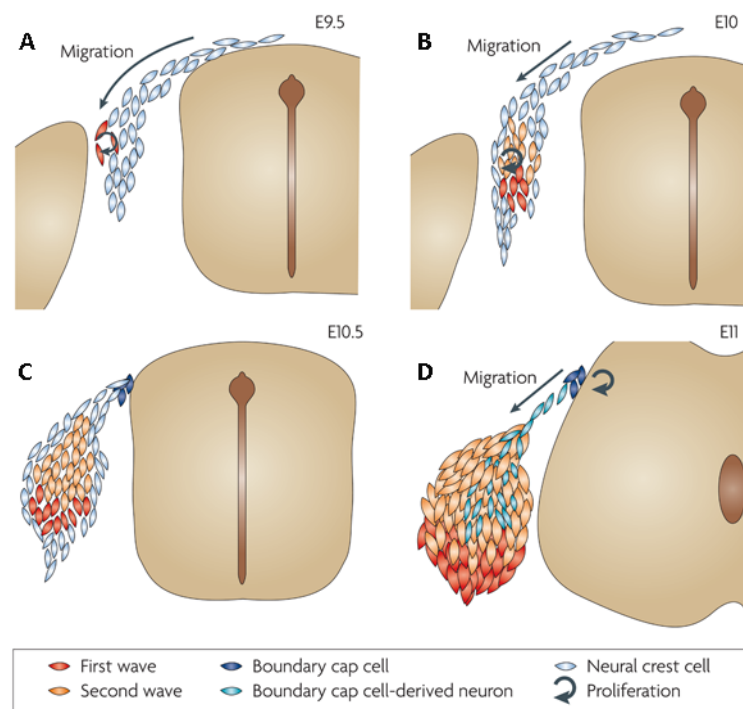
Figure 10. Three neurogenesis waves of DRGs
(A) The first type (red) of neural crest cells migrates laterally and generates large neurons in the first wave. (B and C) In the second wave, the second type (orange) of neural crest cells migrates later and generates large and small neurons of DRGs. (D) In the third wave, boundary cap cells (blue) generate small neurons. Neural crest cells and boundary cap cells generate glia cells of DRGs. Taken from Marmigere and Ernfors (2007).

1.3.3.1 Populations and projection of sensory neurons

DRGs contain a heterogeneous population of sensory neurons that innervate different peripheral targets and transmit different types of sensory information (e.g. pain, touch, vibration, pressure, temperature) to the central nervous system. Different criteria can be used to classify DRG sensory neurons, for instance the size of the pericaryon, ultrastructure, and the expression of certain neurotrophin receptors e.g. members of the family of high-affinity neurotrophin receptors tyrosine kinase receptors (Trk). In general, neurons in DRGs are classified in four main classes (Figure 11). Large proprioceptive neurons express TrkC and innervate sensory organs in muscle and joints. Intermediate neurons express TrkB and innervate mechanoreceptors. Small nociceptive neurons are peptidergic neurons, expressing TrkA, and the fourth class consists of non-peptidergic neurons (Montano et al., 2010).
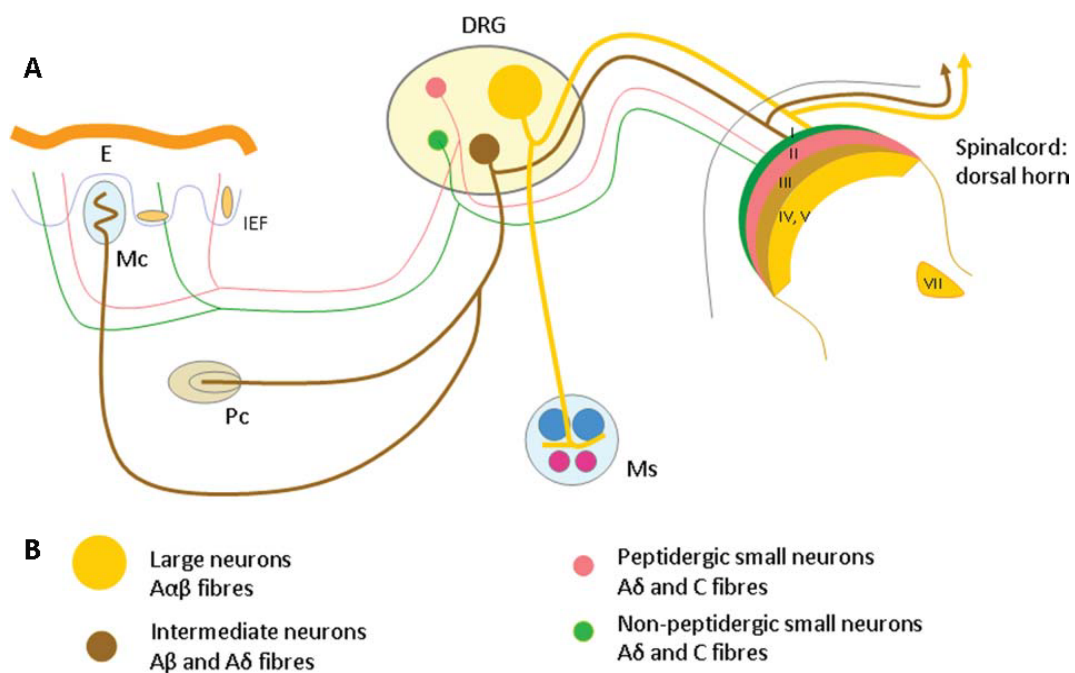
Figure 11. Schematic representation of DRG neuronal populations and their projection
Four main classes of DRG sensory neurons (B) project fibers into the periphery and the dorsal horn of the spinal cord (A). Small neurons have afferent myelinated Aδ and unmyelinated C fibers from the epidermis (E) forming intraepidermic nerve fibers (IEF). These fibers end in spinal cord in laminae I, II, and V. Intermediate neurons have afferent myelinated Aβ fibers from mechanoreceptors like Meisner corpuscles (Mc) and Pacinian corpuscles (Pc) that reach the laminae III and V or to the central nervous system nuclei. Large neurons have afferent input via myelinated Aα fibers from the muscle spindels (MS). Taken from Montano et al. (2010).

DRG sensory neurons extend peripheral processes (Aα, Aβ, Aδ, and C fibers), which innervate various parts of the body including the skin (e.g. sensory organs in the skin and free nerve ending in the

epidermis) (Figure 11). Nociceptive small neurons sense pain and temperature send the messages to laminae I and II through thinly myelinated Aδ and unmyelinated C fibers, in an intermediate or slow conducting form. Mechanoreceptors convey touch by moderately myelinated Aβ fibers from intermediate sized neurons to the laminae III and V or to central nervous system nuclei. The proprioception is mediated by large neurons, which project myelinated Aα fibers with a fast conduction velocity to the skeletal muscles. Fibers end in the lamina VII, and connect directly to the ventral motor neurons (Caspary and Anderson, 2003, Montano et al., 2010).

2   Aim of the study

Previous studies have reported that Panx1 is expressed *in vitro* in neural stem cells (Ray et al., 2005). Other studies confirmed this finding *in vivo* (Wicki-Stordeur et al., 2012, Wicki-Stordeur and Swayne, 2013). Panx1 expression was identified in a defined neuronal population during postnatal (Wicki-Stordeur et al., 2012) and adult (Wicki-Stordeur and Swayne, 2013) neurogenesis of the mouse brain. In neural stem and progenitor cells, Panx1 was shown to regulate cell proliferation by mediating ATP release (Wicki-Stordeur et al., 2012) in addition to influencing on cell migration and neurite extension during neurogenesis (Wicki-Stordeur and Swayne, 2013).

These data have led to hypothesize that Panx1 might be important for embryonic neurogenesis. However, Panx1 expression during early neurogenesis remained largely unknown. There were only some reports showing Panx1 mRNA expression at late stages of mouse and rat development. Therefore, the analysis of the temporal and spatial expression of Panx1 mRNA and protein at the beginning of neurogenesis (E9.5 – E12.5) is essential for understanding its functional implication.

The first aim of the study was therefore to investigate the temporal expression of Panx1 mRNA and protein at early stages of mouse development (E9.5 – E12.5). In those stages expressing Panx1, the spatial distribution of Panx1 mRNA and protein was to be analyzed in whole mount samples or in histological sections of embryos. Panx1 protein expression has never been described before in embryonic stages. In the present study, the temporal protein expression was studied in E9.5 – E12.5 stages. The spatial distribution of Panx1 protein was also investigated in defined regions, in spinal cord and sensory ganglia, to determine cell populations expressing Panx1.

Given that Panx1 mRNA was shown to be abundantly expressed in spinal cord and sensory ganglia of studied embryonic stages, the second aim of the study was a detailed analysis of Panx1 expression in these particular regions. In spinal cord, the spatial distribution of Panx1 was investigated in prenatal (E18.5), postnatal (P9 and P12) and adult stages. Relative gene expression of Panx1 in adult spinal cord was also compared with other associated genes. Possible phenotypic changes due to Panx1 deletion were examined in transgenic animals. In dorsal root ganglia, cell populations expressing Panx1 were determined. Given that different sensory ganglia relay information from different regions of the body (dermatomes), relative gene expression of Panx1 and other related genes was compared between different regions of sensory ganglia i.e. trigeminal ganglion and dorsal root ganglia of cervical, thoracic and lumbar regions.

3 Materials and Methods

3.1 Materials

Devices

Analytical Balance	Sartorius, Göttingen, Germany
Autoclave Systec D-65	Labor-Systemtechnik, Wettenberg, Germany
Camera AxioCam ERc 5s	Carl Zeiss, Göttingen, Germany
Camera AxioCam MRm	Carl Zeiss, Göttingen, Germany
Camera CC-12	Olympus, Hamburg, Germany
Cold-light source CL 1500 ECO	Carl Zeiss, Göttingen, Germany
Cryostat, Leica CM 1950	Leica, Wetzlar, Germany
Embedding Center, MPS/P1 and MPS/C	Slee, Mainz, Germany
Filter Sets (43HE, 38HE, and 49)	Carl Zeiss, Göttingen, Germany
Fluorescent Lamp HXP 120 C	Carl Zeiss, Göttingen, Germany
FUSION-FX7/SL Advance System	PEQLAB, Erlangen, Germany
Gel Electrophoresis System	PEQLAB, Erlangen, Germany
Glass Knives C335	Plano, Wetzlar, Germany
Heraeus Megafuge 16 R Centrifuge	Thermo Fisher Scientific, Heidelberg, Germany
Heratherm Oven	Thermo Fisher Scientific, Heidelberg, Germany
Himac CT 15RE centrifuge	Hitachi Koki, Tokyo, Japan
Historange Microtome 2218	Lkb Bromma, Sollentuna, Sweden
Hybridization Oven, HB-1000	Ultra-Violet Products Ltd, Cambridge, Uk
KERN PLE Scale	KERN & SOHN Gmbh, Balingen, Germany
Life Touch Thermal Cycler	Biozym, Hessisch Oldendorf, Germany
Micro-Plate Reader Infinite M200	Tecan, Crailsheim, Germany
Microscope, Observer.Z1	Carl Zeiss, Göttingen, Germany
Microscope, Olympus BX51 TF	Olympus, Hamburg, Germany
Microtome, HM 350	Techno-Med Gmbh, Bielefeld, Germany
Mini Rocker	PEQLAB, Erlangen, Germany
Nano Drop ND-1000	Thermo Fisher Scientific, Heidelberg, Germany
Orbital Incubator SI500	Bibby Scientific, Stone, UK
Paraffin Tissue Floating Bath	Medax , Neumünster, Germany
Robust Carousel Tissue Processor, mtp	Slee, Mainz, Germany
Semi-Dry Electro Blotter System	PEQLAB, Erlangen, Germany
Sonoplus, Ultrasonic Homogenizer	Bandelin Electronic, Berlin, Germany
StepOnePlus Real Time PCR system	Applied Biosystems, Foster City, USA
Stereo Microscope Discovery. V8	Carl Zeiss, Göttingen, Germany
Stereo Microscope SZX12	Olympus, Hamburg, Germany
Thriller Thermo Shaker Incubator	PEQLAB, Erlangen, Germany
Ultra-Turrax Ika T10	Ika, Staufen, Germany

Universal Oven	Memmert, Schwabach, Germany
UV- Transilluminators	Vilber Lourmat, Eberhardzell, Germany
Vibratome, LEICA VT1000 S	Leica, Wetzlar, Germany
Water Purification System Q-Pod	Merck Millipore, Darmstadt, Germany

Chemicals

Acetic Acid	VWR, Darmstadt, Germany
Acrylamid Mix (Rotiphorese Gel 30)	Carl Roth, Karlsruhe, Germany
Agar	AppliChem, Darmstadt, Germany
Agarose	Biozym Scientific, Hessisch Oldendorf, Germany
Ammonium Acetate	Fisher Scientific, Nidderau, Germany
Ammonium peroxodisulfate	Carl Roth, Karlsruhe, Germany
Ampicillin	Carl Roth, Karlsruhe, Germany
BamHI	New England Biolabs, Hitchin, UK
BCA assay kit	Thermo Fisher Scientific, Heidelberg, Germany
Bis-Tris	AppliChem, Darmstadt, Germany
Blocking Reagent	Roche, Manheim, Germany
Bovine Serum Albumin	MP Biomedicals, Heidelberg, Germany
Bromophenol Blue Dye	Alfa Aesar, Karlsruhe, Germany
cDNA synthesis reaction buffer	Thermo Fisher Scientific, Heidelberg, Germany
CHAPS	Alfa Aesar, Karlsruhe, Germany
Chloroform	Sigma-Aldrich, München, Germany
Chromogenic substrate, TMB	Dako, Hamburg, Germany
Complete, Protease Inhibitor Cocktail Tablets	Roche, Manheim, Germany
Cresyl violet staining	Merck, Darmstadt, Germany
DAPI-Fluoromount-G	Southern Biotechnology, Birmingham, USA
DEPC	Sigma-Aldrich, München, Germany
DIG RNA Labeling Kit	Roche, Manheim, Germany
DNA loading Dye	Thermo Fisher Scientific, Heidelberg, Germany
dNTPs	New England Biolabs, Hitchin, UK
EcoRI	New England Biolabs, Hitchin, UK
EcoRV	New England Biolabs, Hitchin, UK
EDTA	Carl Roth, Karlsruhe, Germany
EGTA	AppliChem, Darmstadt, Germany
Ethanol Pure	Sigma-Aldrich, München, Germany
Formaldehyde	VWR, Darmstadt, Germany
Formamid	AppliChem, Darmstadt, Germany
Freund's Adjuvant	Sigma-Aldrich, München, Germany
Gel Red	Biotium, Hayward, USA
Gene Ruler 1 kb Plus DNA Ladder	Fermentas, Heidelberg, Germany
Gene Ruler Low Range DNA Ladder	Fermentas, Heidelberg, Germany
Glutardialdehyde	Merck, Darmstadt, Germany

Glycine	Carl Roth, Karlsruhe, Germany
Heparin	Carl Roth, Karlsruhe, Germany
Hydrogen Peroxide (H_2O_2)	Thermo Fisher Scientific, Heidelberg, Germany
kanamycin	Sigma-Aldrich, München, Germany
Lamb Serum	Invitrogen, Darmstadt, Germany
Lithium Carbonate	Sigma-Aldrich, München, Germany
Lumi-Light Western Blotting Substrate	Roche, Manheim, Germany
Luxol Fast Blue	Fisher Scientific, Nidderau, Germany
Magnesium Chloride	Merck, Darmstadt, Germany
Masson Goldner Trichrome Staining Kit	Carl Roth, Karlsruhe, Germany
NBT/BCIP	Roche, Manheim, Germany
Nonfat Milk	Carl Roth, Karlsruhe, Germany
Normal Goat Serum	Sigma-Aldrich, München, Germany
NP-40 Alternative	Merck, Darmstadt, Germany
Nuclear Fast Red	Sigma-Aldrich, München, Germany
Oligo (dT)	Thermo Fisher Scientific, Heidelberg, Germany
Page Ruler Plus Prestained Protein Ladder	Thermo Fisher Scientific, Heidelberg, Germany
Paraffin Wax (mp. 44-46°C)	Sigma-Aldrich, München, Germany
Paraffin Wax (mp. 55-57°C)	Carl Roth, Karlsruhe, Germany
Paraformaldehyde	Electron Microscopy Sciences, Hatfield, USA
PCR Reaction Buffer	New England Biolabs, Hitchin, UK
Picric Acid Solution	AppliChem, Darmstadt, Germany
Plasmid Midi Kit (25)	QIAGEN, Erlangen, Germany
Ponceau Red	Carl Roth, Karlsruhe, Germany
Potassium Ferricyanide	Carl Roth, Karlsruhe, Germany
Potassium Ferrocyanide	Carl Roth, Karlsruhe, Germany
Pre-stained protein marker broad range	New England Biolabs, Hitchin, UK
Proteinase K	Roche, Manheim, Germany
Restriction Endonuclease Buffer	New England Biolabs, Hitchin, UK
RevertAid-RT	Thermo Fisher Scientific, Heidelberg, Germany
RNase inhibitor	Thermo Fisher Scientific, Heidelberg, Germany
RNase-free DNase I set	QIAGEN, Erlangen, Germany
RNeasy Lipid Tissue Mini Kit	QIAGEN, Erlangen, Germany
Roti-Histokitt	Carl Roth, Karlsruhe, Germany
Roti-Histol	Carl Roth, Karlsruhe, Germany
Roti-Mount Aqua	Carl Roth, Karlsruhe, Germany
Sodium Chloride	VWR, Darmstadt, Germany
Sodium citrate tribasic dehydrate (S-4641)	Sigma-Aldrich, München, Germany
Sodium Deoxycholate	AppliChem, Darmstadt, Germany
Sodium dodecyl sulfate (SDS)	Carl Roth, Karlsruhe, Germany
T4 DNA Ligase	Fermentas, Heidelberg, Germany
Takyon™ Rox SYBR Master Mix dTTP Blue kit	Eurogentec, Seraing, Belgium
Taq DNA polymerase	New England Biolabs, Hitchin, UK
TEMED	Carl Roth, Karlsruhe, Germany

Tissue Tek	Sakura, Staufen, Germany
Tris base	Sigma-Aldrich, München, Germany
Tris HCl	Carl Roth, Karlsruhe, Germany
Triton X-100	Carl Roth, Karlsruhe, Germany
tRNA	Roche, Manheim, Germany
Tryptone	Sigma-Aldrich, München, Germany
Tween 20	Sigma-Aldrich, München, Germany
X-Gal	Carbolution Chemicals, Germany
Yeast – Extract	Sigma-Aldrich, München, Germany
β-mercaptoethanol	Carl Roth, Karlsruhe, Germany

Consumables

12-well culture plate	SARSTEDT, Nümbrecht, Germany
96-well-plate	SARSTEDT, Nümbrecht, Germany
Coverslips	R. Langenbrinck, Emmendingen, Germany
Filter papers (190 g/m^2)	A. Hartenstein, Würzburg, Germany
Fixogum	Marabu, Tamm, Germany
Nitrocellulose membrane (0.45 μm)	GE Healthcare, Freiburg, Germany
Peel-a-way disposable embedding molds	Polysciences Europe, Eppelheim, Germany
Pipette tips and tubes	SARSTEDT, Nümbrecht, Germany
Razor blades	Electron Microscopy Sciences, Hatfield, USA
Real time qPCR 96 well plate	Applied Biosystems, Foster City, USA
SuperFrost Plus slides	R. Langenbrinck, Emmendingen, Germany

Software

Adobe Photoshop CS4	Adobe Systems Software, California, USA
AxioVision v 4.8.	Carl Zeiss Microscopy, Jena, Germany
Cell^P imaging software	Olympus, Hamburg, Germany
EndNote X6	Thomson Reuters, New York, USA
FUSION-CAPT software	PEQLAB, Erlangen, Germany
Magelan software	TECAN, Crailsheim, Germany
Prism 5	GraphPad Software, San Diego, USA
Slide digital virtual microscopy V 1.2	Olympus, Hamburg, Germany
StepOne software V 2.2	Applied Biosystems, Foster City, USA
ZEN 2011	Carl Zeiss Microscopy, Jena, Germany

3.1.1   Antibodies

Table 1. Primary antibodies

Antibody	Host	Dilution	Code Number	Manufacturer
anti-Panx1 (antiserum)	Rabbit, pAb	1:200 IF / 1:1000 IB	1307	Saarland University*
pre-immune serum (PIS)	Rabbit	1:100 IF / 1:1000 IB	1307	Saarland University*
anti Panx1	Rabbit, mAb	1:10,000 IB	ab124969	abcam
anti Panx1	Rabbit, pAb	1:500 IB	ab139715	abcam
anti Panx1	Mouse, mAb	1:500 IB	MAB7097	R&D
anti Panx2	Rabbit, pAb	1:2000 IB	ARP42778_T100	AVIVA
anti P2X7R	Rat, mAb	1:100 IF	MCA4713	AbD Serotec
anti-DIG-AP	Sheep, pAb	1:2000 ISH	11093274910	Roche
anti β-III-tubulin (Tuj1)	Mouse, mAb	1:500 IF	MMS-435P	Covance

Primary Antibodies used for IF (immunofluorescence), IB (immunoblotting) and ISH (*in situ* hybridization). mAb (monoclonal antibody), pAb (polyclonal antibody). *Prof. Zimmermann, Dr. Jung, Dept. Of Biochemistry, Saarland University.

Table 2. Panx1 antibodies recognize different epitopes of the protein

Anti-Panx1	Epitope region	Caspase cleavage product	Panx1 isoforms
1307 (antiserum)	C-terminus	6, 30 kDa	Panx1 (a, c)
ab124969 (abcam)	C-terminus	6, 30 kDa	Panx1 (a, c)
ab139715 (abcam)	1EL and 2Td	19, 42 kDa	Panx1 (a, c, d)
MAB7097 (R&D)	C-terminus	6, 30, 42 kDa	Panx1 (a, c, d)

Antibodies used for Panx1 detection recognize different regions of the protein. For the present study, the generated antiserum (1307) recognizes a short part of the C-terminus. The antibody ab124969 recognizes the C-terminus of human Panx1 and only 45 % of its epitope sequence is alignment in mouse sequence. The antibody ab139715 recognize a large region of the first extracellular loop (1EL) and the second transmembrane domain (2Td). The antibody MAB7097 recognizes most C-terminus region (87 aa). Different predicted fragments of caspase cleavage are detectable with these antibodies; detectable fragments are listed in size. Not all Panx1 isoforms are detectable with these antibodies, Panx1a (48 kDa), Panx1c (40 kDa), and Panx1d (34 kDa) (Li et al., 2011).

Table 3. Secondary antibodies

Antibody	Host	Dilution	Code Number	Manufacturer
anti-rabbit HRP	Goat	1:10000 IB	A10547	Invitrogen
anti-mouse HRP	Goat	1:50000 IB	115-035-146	Jackson Immune Research
anti-rabbit-Alexa488	Goat	1:3000 IF	A11008	Invitrogen
anti-rabbit-Alexa568	Goat	1:3000 IF	A11011	Invitrogen
anti-rat-Alexa594	Goat	1:3000 IF	A-11007	Invitrogen

Secondary antibodies used for IF (immunofluorescence) and IB (immunoblotting).

3.2 Animal experiments

3.2.1 Animal handling

All animal experiments were performed with the approval of the governmental animal care committee of the Saarland, Germany. All mice were bred and housed under standard conditions in the animal core facility at the Institute for Clinical and Experimental Surgery, Medical faculty of Saarland University. Adult rabbits were housed under standard conditions at the Institute for Medical Biochemistry and Molecular Biology, Saarland University.

3.2.2 Animals

An adult rabbit (New Zealand White Rabbit) was used to generate polyclonal antibodies against Panx1. C57Bl/6N mice (Charles River Laboratories, Sulzfeld, Germany) were used as wildtype mice.

Two transgenic strains, Panx1$^{tg/tg}$ and Panx2$^{tg/tg}$, were provided by Prof. Dr. Hannah Monyer, Department of Clinical Neurobiology, University Hospital of Neurology, Heidelberg, Germany. Generation of transgenic mice Panx1$^{tg/tg}$ (Anselmi et al., 2008) and Panx2$^{tg/tg}$ (Bargiotas et al., 2011) was performed by inserting the *LacZ* gene into the exon1 of Panx1 and Panx2 of C57Bl/6 mice, respectively (Figure 12). For this generation, genomic *Panx1* and *Panx2* fragments, which were obtained after screening a 129/SvJ mouse genomic library, were modified by inserting the bacterial gene *LacZ* and a phosphoglycerate kinase-neomycin cassette flanked by *loxP* into exon1 of both fragments. The modified construct was linearized and transfected into R1 embryonic stem cells using electroporation to replace the target fragment via homologous recombination. Clones of transfected

embryonic stem cells were injected into blastocytes, which were implanted into foster mothers. Chimeric animals were bred to obtain stable transgenic animals. The neomycin cassette was removed from transgenic animals by breeding with Cre-deleter mice.
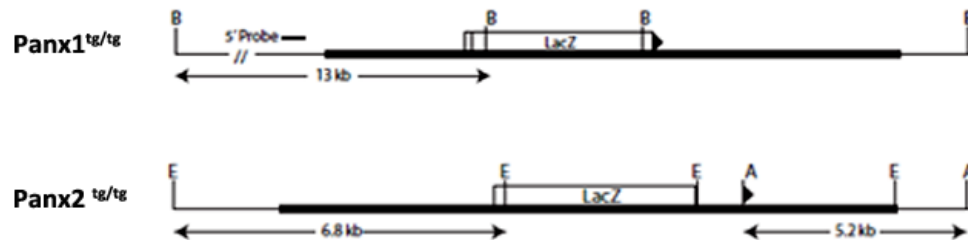
Figure 12. Transgenic mice generation
A scheme shows the location of the LacZ cassette within exon1 of the Panx1 (top) and Panx2 (bottom) allele in transgenic strains Panx1$^{tg/tg}$ and Panx2$^{tg/tg}$. Restriction endonucleases: A, ApaI; B, BamHI and E, EcoRI. Taken from Bargiotas et al. (2011).

3.2.3   Collection of mouse embryos

Female mice were mated with males (2:1) for 15 hours. The vaginal plug was examined at the time of separation. The day, on which a vaginal plug was found, was designated embryonic day (E) 0.5. Pregnant mice were sacrificed by intra-peritoneal injection with Pentobarbital-Sodium "Narcoren" (4 g/kg body weight) (Merial, Hallbergmoos, Germany) or with Phenobarbital-Sodium "Luminal" (500 mg/kg body weight) (Destin, Hamburg, Germany) on day 9.5, 10.5, 11.5, 12.5 or 18.5 of gestation. Uterine horns were dissected from the mouse and were placed in a petri dish containing phosphate buffer (PB) or 0.1 % diethyl pyrocarbonate treated phosphate buffered saline (DEPC-PBS), according to the protocol of the experiment. Embryos were isolated from the decidua, yolk sac and the amniotic sac for staging as described in Chapter 3.2.4. Staged embryos were treated according to specific experimental conditions.

3.2.4   Staging of embryos

Embryos were staged according to the description in the Atlas of Mouse Development (Kaufman, 2003), focussing on the morphological differentiation of limbs at each stage. At embryonic day (E) 9.5, only forelimb buds are visible in the truncal region (Figure 13). At E10.5, hindlimb buds appear at the caudal extremity in the tail region. At E11.5, only the forelimbs are clearly divided into proximal and

distal regions, whereas hindlimb buds do not show this differentiation yet. At E12.5, the handplate shows angular contour, which are future digits, and the footplate is to see in a polygonal shape.
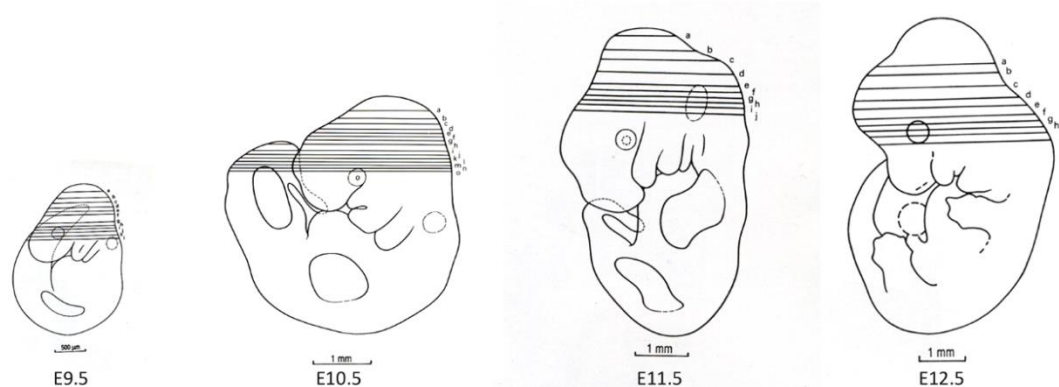
Figure 13. Staging of embryos
A schematic representation of mouse embryos shows staging strategies of studied embryos. At E9.5, the forelimb buds are visible. At E10.5, the hindlimb buds appear at the caudal extremity of the tail region. At E11.5, forelimbs are divided into proximal and distal parts. At E12.5, the handplate shows angular contour and the footplate has a polygonal shape. Black lines indicate sections levels as shown in the original scheme. Taken from Kaufman (2003).

3.2.5   Dissection of organs

Spinal cord, trigeminal ganglia and dorsal root ganglia (DRG) were collected at different ages and studied in histological and molecular biological ways.

- In spinal cord, the cranial thoracic region between T2 and T6 segments was dissected and investigated in different methods. For real time qPCR experiment, the cranial thoracic region was divided into dorsal and ventral parts using razor blades (Electron Microscopy Sciences, Hatfield, USA) and subjected to RNA extraction prior to the cDNA synthesis and real time qPCR.
- Dorsal root ganglia were collected of determined regions. At first, spinal segments were identified according to the description of Harrison et al. (2013). For histological experiments, thoracic ganglia were dissected so that they remained attached to the spinal cord. For real time qPCR experiment, vertebral columns of 9 animals were divided at C1, T1, T7, T13 and L6 segments into four regions (Table 4) Within each region, ganglia were pooled from three animals. All regions were analyzed in triplicate (n=3 per group).

Table 4. Groups of collected dorsal root ganglia

Group	Region	Segments
1	Cervical	C2 to C8
2	Cranial thoracic	T2 to T6
3	Caudal thoracic	T8 to T12
4	Lumbar	L1 to L5

- Dissection and identification of trigeminal ganglia was performed as described in the protocol of Malin et al. (2007). The brain and the brainstem were dissected from the skull. This way, the trigeminal nerve was identified at the income point to the brainstem (Figure 14). Branches of mandibular nerve, ophthalmic nerve and maxillary nerve were cut of the trigeminal nerve. Trigeminal ganglia including the trigeminal nerve were collected and treated as described in Chapter 3.2.6.
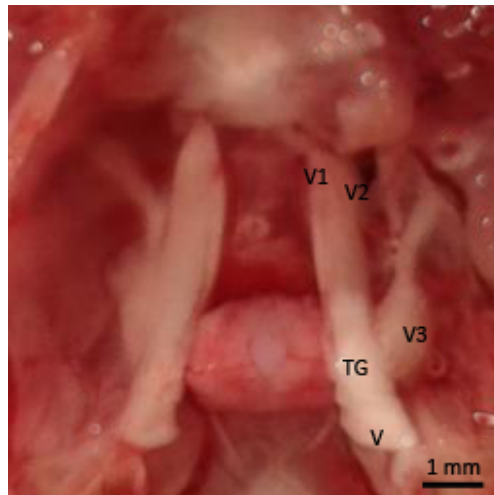
Figure 14. The location of the trigeminal ganglion
A view of the cranial cavity after dissection of the brain shows the location of the trigeminal ganglion (TG) on the trigeminal nerve (V) at the branching point of the mandibular nerve. Ophthalmic nerve (V1), maxillary nerve (V2), mandibular nerve (V3).

3.2.6 Cryopreservation of tissues and cryosectioning

For RNA and protein extraction experiments, 8±2 embryos of E9.5 were pooled prior to freezing. Embryos of E10.5, 11.5 and 12.5 were divided in two parts: head and body. Heads or bodies of litters from each stage were pooled also prior to freezing. The collected samples of embryos or other organs were snap frozen in liquid nitrogen and subjected to RNA or protein extraction.

To cryopreserve samples for cryosectioning, unfixed samples were embedded in OCT medium (Tissue Tek, Sakura, Staufen, Germany) using peel-a-way disposable embedding molds (Polysciences Europe

GmbH, Eppelheim, Germany) and frozen in the gas phase of liquid nitrogen. The frozen samples were stored at -80°C until further use.

Samples were cut on a cryostat, Leica CM 1950 (Leica, Wetzlar, Germany), in a thickness of 10 μm for immunofluorescence and 15 μm for β-Gal staining. Sections were mounted onto SuperFrost Plus slides (R. Langenbrinck, Emmendingen, Germany) and allowed to dry at 37°C for 30 min, before using in the experiment or storing at -80°C until further use.

3.2.7 Genotyping of transgenic animals

Genotyping of transgenic animals was performed using the PCR as described by Bargiotas et al. (2011). Tail tips of studied mice were digested in the genotyping lysis buffer including proteinase K (Roche, Manheim, Germany) at 55°C for 24 hours by mixing intensity of 60 rpm in a Thermoshaker Incubator (PEQLAB, Erlangen, Germany). After that, proteinase K was inactivated at 95°C for 20 min. 2 μl of this tissue extract was used as template for PCR reaction mixture. PCR reaction mixture included 1x PCR reaction buffer (New England Biolabs, Hitchin, UK), 0.2 μM specific primers (Table 5) (Sigma-Aldrich, München, Germany), 0.2 mM dNTPs (New England Biolabs), and 0.3 U *Taq* DNA polymerase (New England Biolabs). Double-distilled water (ddH$_2$O) was added to the reaction mixture to make a final volume of 25 μl. ddH$_2$O was purified using the purification system Q-Pod (Merck Millipore, Darmstadt, Germany). The amplification of the target DNA was performed using the cycler LifeTouch Thermal (Biozym, Hessisch Oldendorf, Germany) under following conditions:

Heated lid	110°C		
Initial denaturation	95°C	5 min	
Denaturation	95°C	30 s	
Annealing	60°C	30 s	35 Cycles
Extension	72°C	40 s	
Final extension	72°C	5 min	
	10°C	∞	

PCR product was separated and visualized using agarose gel electrophoresis as described in Chapter 3.5.6. The amplified size of the PCR product was used to determine the genotype of samples. This experiment was performed and analyzed by Andrea Rabung.

PCR buffer 10x

KCl	500 mM
Tris buffer	100 mM
MgCl$_2$	22.5 mM
DMSO	5 % (v/v)
in ddH$_2$O	

Genotyping lysis buffer

PCR buffer (10x)   1x
Proteinase K   0.2 µg/µl
in ddH$_2$O

Table 5. Primers used for Genotyping of transgenic mice

Primers	Sequence	Amplification product length	Genotype
Panx1	Fwd: 5`GGAAAGTCAACAGAGGTACCC 3`	330 bp	Panx1[wt/wt]
	Rev: 5`CTTGGCCACGGAGTATGTGTT 3`		
	Rev: 5`GTCCCTCTCACCACTTTTCTTACC 3` (*lacZ* region)	630 bp	Panx1[tg/tg]
Panx2	Fwd: 5`TCCTGCTATGAAGCTGGCATCTCTG 3`	350 bp	Panx2[wt/wt]
	Rev: 5`CAAGAAGCCACCCTTGACTGGCAAA 3`	430 bp	Panx2[tg/tg]
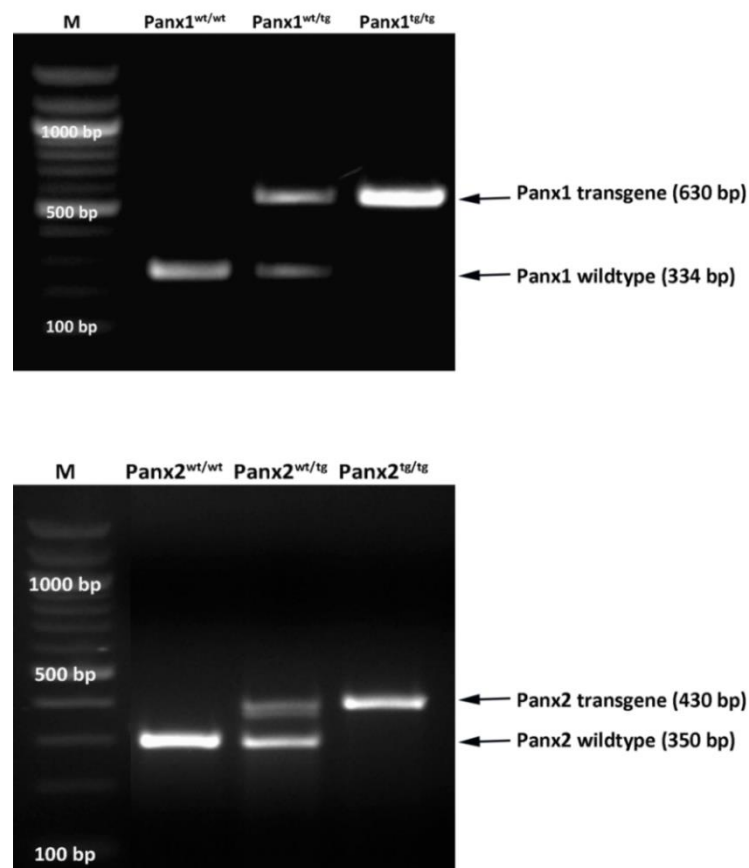
Figure 15. Genotyping of transgenic mice
A specific region of genomic DNA was amplified using standard PCR conditions and analyzed by agarose gel electrophoresis. The size of PCR products was used to determine the genotype of animals. One PCR product was present in homozygous animals Panx1[wt/wt] (334 bp), Panx1[tg/tg] (630 bp), Panx2[wt/wt] (350 bp), and Panx2[tg/tg] (430 bp). Two PCR products were present in heterozygous animals Panx1[wt/tg] (334 and 630 bp) and Panx2[wt/tg] (350 and 430 bp). Broad range DNA ladder (M).

3.3   Reverse transcriptase PCR (RT-PCR)

The expression of a gene of interest was detected using the reverse transcriptase-polymerase chain reaction (RT-PCR) technique. The total RNA including mRNAs was extracted from a tissue to transcribe mRNAs into the complementary DNA (cDNA) using the enzyme reverse transcriptase. The target sequence of the cDNA can be amplified using polymerase chain reaction (PCR) technique in the presence of gene-specific primers. Amplification products can be separated and visualized using agarose gel electrophoresis. Observed specific amplification products on the gel indicate the presence of the mRNA and its gene expression.

3.3.1   RNA extraction

The total RNA was extracted from tissues of interest and embryos. Samples were collected as described in Chapter 3.2.6. Tissue homogenization was performed using the ultrasonic homogenizer Sonoplus (Bandelin Electronic, Berlin, Germany) or the ultra turrax, Ika T10 (Ika, Staufen, Germany). The extraction of RNA was performed using the RNeasy Lipid Tissue Mini Kit (QIAGEN, Erlangen, Germany), according to the manufacturer's instructions. The extraction included an on-column DNase-digestion step using an RNase-free DNase I set (QIAGEN). The RNA of all samples was eluted in 30 µl RNase-free water, except the RNA of cerebellum and brainstem samples, which were eluted in 50 µl of RNase-free water. The RNA was quantified using the spectrophotometer nano drop ND-1000 (Thermo Fisher Scientific, Heidelberg, Germany).

3.3.2   cDNA synthesis

The cDNA was synthesized from total RNA extract (see Chapter 3.3.1) using the enzyme RevertAid Reverse Transcriptase (Thermo Fisher Scientific). Two reactions served as negative controls: one was performed in the absence of the template (NT) and the other without reverse transcriptase (NR). 1 µg of the total RNA was incubated with 0.5 µg Oligo (dT) primer (Thermo Fisher Scientific) and DEPC-H_2O in a volume of 12.5 µl at 65°C for five min, to hybridize primers to the RNA. This reaction mix was supplemented with reaction buffer (Thermo Fisher Scientific), 20 U RNase inhibitor (Thermo Fisher Scientific), 1 mM dNTP (New England Biolabs, Hitchin, UK), 200 U RevertAid-RT (Thermo Fisher Scientific) in a final volume of 20 µl. cDNA synthesis was performed at 42°C for one hour, followed by an inactivation step at 70°C for 10 min.

3.3.3 Polymerase chain reaction (PCR)

The third step of the RT-PCR technique is the amplification of the target cDNA sequence using the polymerase chain reaction (PCR) technique. PCR technique is based on the amplification of a target cDNA sequence using a cDNA polymerase enzyme, which synthesizes a new DNA strand in the presence of target-specific primers and deoxynucleotide triphosphates (dNTPs). PCR was performed at the same time for all samples of cDNA synthesis including negative controls of NT and NR. The PCR reaction mix included 2 µl cDNA as template in addition to 2.5 U *Taq* DNA polymerase (New England Biolabs), 10 µM Primers (Table 7) (Sigma-Aldrich), 10 mM dNTPs (New England Biolabs), 1x PCR reaction buffer (New England Biolabs) and DEPC-H_2O in a final volume of 25 µl. All PCRs had an initial denaturation step of 30 s at 95°C and a final extension step of 10 min at 68°C. The amplification was performed using the LifeTouch Thermal Cycler (Biozym) under different PCR conditions for different primers (see Table 6). The PCR product was separated and visualized using agarose gel electrophoresis as described in Chapter 3.5.5.

Table 6. PCR conditions

Target	Denaturation	Annealing	Extension	Cycles (n)
Panx1 Ct	95°C; 30 s	56°C, 30 s	68°C, 2 min	25
Panx2	95°C; 30 s	57°C, 30 s	68°C, 2 min	30
18S rRNA	95°C; 30 s	56°C, 30 s	68°C, 2 min	20

All PCRs had an initial denaturation step of 30s at 95°C and final extension of 10 min at 68°C. Primers had different annealing temperatures and different number of cycles.

Table 7. Primers used in RT-PCR

Primers	Sequence	Amplification product length
Panx1 Ct	Fwd: 5`AGAGAGGAATTCTGCAAGCTCATCGCCGTG 3` Rev: 5`AGAGAGGGATCCTTTGCTGCAGCCTCGCTG 3`	443 bp
Panx2	Fwd: 5`GAGAAAAAGCATACCCGCCAC 3` Rev: 5`GGTGAGCAGACATGGAATGA 3`	266 bp
18S rRNA	Fwd: 5`AAACGGCTACCACATCCAAG 3` Rev: 5`CCTCCAATGGATCCTCGTTA 3`	155 bp

3.4   Real time quantitative PCR

The previously described RT-PCR was used to determine the qualitative expression of Panx1 mRNA in defined stages of mouse development. Here, real time quantitative PCR technique was used to quantify relative Panx1 mRNA expression in different tissues. This experiment was performed using the Rox SYBR Green system. SYBR Green is a fluorescent dye binding to the double-strand DNA and emits a fluorescent signal. Rox dye was used as internal passive reference dye to normalize the SYBR Green signal in samples. During the amplification process, the increased fluorescent signal was measured to evaluate the double-strand DNA concentration. Reference genes were used to normalize differences in total RNA between samples.

Samples of spinal cord, trigeminal ganglia, and DRGs were collected as described in Chapter 3.2.5. Triplet samples (n=3) of the cranial thoracic region of spinal cord were collected from three animals (47±3 weeks-old). On the other hand, trigeminal ganglia and DRGs were collected from nine animals (27±3 weeks-old) to obtain enough quantity of RNA for cDNA synthesis. Ganglia from each studied region were pooled from three animals to obtain finally triplet ganglia samples (n=3). The cDNA synthesis was performed using 0.5 µg total RNA for spinal cord samples and 1 µg total RNA for trigeminal ganglia and DRGs samples in a final reaction volume of 20 µl as described in Chapter 3.3.2.

Prior to use in the experiment, all cDNA templates were diluted 1:5 with DEPC-H_2O. The experiment was carried out in a 20 µl reaction mix, including 2.5 µl diluted cDNA template, 300 nM primers (Table 8) and 10 µl master mix of Takyon^{TM} Rox SYBR Master Mix dTTP Blue kit (Eurogentec, Seraing, Belgium). The Takyon master mix contains Takyon DNA polymerase, $MgCL_2$, SYBR Green, dNTPs, Rox passive reference and stabilizers. The measurement was performed in a 96 well plate (Applied Biosystems, Foster City, USA) using the StepOnePlus Real Time PCR system (Applied Biosystems) under the regular amplification conditions, as recommended in the manufacturer's instructions of Takyon Kit (Eurogentec). These includes an initial Takyon activation at 95°C for 3 min followed by 40 cycles of denaturation at 95°C for 10 s and annealing /extension at 60°C for 1 min.

Subsequently, melting curve analysis was performed to identify any primer-dimers or other artifacts. Melting curve analysis was performed under the following conditions: 15 s denaturation at 95°C, 1 min annealing at 60°C, and continued measurement by increasing the temperature in a ratio of 0.3 °C/s from 60°C to 95°C. StepOne™ Software v2.2 (Applied Biosystems) was used to readout data of real time qPCR and melting curve.

3.4.1   Relative quantification of real time qPCR data

The relative quantification of real time qPCR data was used to describe the relative expression of a gene in target samples compared to another calibration sample. Firstly, a threshold was determined for each individual gene during the exponential phase of the reaction. This determination of a threshold was used to distinguish the significantly increased signal from the initial fluorescent signal (background). The threshold cycle (Ct) indicated the cycle number at which the fluorescence value crosses the threshold. In all samples, the mean of a gene of interest was normalized (ΔCt) to the mean of the reference gene 18S rRNA as follows:

$$\Delta Ct_{target} = Ct_{target} - Ct_{reference}$$

ΔCt values of target samples were related to a calibration sample. In the spinal cord experiment, for instance, samples of the ventral region were used as calibration samples (see Chapter 4.6.3). Trigeminal ganglia samples were used as calibration samples for sensory ganglia samples (see Chapter 4.6.6). The relation between samples was calculated by:

$$\Delta\Delta Ct_{target} = \Delta Ct_{target} - \Delta Ct_{calibration\ sample}$$

The relative gene expression in the target sample was calculated by:

$$\text{Relative quantity} = 2^{-\Delta\Delta Ct}$$

All regions were analyzed in triplicate (n=3 per group). Data were presented as means ± standard errors of the mean (SEM). The statistical analysis of data was performed as described in Chapter 3.14.

Table 8. Primers used in real time qPCR

Primers	Sequence	Amplification product length
Panx1	Fwd: 5` AGCCAGAGAGTGGAGTTCAAAGA 3` Rev: 5` CATTAGCAGGACGGATTCAGAA 3`	104 bp
Panx2	Fwd: 5` GTCACCCTGGTCTTCACCAA 3` Rev: 5` AGCTCTGTCCAGCAGTAGCC 3`	113 bp
P2X3R	Fwd: 5` CTGCCTAACCTCACCGACAAG 3` Rev: 5` AATACCCAGAACGCCACCC 3`	150 bp
P2X7R	Fwd: 5` CCTCTGCTATGCCTTTGACC 3` Rev: 5` CAGAGCACGAATTATGGCAC 3`	148 bp
18S rRNA	Fwd: 5` AAACGGCTACCACATCCAAG 3` Rev: 5` CCTCCAATGGATCCTCGTTA 3`	155 bp

3.5 Cloning of DNA templates for the *in vitro* transcription

For whole-mount *in situ* hybridization (WM-ISH), it was required to prepare recombinant plasmids carrying DNA fragments of Panx1. These plasmids are required for *in vitro* transcription of cRNA probes.

The source of murine pannexin1 (mPanx1) DNA fragment was a recombinant plasmid, which was obtained as a gift from Prof. Dr. Georg Zoidl (Ruhr-University Bochum, Germany). In this recombinant plasmid, mPanx1 was inserted into the plasmid pEYFP-N1 (Figure 16) at the restriction site of EcoRI.
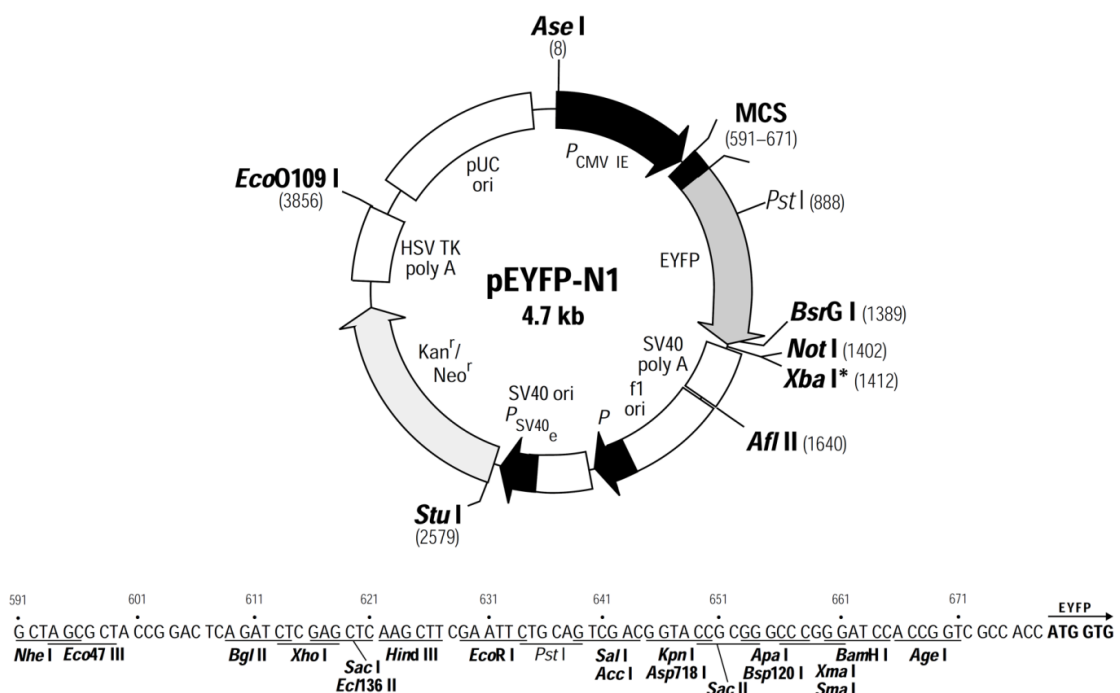
Figure 16. The map of the pEYFP-N1 vector
The full-length mPanx1 DNA fragment was inserted into the plasmid pEYFP-N1 at the restriction site of EcoRI. This recombinant plasmid was used as the source of mPanx1 DNA fragment. Taken from BD Biosciences (Heidelberg, Germany).

For *in vitro* transcription, two DNA fragments of Panx1 (full-length and short-length) were inserted into appropriate plasmids, pSPT18 and pSPT19 (Figure 17). These plasmids contain T7 and SP6 RNA polymerase promoters.

3.5.1 Preparation of the Panx1 short-length DNA fragment

The recombinant plasmid pEYFP-N1-mPanx1 was used as a template to amplify a short DNA fragment of 443 base pairs (bp) (bases 1231 to 1673) encoding the carboxy-terminus of murine Panx1 (Panx1

Ct). Primers were designed using tools of the program NCBI Primer-BLAST. Sequences of restriction endonucleases were designed at the 5´-end of primers to allow insertion of the short fragment into vectors. The forward primer included an EcoRI sequence and the reverse primer included a BamHI sequence (Table 9).

Table 9. Primers used for Panx1 Ct amplification

Primers	Sequence	Amplification product length
Panx1 Ct	Fwd: 5` AGAGAGGAATTCTGCAAGCTCATCGCCGTG 3` Rev: 5` AGAGAGGGATCCTTTGCTGCAGCCTCGCTG 3`	443 bp

Primer included sequences of restriction endonucleases EcoRI (**GAATTC**) and BamHI (**GGATCC**).

The short fragment (Panx1 Ct) was amplified by PCR using 0.3 µg purified plasmid pEYFP-N1-mPanx1 in a reaction volume of 50 µl including 2.5 U *Taq* DNA polymerase (New England Biolabs), 10 µM Primers (Sigma-Aldrich) (Table 9), 10 mM dNTPs (New England Biolabs), 1x reaction buffer (New England Biolabs) and ddH$_2$O. An additional reaction mix, which contained all reaction components without the template, served as negative control. The amplification was performed under cycling conditions of an initial denaturation step at 95°C for 30s followed by 30 cycles of denaturation at 95°C for 30s, annealing at 56°C for 30s, and extension at 68°C for 2 min. Finally, the reaction had an extension step at 68°C for 10 min. PCR amplification was performed using the LifeTouch Thermal Cycler (Biozym).

PCR product was examined by agarose gel electrophoresis (see Chapter 3.5.6) to ensure the specificity of the amplified fragment according to its size and by comparing it to the negative control without template. The amplified fragment was separated from the template by cutting out the specific amplification product under UV light as a gel block using UV-transilluminators (Vilber Lourmat, Eberhardzell, Germany). This DNA fragment was purified from the isolated gel block using the method freeze-squeeze (Thuring et al., 1975). In this method, the isolated gel block was frozen at -20°C overnight. The frozen gel block was squished gently using a Parafilm section to extract an aqueous solution from the gel. The resulting liquid consists of solution of agarose gel and separated DNA. DNA was purified from the collected aqueous solution by isopropanol precipitation as described in Chapter 3.5.5. After purification, the PCR product was eluted in 10 µl ddH$_2$O. This purified DNA fragment (Panx1 short-length) was joined to the linearized plasmid pSPT19 (Figure 17) using the enzyme T4 DNA ligase (Fermentas, Heidelberg, Germany) as described in Chapter 3.5.3.

3.5.2 Preparation of the Panx1 full-length DNA fragment

The recombinant plasmid pEYFP-N1-mPanx1 contains the full-length fragment of mPanx1 (1280 bp), which is flanked by restriction sites of EcoRI at both termini. This recombinant plasmid does not allow *in vitro* transcription, as this plasmid does not contain any promoters for RNA polymerase. Therefore, it was required to transfer the Panx1 full-length fragment from pEYFP-N1-mPanx1 into appropriate plasmids, pSPT18 and pSPT19, which are flanked by T7 and SP6 RNA polymerase promoters. Firstly, the recombinant plasmid pEYFP-N1-mPanx1 was digested using the restriction endonuclease EcoRI. 3 µg purified recombinant plasmid of pEYFP-N1-mPanx1 was digested in the presence of 10 units of the restriction endonuclease EcoRI (NEB), 1x restriction endonuclease buffer (NEB) and ddH$_2$O in a final volume of 20 µl. Digestion was performed at 37°C for one hour. After digestion, Panx1 full-length fragment was separated from the plasmid pEYFP-N1 by agarose gel electrophoresis (see Chapter 3.5.5). This fragment was also isolated from the gel using the method freeze-squeeze (see Chapter 3.5.1), followed by isopropanol precipitation as described in Chapter 3.5.5. This purified DNA fragment (Panx1 full-length) was finally inserted into linearized plasmids pSPT18 and pSPT19 using the enzyme T4 DNA ligase (Fermentas) as described in Chapter 3.5.3.

3.5.3 Ligation of fragments into Vectors

The enzyme T4 DNA ligase binds 5'-phosphate to 3'-hydroxyl termini in double-strand DNA. Ligation of DNA was performed in a 20 µl reaction volume including 35 ng of linearized plasmid (see Table 10) and 0.3 µg of DNA insert in addition to 5 units T4 DNA Ligase (Fermentas), 1x T4 ligase buffer (Fermentas) and ddH$_2$O. The mixture was incubated at 16°C for one hour. The resulting recombinant plasmid was amplified using competent bacteria as described in Chapter 3.5.4.

Table 10. Linearization of plasmids prior to DNA insertion

Plasmid	linearization site of the plasmid	DNA insert
pSPT 19	EcoRI BamHI	Panx1 short-length
pSPT 19	EcoRI	Panx1 full-length
pSPT 18	EcoRI	Panx1 full-length

3.5.4 Bacterial transformation

Bacterial transformation was performed in a S1 approved laboratory. All transformed organism were recorded at the governmental committee of the University of Saarland, Germany. Not required organisms were directly destroyed by autoclaving.

Bacteria take up DNA from their environment via transformation in a special physiological state called competent. This advantage is commonly used to amplify a large amount of plasmids. Escherichia coli XL1-blue cells had previously been made competent and were stored at -80°C. 0.5 µg plasmids were transferred to 200 µl competent bacteria. The mixture of bacteria and plasmids was placed on ice for 30 min following a heat shock at 42°C for 45 seconds; a process which allows the DNA to enter into bacteria. Bacteria were returned to ice for 1-2 minutes. 800 µl LB-Medium was added to the transformation mixture and placed on a shaker incubator (PEQLAB) at 37°C with mixing intensity of 700 rpm for one hour. This pre-culture was briefly centrifuged, and plated out on an agar plate. The agar plate contained the LB-Medium and 2 % agar (w/v) (AppliChem, Darmstadt, Germany) in addition to the appropriate selective antibiotic. All antibiotics were used in a concentration of 50 µg/ml. The plasmid pEYFP-N1 was selected using kanamycin (Sigma-Aldrich). Ampicillin (Carl Roth, Karlsruhe, Germany) was used to select plasmids of pSPT 18, pSPT 19, and pBS. The plasmid pBS included the DNA insert of mMyoD. This recombinant plasmid pBS mMyoD was obtained as a gift from Prof. Beate Brand-Saberi (Ruhr-University Bochum, Germany) and served as positive control for *in situ* hybridization and preparatory procedures.

After plating transfected bacteria, plates were incubated at 37°C overnight. A single visible isolated colony was inoculated into a starter culture (3ml LB-Medium containing the selective antibiotic) and incubated at 37°C overnight with shaking at 200 rpm using the orbital incubator SI500 (Bibby Scientific, Stone, UK). The starter culture was used to increase the quantity of bacteria and to inoculate the main culture of 100 ml LB-Medium containing the selective antibiotic. Bacteria were harvested from the main culture by centrifugation at 4°C and 2857 xg for 15 min using the centrifuge Heraeus Megafuge 16 R (Thermo Fisher Scientific). Plasmid isolation from the bacterial pellet was performed using a plasmid midi kit (QIAGEN) according to the manufacturer's protocol. Transformed DNA fragments were tested by restriction analysis and sequencing by Eurofins Genomics (Ebersberg, Germany). Sequencing results confirmed the sequence of Mus musculus pannexin 1 (mPanx1), NM_019482.2.

LB-Medium pH 7.0

Tryptone	1 % (w/v)
Yeast – Extract	0.5 % (w/v)
NaCl	1 % (w/v)
in distilled water (dH$_2$O)	

Autoclave at 120°C 20 min

3.5.5   Isopropanol precipitation of DNA

DNA can be precipitated from an aqueous solution in the presence of alcohol and a high concentration of salt. In this study, DNA was precipitated by addition of salt and alcohol in final concentration of 0.3 M sodium acetate and 30 % isopropanol (v/v). The precipitation mixture was incubated at -20°C overnight followed by centrifugation at 4°C and 215 xg for 30 minutes using the centrifuge Himac CT 15RE (Hitachi Koki, Tokyo, Japan). The supernatant was removed and the DNA pellet was washed twice in 70 % ethanol in ddH_2O (v/v) by centrifugation at 4°C and 215 xg for 10 min. Finally, the pellet was air-dried for 30 minutes and re-suspended in 10 µl ddH_2O. DNA was quantified using the nano drop ND-1000 spectrophotometer (Thermo Fisher Scientific, Wilmington, USA).

3.5.6   Agarose gel electrophoresis

Agarose gels were prepared by boiling a solution of Tris-Acetate-EDTA buffer (TAE buffer) and 1.5 % agarose (w/v) (Biozym) in the microwave for 2 min. The solution was allowed to cool down to 60°C and supplemented with the fluorescent nucleic acid gel stain, Gel Red (Biotium, Hayward, USA). 1x DNA loading Dye (Thermo Fisher Scientific) was applied to DNA samples. The mixture of samples was loaded into gel wells. DNA Ladder of low range or broad range (Fermentas) was pipetted next to the samples. DNA samples were separated in a horizontal gel electrophoresis system (PEQLAB) at 120 V and 75 mA for 45 minutes. Amplification products of DNA were photographed using FUSION-FX7/SL Advance system (PEQLAB).

Tris-Acetate-EDTA (TAE) buffer

Tris base	40 mM
Acetic acid	0.11 % (v/v)
0.5 M EDTA (pH 8.0)	0.2 % (v/v)
in dH_2O	

3.6 Probe synthesis for *in situ* hybridization

Digoxigenin-labeled complementary RNA probes (DIG-labeled cRNA probes) were prepared by *in vitro* transcription for whole-mount *in situ* hybridization. Prior to the synthesis of cRNA probes, recombinant plasmids were linearized and utilized for *in vitro* transcription. After that, cRNA probes were precipitated with ammonium acetate and ethanol. The quality of cRNA probes was tested by Northern blot analysis.

3.6.1 Linearization of plasmid DNA

A RNA polymerase synthesizes a cRNA in the direction 3`→5` of the DNA template. To terminate the reaction "*run off*", each recombinant plasmid was linearized by a restriction at the site downstream from the site of interest (Table 11). 3 µg of the purified recombinant plasmid was digested in the presence of 10 units restriction endonuclease (NEB), 1x restriction endonuclease buffer (NEB) and DEPC-H_2O in a final volume of 20 µl. Digestion was performed at 37°C for one hour. The linearized plasmid was purified by isopropanol precipitation as described in Chapter 3.5.5. Prior to *in vitro* transcription, this plasmid was eluted in 13 µl DEPC-H_2O.

3.6.2 *In vitro* transcription

RNA transcription can be performed *in vitro* using a bacteriophage RNA polymerase of T3, T7, or SP6 (Schenborn, 1995). In contrast to DNA polymerase, RNA polymerase does not require primers to produce the single strand of RNA. Plasmids are commonly used tools for *in vitro* transcription, which include the cognate promoter of a RNA polymerase in the multiple cloning site (MCS). In this study, recombinant plasmids of pSPT18, pSPT19 and pBS mMyoD were used for *in vitro* transcription. These plasmids contain promoters of T7 and SP6 RNA polymerase. *In vitro* transcription was performed using the DIG RNA Labeling Kit (Roche) according to the manufacturer's instructions. *In vitro* transcription reaction mixture of 20 µl included the whole volume of 13 µl of the linearized plasmid (see Chapter 3.6.1) and the corresponding RNA polymerase (see Table 11 and Figure 17) in addition to a mixture of NTPs including Digoxigenin-UTP. RNA polymerase T7 was used to generate antisense probes, whereas RNA polymerase SP6 was used to generate DIG labeled sense cRNA probes. It was not required to remove the DNA template from the reaction mixture after the transcription.
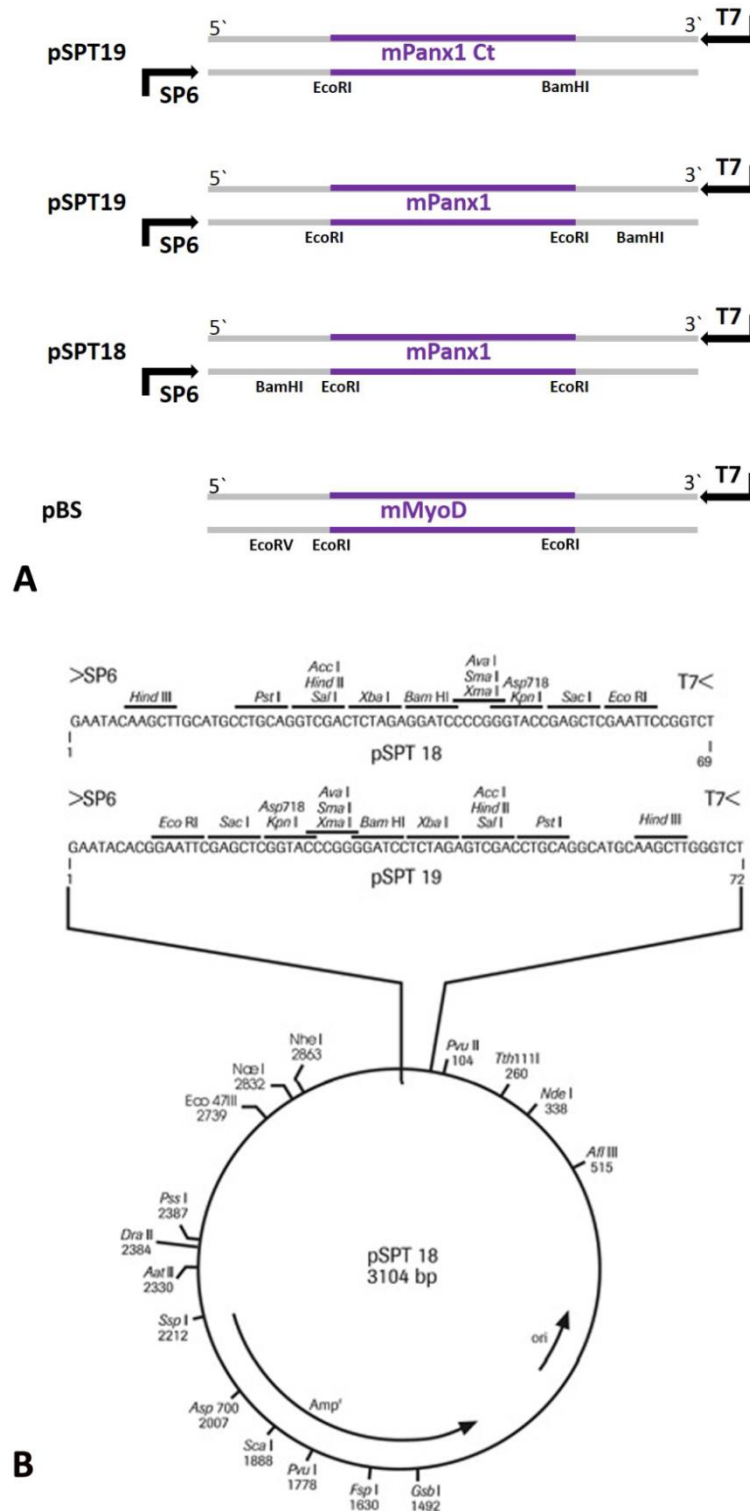
Figure 17. Recombinant plasmids used for *in vitro* transcription
(A) A part of each recombinant plasmid is represented to illustrate the location of the insert within the plasmid. Linearization sites are represented in Table 11. The promoter T7 served to generate antisense probes, whereas SP6 served to generate sense cRNA probes. (B) Maps of pSPT18 and pSPT19 vectors. Taken from Roche.

Table 11. *In vitro* transcription of cRNA probes

DNA Template	linearization site	RNA polymerase	cRNA probes	Length in bases
pSPT 19 mPanx1 Ct	EcoRI	T7	antisense Panx1 Ct	443
pSPT 19 mPanx1 Ct	BamHI	SP6	sense Panx1 Ct	443
pSPT 18 mPanx1	BamHI	T7	antisense Panx1	1280
pSPT 19 mPanx1	BamHI	SP6	sense Panx1	1280
pBS mMyoD	EcoRV	T7	antisense MyoD	1833

The table shows DNA templates used for *in vitro* transcription, the linearization site of each recombinant plasmid, RNA polymerase used for each reaction, cRNA probe generated through each reaction, and the length of each cRNA probe in bases.

3.6.3   Ammonium acetate precipitation

Ammonium acetate precipitation is an alternative method to sodium acetate precipitation. It reduces co-precipitation of NTPs. Probes of cRNA were precipitated immediately after transcription. The precipitation mixture (20 µl) was supplemented with ammonium acetate (Fisher Scientific, Nidderau, Germany) in a final concentration of 1M and with 82 % ethanol pure (v/v) (stored at -20°C). The precipitation mixture was immersed in liquid nitrogen for 3 min followed by centrifugation at room temperature at 162 xg for 10 minutes using a Himac CT 15RE centrifuge (Hitachi Koki). The supernatant was removed and the pellet was washed with 500 µl of 80 % ethanol pure in ddH$_2$O (v/v) and centrifuged at 215 xg at RT for 10 min. The supernatant was removed; the pellet was air-dried at RT for 30 min. The pellet of cRNA was eluted in 100 µl DEPC-H$_2$O. Aliquots of cRNA probes were stored at -20°C until use. The quality of cRNA probes was controlled by agarose gel electrophoresis using 10 µl of each probe as described in Chapter 3.5.6.

3.7   Whole-mount *in situ* hybridization

In mouse embryos, the distribution of Panx1 mRNA expression was analyzed using whole-mount *in situ* hybridization. The technique was based on the hybridization of a DIG-labeled cRNA probe complementary to the target mRNA. This cRNA probe was detected using anti-DIG antibodies conjugated to a reporter molecule alkaline phosphatase (AP). Antibody binding was made visible using the substrate Nitro Blue Tetrazolium Chlorid / 5-Bromo-4-Chloro-3-Indolyl Phosphate (NBT/BCIP), which reacts in the presence of alkaline phosphatase to a purple staining at sites of hybridization.

3.7.1   Material and reagents for *in situ* hybridization

All *in situ* hybridization procedures were performed under RNase-free conditions. Operation instruments were rinsed using the cleaning unit Elmasonic S 10 (Elma Hans Schmidbauer, Singen, Germany). Glassware and metal instruments were baked at 200°C in an oven (Thermo Fisher) for four hours. Disposable plastic wares were used sterile and RNase-free. Unsterile plastic equipment, e.g. pH electrode, was rinsed in 70 % ethanol DEPC-H_2O (v/v) for 30 s followed by washing in 1M NaOH for 5 min and a final wash in DEPC-H_2O.

Diethyl pyrocarbonate (DEPC) (Sigma-Aldrich) was used to inactivate RNases in water and solutions. Solutions were treated with 0.1 % DEPC (v/v) by stirring at RT for 1 hour. After treatment, DEPC was inactivated by autoclaving. DEPC is highly unstable in the presence of Tris. It decomposes rapidly into ethanol and CO_2 (Hilario and Mackay, 2007). Therefore, Tris was not treated directly with DEPC during the preparation of Tris buffer, but Tris was dissolved in DEPC-H_2O.

DEPC-H_2O
1 l ddH_2O was treated with 1 ml DEPC by stirring the solution at RT for 1 hour. DEPC was inactivated by autoclaving the solution.

Hybridization solution

Formamid	50 % (v/v)
20x SSC	5x SSC
CHAPS	0.5 % (w/v)
Triton X-100	0.1 % (v/v)
0.5 M EDTA (pH 8.0)	5 mM
Blocking reagent	2 % (w/v)
DEPC	0.1 % (v/v)
in ddH_2O	

All components were mixed by stirring at 60-65°C in a water bath for 2 hours. The mixture was allowed to cool on ice. After cooling, the following components were added:

Heparin	50 μg/ml
tRNA	1 mg/ml

The solution was again mixed by stirring, aliquoted in RNase free tubes, and stored at -20°C until use.

Saline sodium citrate (SSC) pH 7.0

NaCl	0.15 M
Sodium citrate tribasic dihydrate	15 mM

DEPC   0.1 % (v/v)

in ddH$_2$O

The solution was sterilized by autoclaving and stored at RT.

10x Sodium potassium buffer (KTBT)

NaCl	1.5 M
KCl	20 mM
Tris HCl 1 M (pH7.3)	25 % (v/v)
Tween 20	1 % (v/v)

The solution was prepared in DEPC-H$_2$O, sterilized by autoclaving, and stored at RT.

Alkaline phosphate buffer (AP-buffer)

5 M NaCl	2 % (v/v)
1 M MgCl$_2$	5 % (v/v)
1 M Tris HCl (pH 9.5)	10 % (v/v) (dissolved in DEPC-H$_2$O)
Triton X-100	0.1 % (v/v)

AP-buffer was always made fresh using ddH$_2$O.

10x DEPC-PBS pH 7.4

NaCl	0.136 M
KCl	2.6 mM
Na$_2$HPO$_4$	10.1 mM
KH$_2$PO$_4$	1.76 mM
DEPC	0.1 % (v/v)

in ddH$_2$O

All components were mixed by stirring. The solution was sterilized by autoclaving.

3.7.2   Whole-mount *in situ* hybridization procedure

Whole-mount *in situ* hybridization was performed in the following steps:

- Embryos of different stages were dissected as described in Chapter 3.2.3. After that, embryos were transferred into a 12-well culture plate containing 4 % PFA (v/v), RNase free, (Electron Microscopy Sciences, Hatfield, USA) diluted in PBS-Triton for fixation at 4°C for 4 hours. Fixation was followed by washing twice in DEPC-PBS-Triton (DEPC-PBS in 0.1 % Triton X-100 (v/v) (Carl Roth)) on ice.

- Subsequently, embryos were treated with 20 µg/ml Proteinase K (Roche) for 20 min at RT. Proteinase K makes the tissue permeable and unmasks the target mRNA. This allows the cRNA probe to access its target mRNA. The same digestion duration was used for all stages.

- The digestion was stopped by washing embryos in DEPC-PBS-Triton for 10 min on ice.

- Embryos were post-fixed in postfixation solution (0.2 % glutardialdehyde (v/v) (Merck, Darmstadt, Germany), 4 % PFA (v/v) in PBS-Triton) for 20 min by shaking on ice, followed by washing in PBS-Triton for 10 min on ice.
- Pre-hybridization of embryos was performed in a hybridization oven, HB-1000 (Ultra-Violet Products Ltd, Cambridge, UK), with pre-warmed hybridization solution at 65°C twice; at first for 2 hours and then overnight.
- Embryos were hybridized with 1 µl/ml DIG-labeled cRNA probes (Table 11) in fresh pre-warmed hybridization solution at 65°C overnight.
- Non-bound cRNA probes were removed by washing at 65°C in the following steps:
- In 2x saline sodium citrate (SSC) for 20 min.
- In 2x SSC containing 0.1 % CHAPS (3-[(3-Cholamidopropyl)dimethylammonio]-1-propansulfonat) (w/v) twice for 30 min each.
- In 0.2X SSC containing 0.1 % CHAPS (w/v) twice for 30 min each.
- Embryos were rinsed in KTBT buffer three times at RT for 10 min.
- Non-specific antibody binding sites were blocked with lamb serum solution (20 % lamb serum (v/v) (Invitrogen, Darmstadt, Germany) diluted in KTBT) at RT for 4 hours.
- DIG labeled cRNA probes were detected with anti-DIG-AP (Table 1), diluted 1:2,000 in lamb serum solution, at 4°C overnight.
- Non-bound antibodies were removed by washing in KTBT buffer in steps: firstly, three times at RT for 10 min each, secondly, six times at RT for 1 hour each, and finally one time at 4°C overnight.
- Embryos were equilibrated with the alkaline phosphate buffer three times at RT for 10 min each.
- The color reaction was carried out using the staining solution of alkaline phosphate buffer and 2 % NBT/BCIP (v/v) (Roche). The color was allowed to develop in the dark at RT for one hour or until the signal or the background become visible.
- Staining solution was removed, and embryos were washed with KTBT buffer twice at RT for 10 min. Color reaction was terminated by washing in DEPC-PBS.
- Embryos were photographed using a stereo microscope SZX12 (Olympus, Hamburg, Germany), equipped with a color camera CC-12 (Olympus) and the software Cell^P imaging (Olympus).

3.7.3 Vibratome sectioning post *in situ* hybridization

Post whole-mount *in situ* hybridization, embryos were embedded in warm agarose gel (3 % agarose (w/v) in TAE buffer) and cooled at 4°C. 50 µm transversal sections were immediately cut using the vibratome VT1000 S (Leica) equipped with a razor blade (Electron Microscopy Sciences). The agarose

block containing the tissue was immersed in PBS in the bath of the vibratome. PBS was prepared as described in Chapter 3.9. The vibration amplitude, the speed, and the angle of the blade were controlled. Sections were mounted onto SuperFrost Plus slides (R. Langenbrinck) using the embedding medium of Roti-Mount Aqua (Carl Roth). After drying, sections were photographed using the stereo microscope SZX12 (Olympus).

3.8 Generation of anti-Panx1 polyclonal antibodies

A polyclonal antibody against mouse Panx1 was generated in an adult rabbit (New Zealand White Rabbit) (see Chapter 3.2.2). Immunization was performed using synthetic peptides, which were synthesized at the Institute for Medical Biochemistry and Molecular Biology of Saarland University. The amino acid (aa) sequence (QRVEFKDLDLSSEAA) was derived from the carboxy terminus (395-409 aa) of mouse Panx1. In a previous study, the sequence was used to generate a polyclonal antibody against Panx1 by Penuela et al. (2007).

Immunization of animals and collection of serum was performed at the Institute for Medical Biochemistry and Molecular Biology of Saarland University. Firstly, the pre-immune serum (PIS) was collected prior to immunization. The animal was immunized subcutaneously with the antigen every two weeks for six times. Each injection contained 200 µg antigen dissolved in 250 µl complete Freund's adjuvant. The antiserum was collected ten days after each immunization. Finally, the animal was sacrificed and the whole endserum was collected.

3.8.1 Determination of antibody titer by ELISA

The enzyme-linked immune-sorbent assay (ELISA) was used to determine the antibody titer of the first antiserum. An equal amount of peptides (80 ng) was coated onto a 96 well plate. Serial dilutions (1:1000 – 1:128,000) of Panx1 antibody (the first antiserum) and of the negative control of PIS were allowed to bind to coated peptides. The peptide-antibody complex was detected using a horseradish-peroxidase (HRP)-conjugated goat anti-rabbit antibody (Table 3). The antibody detection was visualized using a chromogenic substrate of 3,3'-5,5' tetramethylbenzidine (TMB) (Dako, Hamburg, Germany) which catalyzes a color in the presence of HRP. The absorbance of color was measured using the micro-plate reader infinite M200 (TECAN, Crailsheim, Germany). This experiment was carried out in our laboratory by Dr. Anja Beckmann and Jessica Kilper according to the following protocol:

- Peptides were dissolved in 50 mM sodium bicarbonate (coating-buffer).

- 50 µl of peptide solution was pipetted in a 96 well plate so that all wells contained an equal quantity of peptides (80 ng). The plate was sealed with parafilm and incubated at 37°C for three hours.
- Wells were washed three times with 200 µl washing buffer (0.1 % Tween (v/v) in PBS)
- Wells were incubated with 200 µl blocking solution (5 % nonfat milk powder (w/v) and 0.1 % Tween (v/v) in PBS) at 4°C overnight.
- Wells were washed three times with 200 µl washing buffer.
- Serial dilutions (1:1,000 – 1:128,000) of the first antiserum and PIS (Table 1) in washing buffer were allowed to bind to coated peptides. Antibody detection was performed at RT for 30 min.
- Wells were washed three times with 200 µl washing buffer.
- Wells were incubated with 150 µl of the secondary antibody HRP goat anti-rabbit (Table 3) at RT for 30 min. The antibody was diluted 1:20,000 in washing buffer.
- Wells were washed three times with 200 µl washing buffer.
- Color detection was performed using 50 µl of the chromogenic substrate TMB, which produces a blue color, for 5 min.
- The enzymatic reaction was stopped with 50 µl 1M sulfuric acid, which converts the blue color to a yellow color.
- The developed yellow color was measured at 450 nm using the micro-plate reader infinite M200 (TECAN).
- As described by Liu et al. (2009), results were taken as positive if the ratio of the absorbance of analyzed sample to the absorbance of negative control is greater than 2.1.

3.8.2   Serum neutralization assay

Unpurified polyclonal antibodies are able to bind non-specifically to proteins. To determine whether antibody signals are specific, a peptide preabsorbtion experiment was performed. Prior to use in the experiment, peptides were diluted in PBS and incubated with the antiserum (Table 1) at 4°C for 48 hours. Peptides were used in a ratio of w/w to the concentration of proteins in the antiserum. Serial dilutions of peptides were prepared to determine the optimal dilution of peptides required for a complete inhibition.

3.9 Immunoblotting

The presence of a protein in a tissue was detected using immunoblotting analysis. This analysis was achieved in multiple steps. Initially, proteins were isolated from a tissue and denatured by heat. Proteins were separated by size in an electrical field using gel electrophoresis. These separated proteins were transferred onto a membrane for immunodetection of a specific protein via antibodies. The molecular weight of the detected protein was determined by comparing its molecular weight to that of proteins of known molecular weight included in a protein marker mixture.

Reagents for immunoblotting

Lysis buffer

Tris HCl 0.5 M (pH 6.8)	6.2 % (v/v)
SDS	2 % (w/v)
Glycerol	10 % (v/v)
β-mercaptoethanol	2 mM
Protease inhibitor	4 % (v/v)
in dH$_2$O	

5x Laemmli buffer

Tris HCl 0.5 M (pH 6.8)	31 % (v/v)
SDS	10 % (w/v)
Glycerol	50 % (v/v)
Bromophenol blue dye	0.05 % (w/v)
β-mercaptoethanol	10 mM (v/v)
in dH$_2$O	

10x PBS pH 7.4

NaCl	0.136 M
KCl	2.6 mM
Na$_2$HPO$_4$	10.1 mM
KH$_2$PO$_4$	1.76 mM
in dH$_2$O	

PBST

Tween 20	0.1 % (v/v)
in PBS	

5 % Stacking gel

1 M Tris HCl (pH 6.8)	12.7 % (v/v)
30 % Acrylamid Mix (w/v)	16.7 % (v/v)
10 % SDS in dH$_2$O (w/v)	1 % (v/v)
10 % Ammonium peroxodisulfate (APS) in dH$_2$O (w/v)	1 % (v/v)
TEMED	0.1 % (v/v)
in dH$_2$O	

12 % Resolving gel

1.5 M Tris HCl (pH 8.8)	25 % (v/v)
30 % Acrylamid Mix (w/v)	40 % (v/v)
10 % SDS in dH$_2$O (w/v)	1 % (v/v)
10 % APS in dH$_2$O (w/v)	1 % (v/v)
TEMED	0.04 % (v/v)
in dH$_2$O	

10x Electrophoresis buffer

Tris base	250 mM, pH 6.8
Glycine	2 M
SDS	1 % (w/v)
in dH$_2$O	

Transfer buffer pH 8.3

Tris base	25 mM
Glycin	192 mM
Methanol	20 % (v/v)
in dH$_2$O	

Ponceau Red solution

Ponceau Red	0.1 % (w/v)
Acetic acid	5 % (v/v)
in dH$_2$O	

Blocking solution

Nonfat milk powder	1 % or 5 % (w/v)
Tween 20	0.1 % (v/v)
in PBS	

Dissociation buffer

Tris HCl	62.5 mM (pH 6.7)
SDS	2 % (w/v)
β-mercaptoethanol	100 mM

in dH$_2$O

Protein isolation

Proteins were isolated from tissues using the lysis buffer. 4 % (v/v) of the protease inhibitor cocktail, Complete (Roche), were included in this buffer to protect proteins during protein isolation. The lysis buffer also included 2 mM β-mercaptoethanol (Carl Roth) to reduce disulfide bonds in proteins. 2 % (w/v) sodium dodecyl sulfate (SDS) (Carl Roth) was also included in the lysis buffer to charge protein molecules negatively so that all protein molecules migrate towards the anode in an electrical field.

Collected samples for immunoblotting (see Chapter 3.2.6) were thawed on ice. Samples were homogenized in 300-800 µl of the lysis buffer. The amount of the lysis buffer needed for homogenization was determined so the protein extract was not too diluted and had a protein concentration of 2-4 µg/µl. Samples were homogenized using an electric ultra-homogenizer; Ultra-Turrax T-10 (IKA, Staufen, Germany) and centrifuged at 215 xg using a Himac CT 15RE (Hitachi Koki) centrifuge at 4°C for 30 minutes. The supernatant of the lysate was transferred into a new tube. The lysate was placed on ice and served for determination of the protein concentration in the sample.

Protein concentration determination

The total protein concentration in the lysate was determined by a bicinchoninic acid (BCA) assay kit (Thermo Fisher Scientific) according to the manufacturer's instructions. In this assay, a cuprous ion Cu$^+$ becomes reduced from Cu^{++} by proteins in an alkaline medium. This cuprous ion interacts with two molecules of bicinchoninic acid (BCA) to produce a purple color. The absorption of light through this color can be measured to determine the protein concentration.

The reaction was carried out in 96-well-plate (Sarstedt, Nümbrecht, Germany). The absorbance was measured at 562 nm using the micro-plate reader; infinite M200 (TECAN). The protein concentration was calculated by comparison to known concentrations of the standard protein, bovine serum albumin (BSA). Data were analyzed using Magelan software (TECAN).

Protein denaturation

After determination of its protein concentration, the protein lysate was diluted with 5x Laemmli buffer to obtain an equal protein concentration of 1 µg/µl in all samples. 5x Laemmli buffer also included the

blue dye Bromophenol Blue (Alfa Aesar, Karlsruhe, Germany) to indicate samples on the gel. Proteins in diluted samples were denatured by boiling the mixture at 95°C for 5 min. After heating, samples were cooled and stored at -20°C until use. Through this denaturation step, proteins lose their secondary and tertiary structure. This helps proteins to be completely denatured and become separated only according to their molecular weight.

SDS-PAGE electrophoresis

Proteins were separated according to their molecular weight in an electrical field using sodium dodecyl sulfate polyacrylamide gel electrophoresis (SDS-PAGE). In the vertical Dual Gel Electrophoresis System (PEQLAB), the SDS-PAGE gel included two polyacrylamide gels: a 5 % stacking gel and a 12 % resolving gel. The stacking gel was poured over the resolving gel. Equal amounts of proteins (15 µg) were loaded into gel wells. Glycerol, which is included in Laemmli buffer, allowed protein samples to sink easily into gel wells. Either the page ruler plus prestained protein ladder (Thermo Fisher Scientific) or the pre-stained protein marker broad range (New England Biolabs) was used in a volume of 8 µl to determine the molecular weight of immunoreactive proteins. The gel was allowed to run in the presence of the electrophoresis buffer at 300 V and 25 mA/gel for 1 hour.

Semi-dry blotting

Negatively charged proteins in the gel can migrate out of the gel into a nitrocellulose membrane in a horizontal electrical field. Migrated proteins bind to the membrane that can then be used for immunodetection of proteins.

After proteins were separated by size in SDS-PAGE, proteins were transferred from the gel onto a nitrocellulose membrane (0.45 µm pore size) (GE Healthcare Europe GmbH, Freiburg, Germany) using a semi-dry electro blotter system (PEQLAB). A horizontal gel-membrane-sandwich was made as following. Firstly, the gel and the nitrocellulose membrane were soaked in transfer buffer for 10 minutes. Six sheets of filter paper 190 g/m^2 (A. Hartenstein, Würzburg, Germany) were saturated with the transfer buffer. Three sheets of these papers were placed on the anode plate of the system. The nitrocellulose membrane was placed onto these papers. Thereon, the gel was placed and covered with three filter papers. Finally, the gel-membrane-sandwich was covered with the cathode plate of the system. The electro blotting was performed at 14 Volt and 180 mA/gel for 30 minutes. After blotting, the membrane was incubated in Ponceau Red (Carl Roth) solution for 2 min. This staining was used to control the efficiency of protein transfer to the membrane. After that, the membrane was discolored by washing in water.

Immunodetection of blotted proteins

The immunological detection of proteins was performed using chemiluminescence technique. After electro blotting, the membrane was washed in dH_2O for 3 min. Non-specific binding of antibodies was prevented by incubating the membrane in the blocking solution (5 % nonfat milk powder (w/v) in PBST) at RT for one hour. After that, the membrane was incubated with a primary antibody that was diluted in 1 % blocking solution (1 % nonfat milk powder (w/v) in PBST) as described in Table 1 at 4°C overnight. Thereafter, the membrane was washed three times in 1 % blocking solution for 10 minutes each. The membrane was incubated with the HRP-conjugated secondary antibody that was diluted in 1 % blocking solution as described in Table 3 at RT for one hour. Finally, the membrane was washed in PBST twice for 10 minutes. The lumi-light substrate (Roche) was applied on the membrane for 1-5 min. The substrate was removed; signal imaging was performed using FUSION-FX7/SL Advance system (PEQLAB). The molecular weight of the immunoractive product was determined using the FUSION-CAPT software (PEQLAB).

Antibody removal

For a second detection of proteins on the same membrane, the primary and secondary antibodies were removed from the membrane. This method was used often to detect the signal of the loading control actin. After the first detection, the membrane was incubated in the dissociation buffer at 50°C for 15 min. After that, the membrane was washed twice in PBST at RT for 10 min. After antibody removal, further proteins were detected on the membrane as described above.

3.10 Immunolabeling

The localization of an antigen in a histological section was detected using a specific antibody to the antigen. Detection sites of primary antibodies were visualized indirectly using secondary fluorescence-labeled antibodies (Alexa Fluor-conjugated antibodies) (Table 3). Nuclear DNA was labeled using 4',6-diamidino-2-phenylindole, dihydrochloride staining (DAPI) to visualize all cell nuclei in the section. The experiment was carried out in the following steps:

- 10 µm thick cryosections (see Chapter 3.2.6) were fixed in absolute ethanol at -20°C for 20 min, and washed in PBS three times for 10 min. PBS was prepared as described in Chapter 3.9.
- Non-specific binding sites were blocked in blocking solution (10 % normal goat serum (NGS) (v/v), 0.1 % Triton X-100 (v/v) in PBS) at RT for one hour.

- The primary antibody was diluted in the blocking solution as described in Table 1. Sections were incubated with the diluted primary antibody at 4°C overnight.

- Thereafter, washing in PBS was performed three times at RT for 10 min to remove non-bound antibodies.

- The second step of blocking was used to prevent the non-specific binding of secondary antibodies. Blocking was performed using 0.2 % bovine serum albumin (BSA) (v/v) (MP Biomedicals, Heidelberg, Germany) diluted in PBS at RT for 30 min.

- The secondary antibody was diluted in BSA solution as described in Table 3. Sections were incubated with the diluted secondary antibody in the dark at RT for 2 hours.

- Finally, sections were washed twice in PBS for 10 min. Mounting of sections was performed using the medium DAPI-Fluoromount-G (Southern Biotechnology, Birmingham, USA) which includes the nuclear staining DAPI. After mounting, sections were dried and stored in the dark at 4°C for microscopy.

- Sections were photographed using the microscope Observer.Z1 (Carl Zeiss, Göttingen, Germany). The microscope was equipped with a fluorescent lamp, HXP 120 C (Carl Zeiss), and filter sets; 43HE for red, 38HE for green, and 49 for blue (Carl Zeiss). The photograph system was equipped with the digital camera AxioCam MRm (Carl Zeiss) and managed by AxioVision software (Carl Zeiss).

3.10.1 Whole mount immunolabeling

Whole mount immunolabeling of embryos was performed as described by De Bellard et al. (2002).

- E9.5 embryos were fixed in 4 % formaldehyde (v/v) (VWR, Darmstadt, Germany) in PBS at 4°C for 4 hours. PBS was prepared as described in Chapter 03.9.

- Embryos were washed three times in PBS for one hour each.

- Non-specific binding sites were blocked using 5 % BSA (v/v), 0.1 % H_2O_2 (v/v) (Thermo Fisher Scientific), 1 % Triton X-100 (v/v) in PBS at 4°C overnight.

- Embryos were washed in 5 % BSA (v/v) and 1 % Triton X-100 (v/v) in PBS three times for one hour each.

- Embryos were incubated with the primary antibody (Table 1) diluted in a solution of 10 % BSA, 1 % Triton X-100 in PBS at 4°C for two days.

- The second step of blocking was performed three times using 1 % NGS (v/v), and 1 % Triton X-100 (v/v) in PBS for one hour each.

- Embryos were incubated with the secondary antibody (Table 3) diluted 1:1,000 in 1 % NGS (v/v) 1 % Triton X-100 (v/v) in PBS at 4°C overnight.

- Embryos were washed three times in 1 % NGS (v/v) 1 % Triton X-100 (v/v) in PBS for one hour each.

- Embryos were photographed using a stereo microscope SZX12 (Olympus), equipped with a color camera CC-12 (Olympus), a fluorescent lamp (Olympus), and the software Cell^P imaging (Olympus).

3.11 β-Gal staining

Transgenic mice of Panx1[tg/tg] and Panx2[tg/tg] express β-galactosidase under the control of *Panx1* or *Panx2* promoter, respectively, as described in Chapter 3.2.2. In β-Gal staining, β-galactosidase activity was used to determine expression of pannexin genes indirectly. Using the substrate of 5-bromo-4-chloro-3-indolyl-b-D-galactopyranoside (X-Gal) (Carbolution Chemicals, Germany), β–galactosidase cleaves X-Gal to produce a blue staining. In this study, β-Gal staining was performed as described by Kranz et al. (2013).

Reagents for β-Gal staining

Phosphate buffer (PB) 0.1 M pH 7.4
Phosphate buffer was prepared by mixing 0.1M sodium phosphate monobasic (H_2O free) and 0.1M sodium phosphate dibasic (H_2O free), dissolved in dH_2O, at a ratio of 2:8 to reach pH 7.4.

Washing solution

Phosphate Buffer pH 7.4	0.1 M
EGTA	2 mM
Sodium deoxycholate	0.01 % (w/v)
NP-40 Alternative	0.02 % (v/v)
$MgCl_2$	2 mM
in dH_2O	

Staining solution

Potassium Ferricyanide (K3[Fe(CN6)])	5 mM
Potassium Ferrocyanide (K4[Fe(CN6)])	5 mM
X-Gal	2 mg/ml
in washing solution	

3.11.1 Whole-mount β-Gal staining

For whole-mount staining, embryos or organs were dissected in 0.1 M PB, pH 7.4, and transferred to 15 ml tubes containing 0.2 % glutardialdehyd (Merck) diluted in PB for fixation at 4°C for 2 hours. Two rinses in washing solution followed. Embryos or organs were incubated in staining solution at 37°C overnight. Post staining, samples were washed twice in PB for 10 min. Stained embryos or organs were photographed using the stereo microscope Discovery. V8 (Carl Zeiss).

Post β-Gal staining, embryos were embedded in paraffin, and paraffin blocks were cut using a microtome to observe more details of stained sites. Firstly, embryos were dehydrated using a serial of ethanol dilutions as follows: one time in 50 % ethanol (v/v) in dH_2O overnight, two times in 70 % and 90 % ethanol for 30 min each, and three times in absolute ethanol for one hour each. After dehydration, embryos were embedded in paraffin using a low-melting-point paraffin wax (44-46°C) (Sigma-Aldrich). Embryos were incubated in paraffin at 49°C with three changes of the paraffin solution; a) after one hour, b) after an overnight incubation, and c) four hours, respectively. Finally, embryos were embedded in paraffin blocks and allowed to cool overnight. Paraffin blocks were cut using the microtome HM 350 (Techno-med GmbH, Bielefeld, Germany). At section levels of interest, the paraffin block was photographed using the microscope stereo Discovery. V8 (Carl Zeiss) equipped with the camera AxioCam ERc 5s (Carl Zeiss). The photograph system was managed by the software ZEN 2011 (Carl Zeiss).

3.11.2 β-Gal staining of cryosections

Cryosections from unfixed frozen tissue were prepared at a thickness of 15 µm and mounted onto SuperFrost-slides (R. Langenbrinck). Sections were allowed to dry and circled with a flexible mounting glue, Fixogum (Marabu, Tamm, Germany), to avoid leaking of solutions during the incubation. Sections were fixed in 0.2 % glutardialdehyd diluted in 0.1 M, PB pH 7.4, at RT for 10 min, followed by two washes in washing solution. Sections were stained in staining solution at 37°C overnight. Stained sections were washed for 10 min in 0.1 M PB. The Fixogum was removed and salt crystals were cleaned up by briefly washing in 70 % ethanol (v/v) in dH_2O followed by a rehydration in dH_2O. Post β-Gal staining, sections were stained with a red nuclear counterstain named nuclear fast red (Sigma-Aldrich). Sections were incubated in the histochemical reagent of nuclear fast red at RT for 7 min following by a wash in tap water and then in dH_2O. After staining, sections were dehydrated in 70 % ethanol, 90 % ethanol and two changes in absolute ethanol for three min in each step. After dehydration, sections were treated for three changes in Roti-Histol (Carl Roth) for 3min in each. Finally, sections were

mounted in Roti-Histokitt (Carl Roth). Stained sections were scanned on the microscope Olympus BX51 TF (Olympus). This system was managed by the software slide digital virtual microscopy V 1.2 (Olympus).

3.12 Preparation and staining of paraffin sections

12-day-old mice (P12) of different strains were used to prepare paraffin sections. Trigeminal ganglia in addition to the thoracic part of the spinal cord attached to dorsal root ganglia were dissected and fixed in Bouin fixation solution (see below). Tissues were immersed in Bouin fixation solution and stored at RT until using. Paraffin infiltration was achieved post fixation using a robust carousel tissue processor; mtp (SLEE, Mainz, Germany). Tissues were dehydrated using a graded series of isopropanol, followed by washing steps in methyl benzoate to remove alcohol and water residues. Finally, tissues were infiltrated with a paraffin wax its melting point is 55-57 °C; Roti®-Plast (Carl Roth).

Infiltration of paraffin was performed as follows:

Isopropanol 70 % (v/v)	60 min
Isopropanol 80 % (v/v)	90 min
Isopropanol 90 % (v/v)	90 min
Isopropanol 100 %	90 min
Isopropanol 100 %	90 min
Methyl benzoate	90 min
Methyl benzoate	90 min
Methyl benzoate	90 min
Paraffin at 65°C	120 min
Paraffin at 65°C	120 min

After paraffin infiltration, samples were embedded in paraffin blocks using the embedding center of MPS/P1 and MPS/C (SLEE). Embedded samples were allowed to cool at RT until use. Paraffin sections were cut in a thickness of 6 µm using the historange microtome 2218 (LKB Bromma, Sollentuna, Sweden) which was equipped with a glass knives C335 (Plano, Wetzlar, Germany). Sections were collected on SuperFrost-Slides (R. Langenbrinck), dried at 37°C, and stored at RT until use.

Bouin fixation solution
Bouin fixation solution was prepared by mixing 1.2 % picric acid solution (v/v) (AppliChem) with 37 % formaldehyde (v/v) (VWR) in a ratio of 3:1. Prior to use, the mixture was supplemented with 5 % (v/v) of acetic acid (VWR).

3.12.1 Masson Goldner trichrome staining

The morphology of spinal cord was illustrated using Masson Goldner Trichrome staining. The staining works with three different stains, Goldner`s stain I, II and III, which allow a differentiated visualization of tissue. In this staining, nuclei stain dark brown, cytoplasm and muscle fibers stain red, and connective tissue stain green. Paraffin sections were firstly deparaffinized in three changes of Roti-Histol (Carl Roth) for three min each. After deparaffinization, sections were rehydrated using a graded series of ethanol, diluted in dH$_2$O, as follows:

Absolute ethanol	3 min
Absolute ethanol	3 min
90 % ethanol (v/v)	3 min
70 % ethanol (v/v)	3 min
dH$_2$O	3 min

The staining was carried out using Masson Goldner Trichrome staining kit (Carl Roth) according to the manufacturer's instructions. Staining procedures were adapted to experimental conditions. After rehydration, nuclei were stained with iron hematoxylin solution according to Weigert for 5 min. Thereafter, sections were blued in flowing tap water for 10 min. Goldner's stain I was applied for 5 min followed by washing in 1 % acetic acid (v/v) in dH$_2$O for 30 seconds. Sections were stained with Goldner's stain II until decolouration of connective tissue for 7 min followed by washing in 1 % acetic acid for 30 seconds. Counterstaining was performed using Goldner's stain III for 10 min, which was followed by washing in 1 % acetic acid for 2 min. Finally, sections were dehydrated directly in absolute ethanol three times for 3 min each, followed by clearing for three changes in Roti-Histol (Carl Roth) for three min each. Sections were mounted in Roti-Histokitt (Carl Roth) and covered with coverslips (R. Langenbrinck).

3.13 Histological image analysis

Images of histological sections were analyzed using the software ZEN 2011 (Carl Zeiss). Measurements were performed in the unit of pixels and results were converted into the unit of millimeters. Converting of pixel into millimeter was calculated using a formula which was obtained from the imaging program for each image. The measurement of areas was obtained by outlining the region of interest using tools for the contour outline. Cell counting was used to estimate the cell density and the cell ratio in a definite area.

3.14   Statistical analysis

Data of groups (n=3 per group) were presented as mean ± standard error of mean (SEM). Firstly, a normality test was performed for all data using Kolmogorov-Smirnov test. Normally distributed data were analyzed using one-way ANOVA test followed by a Bonferroni post-hoc test to compare means. Nonnormally distributed data were analyzed using Kruskal-Wallis test followed by Dunn's post test to compare means. The Mann-Whitney U test was used to compare differences between two independent groups. Statistical significance was set at the 95 % confidence level ($p < 0.05$). Results were considered statistically significant for *$p < 0.05$, **$p < 0.01$, and ***$p < 0.001$. Analyses were performed using the Prism 5 software (GraphPad Software, San Diego, USA). $SEM = S / \sqrt{n}$ (SEM: standard error of the mean, S: sample standard deviation, n: number of samples).

4 Results

4.1 Temporal expression of pannexin mRNA in mouse development

A qualitative gene expression analysis was performed using reverse transcription polymerase chain reaction (RT-PCR) to determine whether pannexins are expressed in early stages of mouse development. Embryos were prepared as described in Chapter 3.2.6. Six embryos of E9.5 were pooled and RNA was isolated from whole embryos. Embryos of E10.5, E11.5 and E12.5 (four, three and one embryo(s), respectively) were analyzed in samples of heads and bodies separately. The total RNA was isolated and transcribed into cDNA. cDNA synthesis was controlled using negative controls without reverse transcriptase (NR) from each sample in addition to a negative control without template (NT). Resulting cDNA samples and negative control samples were used as template for the amplification of target genes Panx1 and Panx2 and the reference gene 18S rRNA using the polymerase chain reaction (PCR).
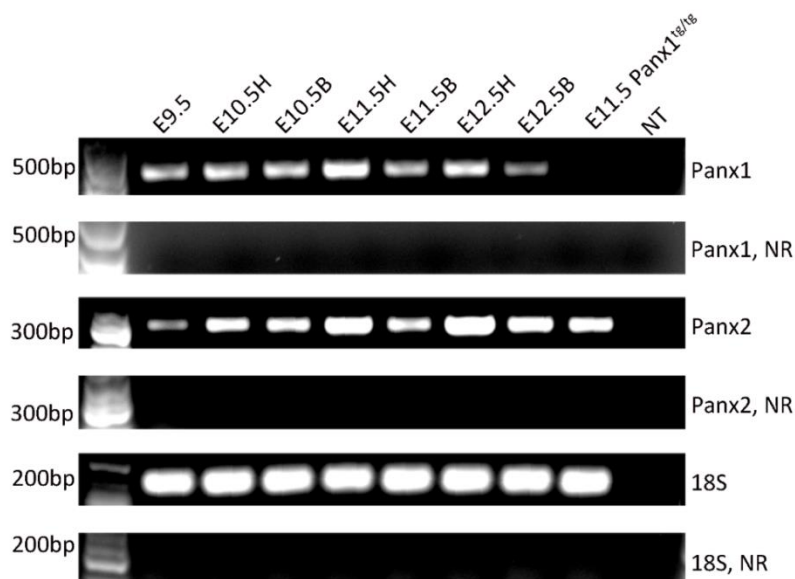

Figure 18. Panx1 and Panx2 mRNA expression in mouse development
Expression of Panx1 and Panx2 mRNAs was detectable in all investigated stages i.e. in E9.5 embryos as well as in heads and bodies of E10.5, E11.5 and E12.5 embryos. The transgenic embryo E11.5 Panx1[tg/tg] did not show any expression of Panx1 whereas it showed Panx2 expression. Negative controls without template (NT) or without reverse transcriptase (Panx1 NR, Panx2 NR and 18S NR) did not show any expression product for any primers. The reference gene 18S rRNA served as a loading control of equal cDNA template. Amplified products of Panx1, Panx2 and 18S were 500 bp, 300 bp and 200 bp in size, respectively.

In this experiment, the temporal expression of Panx1 and Panx2 was investigated in four early embryonic stages (E9.5, E10.5, E11.5 and E12.5). mRNA expression of Panx1 and Panx2 was detectable in all analyzed embryonic stages, in whole-mount of E9.5 as well as in heads and bodies of E10.5, E11.5 and E12.5 (Figure 18). To determine the spatial distribution of mRNA expression, the three stages E9.5, E10.5 and E11.5 were investigated using the whole-mount *in situ* hybridization technique.

4.2 Designing cRNA probes for *in situ* hybridization

Whole-mount *in situ* hybridization provides information about the temporal and spatial distribution of gene expression and was applied during embryogenesis for a better understanding of their function during development. The technique is based on the complementary hybridization of a digoxigenin-labeled cRNA probe with the target mRNA in whole embryos and detection of the cRNA probe using antibodies conjugated with a reporter enzyme of alkaline phosphatase (AP). Detection can be made visible using a NBT/BCIP substrate, which reacts in the presence of AP to produce a purple staining at sites of hybridization. Usually, the best results for *in situ* hybridization can be obtained using cRNA probes of 50-300 bp in length (Piette et al., 2008). As the full-length probe generated for Panx1 (full-length) has ~1280 bp length, an additional shorter DNA fragment of 433 bp length was generated. This short DNA fragment was called Panx1 Ct. Thus, five types of cRNA probes were used: antisense Panx1 (full-length), antisense Panx1 Ct (short-length), and antisense mMyoD (served as positive control) in addition to negative controls of sense Panx1 (full-length) and sense Panx1 Ct (short-length).

4.2.1 Cloning of DNA template for the *in vitro* transcription

Specific DNA fragments of Panx1 were inserted into vectors for *in vitro* transcription of cRNA probes. Firstly, the short DNA fragment of Panx1 Ct 443 bp (1231-1673 of the sequence NM_019482.2) corresponding to the carboxy-terminus of Panx1 was PCR-amplified and analyzed by agarose gel electrophoresis (Figure 19). Panx1 Ct (short-length) fragment was inserted subsequently into the plasmid pSPT19 (Figure 20).
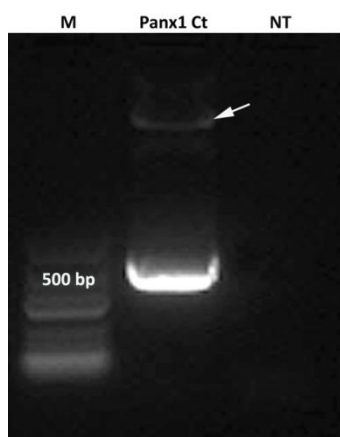
Figure 19. PCR amplification of Panx1 Ct fragment

Agarose gel electrophoresis analysis of Panx1 Ct amplification. The amplified product of Panx1 Ct was 500 in size. The DNA template of pEYFP-N1-mPanx1 was very lightly present at the top of the gel (arrow). No product was present in the negative control without the template (NT). Low range DNA ladder (M).

As mentioned above, it was required to transfer the Panx1 full-length fragment from the plasmid pEYFP-N1-mPanx1 into appropriate plasmids of pSPT18 and pSPT19, which are available for *in vitro* transcription (see Chapter 3.5.2). Recombinant plasmids pSPT18 Panx1, pSPT19 Panx1 and pSPT19 Panx1 Ct were tested by restriction enzyme analysis to identify the correct insert according to the molecular weight of DNA insert (Figure 20). DNA fragments of interest were detected at ~1500 bp for Panx1 (full-length) and at 500 bp for Panx1 CT. Uncut plasmids of pSPT19 Panx1 and pSPT19 Panx1 Ct showed the supercoiled form. On the other hand, the plasmid of pSPT18 Panx1 showed two bands of linear and opencircular forms. After agarose gel analysis, DNA fragments of interest were analyzed by sequencing. Results confirmed the sequence of Mus musculus pannexin 1 (Panx1), NM_019482.2 (see Chapter 3.5.43.5.4).
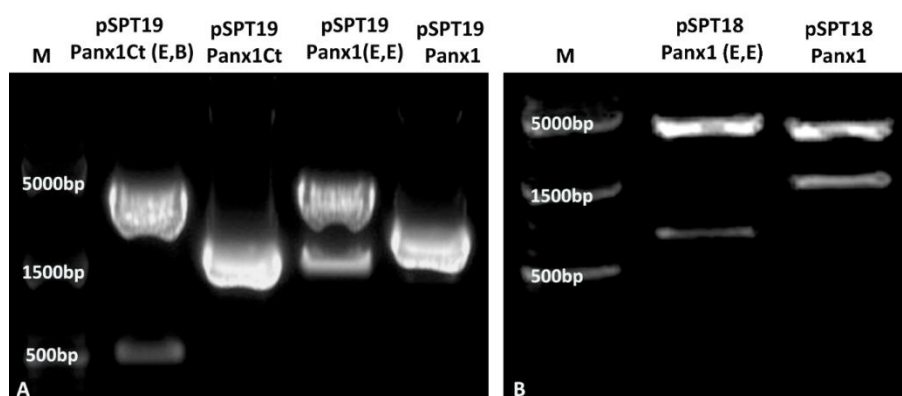

Figure 20. Restriction enzyme analysis of recombinant plasmids

(A) The recombinant plasmid pSPT19 Panx1 Ct was digested with two restriction enzymes EcoRI (E) and BamHI (B) (pSPT19 Panx1 Ct (E,B)). The insert of Panx1 Ct (short-length) appeared at 500 bp. The recombinant plasmid pSPT19 Panx1 was digested with EcoRI (pSPT19 Panx1 (E,E)) and showed the insert of Panx1 (full-length) at ~1500 bp. These recombinant plasmids (pSPT19 Panx1 Ct and pSPT19 Panx1) showed the supercoiled form of uncut plasmids at 1500 bp. (B) The recombinant plasmid pSPT18 Panx1 was digested with EcoRI (pSPT18 Panx1 (E,E)) and showed the insert of Panx1 (full-length) at ~1200 bp. pSPT18 Panx1 without digestion showed two bands of linear and opencircular forms. Broad range DNA ladder (M).

4.2.2   Probe synthesis of DIG-labeled cRNA

DIG-labeled cRNA probes were synthesized using the *in vitro* transcription processes in the presence of RNA polymerases (SP6 or T7). Northern blot analysis was used to evaluate the quality of cRNA probes, compared to a known probe of MyoD (Figure 21). cRNA was present in all samples on agarose gel electrophoresis. In both Panx1 and Panx1 Ct probes, probes equal in length (sense and antisense) appeared at the same level.
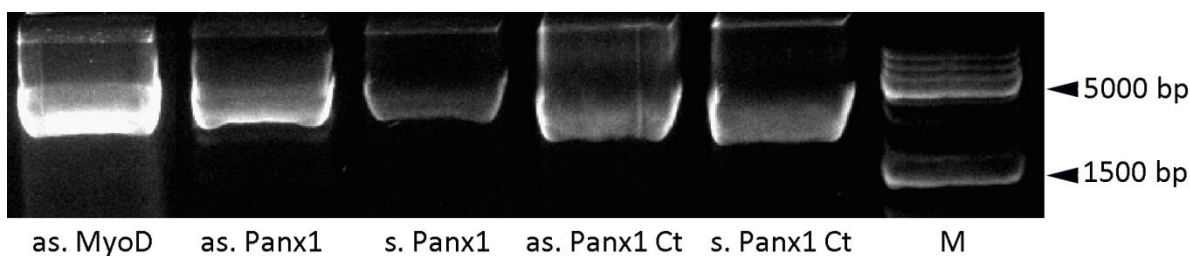

Figure 21. Northern blot analysis of DIG labeled cRNA probes
Antisense MyoD probe was used to control the quality of Panx1 (full-length) and Panx1 Ct (short-length) cRNA probes. All cRNA probes were detected on the gel. Sense (s.) and antisense (as.) probes of Panx1 or Panx1 Ct, respectively, are equal in length. Panx1 Ct probes (443 bases) appeared lower than Panx1 probes (~1200 bases). However, DIG labeled probes did not appear at predicted sizes, as DIG retards the migration of labeled probes on the gel.

4.3   Spatial distribution of Panx1 mRNA in the mouse embryo

To date, there are a limited number of studies describing the expression pattern of pannexin family members in early stages of mouse development. In this study, the distribution of Panx1 mRNA expression was investigated using whole-mount *in situ* hybridization in early developmental stages (E9.5, E10.5 and E11.5). In all experimental steps, the antisense MyoD probe was used as positive control to check the quality of cRNA probes and to determine the optimal conditions for the *in situ* hybridization. MyoD is a myogenic regulatory factor, which is required for the formation of skeletal muscle in vertebrates (Rudnicki et al., 1993, Ishibashi et al., 2005). Normally, E9.5-E9.75 are the earliest

stages to observe MyoD expression by *in situ* hybridization in mouse embryos (Chen and Goldhamer, 2004). In this study, MyoD expression was observed from E10.5 onwards, there was no staining visible in E9.5 embryos. In E10.5 embryos, MyoD hybridization resulted in a clear staining of interlimb somites (Figure 22). The expression level increased at E11.5 and appeared in several regions. It appeared as strongly stained parallel lines in interlimb somites and occipito-cervical somites. Further regions were also stained at this stage, i.e. in branchial arches, forelimb buds, hindlimb buds, and caudal somites. These expression sites were always observed by detecting of MyoD, which was used as a positive control in all *in situ* hybridization experiments.

As mentioned above, two cRNA probes were used for the determination of Panx1 mRNA expression *in situ*: antisense Panx1 (full-length) and antisense Panx1 Ct (short-length), in addition to two sense cRNA probes as negative controls. In all studied stages, samples hybridized with antisense Panx1 Ct (short-length) exhibited a more intense purple staining in several regions (Figure 22), which was in contrast to samples hybridized with antisense Panx1 (full-length), which showed a very light purple staining in restricted regions (e.g. ventricle walls) (Figure 23). In negative controls of both sense cRNA probes, no staining was observed.

Panx1 Ct (short-length) showed the expression in all studied stages in both head and body (Figure 22), thereby confirming that confirms RT-PCR results (see Chapter 4.1). On the other hand, Panx1 (full-length) probe did not detect any expression in the trunk, but only in the restricted regions of brain vesicles. At E9.5, the expression was detected lightly in the walls of forebrain, midbrain, and hindbrain vesicles, whereas at E10.5 and E11.5, the staining was observed only in the wall of telencephalic vesicle (Figure 23). Therefore, Panx1 mRNA expression pattern was determined in this project using the Panx1 Ct (short-length) probe. The specificity of this probe was confirmed in negative controls using sense Panx1 Ct probe, which did not show any staining (Figure 22).
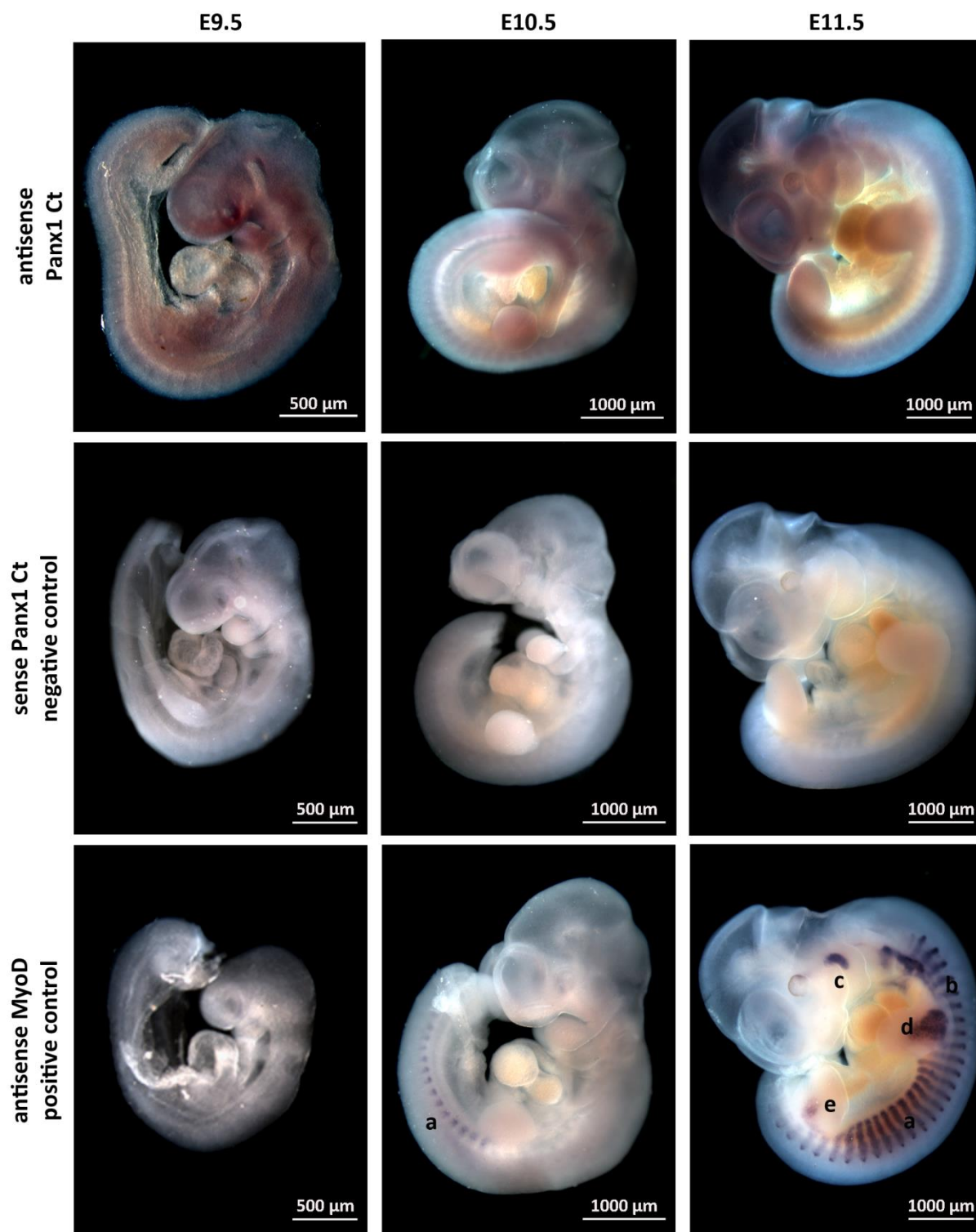
Figure 22. Overview of whole-mount *in situ* hybridization experiment
Lateral views of studied stages E9.5, E10.5 and E11.5 hybridized with antisense Panx1 Ct, sense Panx1 Ct (negative control), and antisense MyoD (positive control). Embryos hybridized with antisense Panx1 Ct show the purple staining in all studied stages. No staining is present in the negative control using sense Panx1 Ct probe. Antisense MyoD probe shows the specific expression at E10.5 and E11.5 in interlimb somites (a), occipito-cervical and truncal somites (b), branchial arches (c), in forelimb buds (d), and in hindlimb buds (e). No MyoD expression was detected at E9.5.
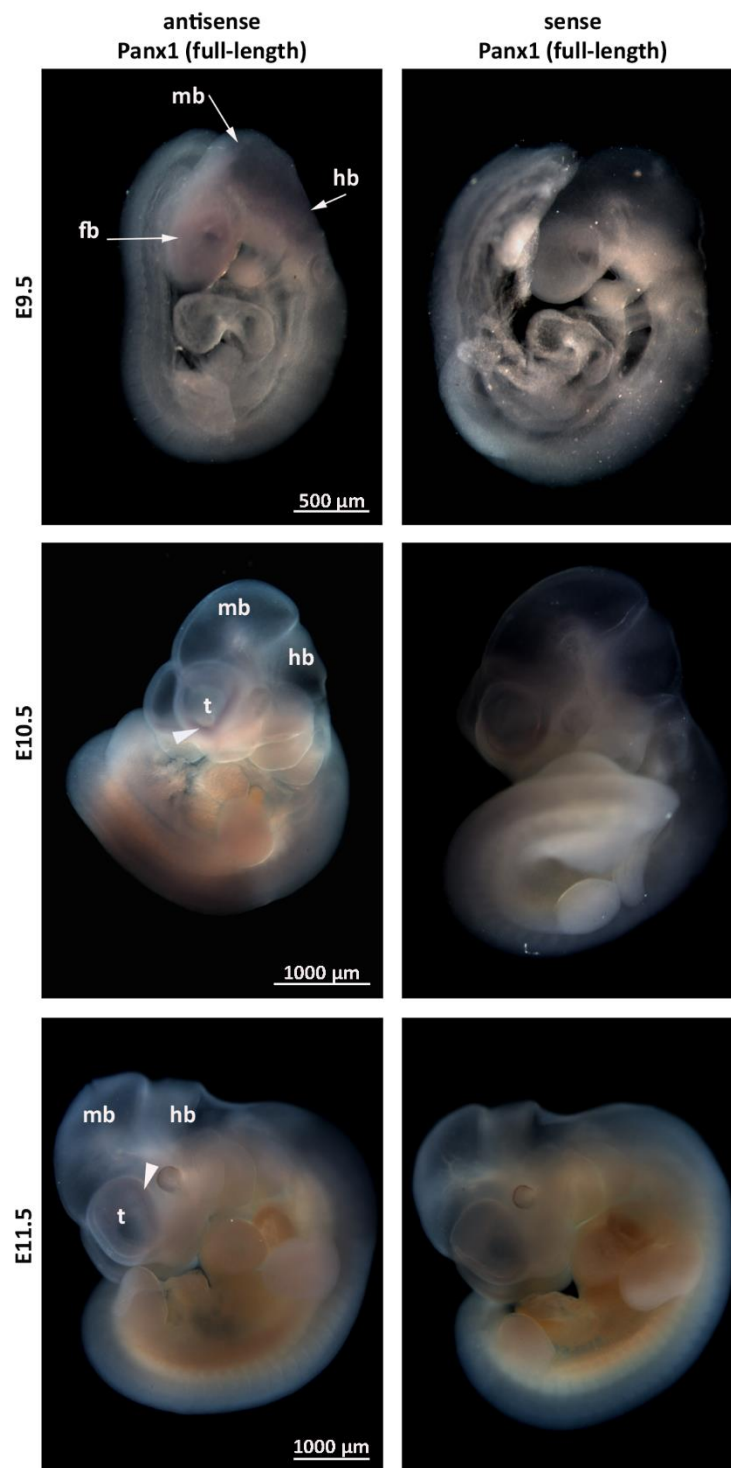
Figure 23. Overview of whole-mount *in situ* hybridization using Panx1 (full-length) cRNA
Samples hybridized with antisense Panx1 (full-length) probe exhibited a very light purple staining in the head of E9.5, E10.5 and E11.5 embryos, no staining was observed in the body at these stages. At E9.5, Panx1 was detected in the wall of brain vesicles; in forebrain (fb), midbrain (mb), and hindbrain (hb). At E10.5 and E11.5, the staining was restricted to the wall of telencephalic vesicle (t) (arrowhead). No staining was detectable in the negative control using sense Panx1 (full-length) probe (right panel).

4.3.1 Panx1 mRNA expression at E9.5

For a better attribution of Panx1 expression sites at E9.5 to structures of the nervous system, whole-mount immunolabeling was performed using the neuronal marker neuronal class III β-tubulin (monoclonal antibody Tuj1) to identify the localization of nervous system regions in this stage (Figure 24). Panx1 mRNA expression at E9.5 was determined using antisense Panx1 Ct (short-length) and expression sites were observed in both head and body of the embryo (Figure 24). In cephalic regions, the wall of forebrain and the basal plate of the mesencephalic vesicle were Panx1-positive. In the maxillary region, the area of trigeminal ganglion tissue (V) was Panx1-positive. This signal appears dorsal of the first branchial arch. Likewise, the facio-acoustic ganglion complex (VII-VIII) exhibited the purple staining on the dorsal region of the second branchial arch. The otic pit, which appears on the caudal part of hindbrain vesicle, showed a less intense Panx1 expression signal. Panx1 expression was also observed in the first branchial arch. In the body, the occipito-cervical and truncal region of neural tube appeared to be Panx1-positive, as well as the forelimb buds.
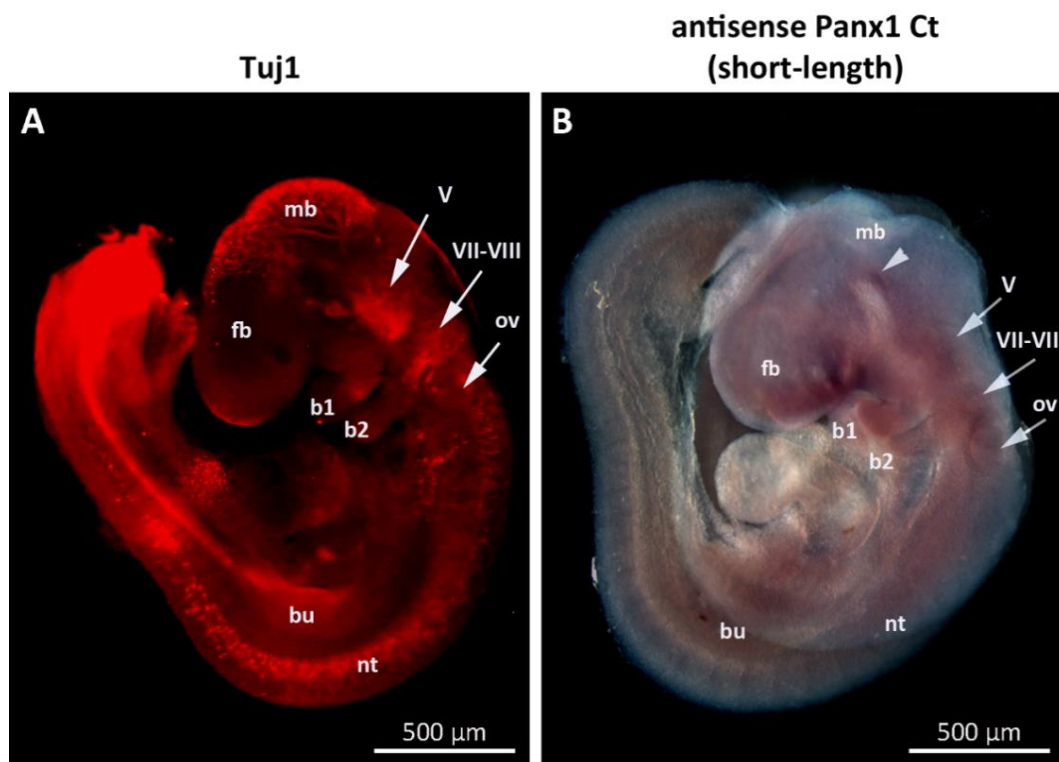

Figure 24. Panx1 mRNA expression in E9.5 embryo
(A) Whole-mount immunolabeling of the neuronal marker β-III-tubulin in an E9.5 embryo used to present nervous system structures at this developmental stage. (B) Lateral view of mouse embryo E9.5 shows Panx1 mRNA expression sites using DIG-labeled probes of antisense Panx1 Ct (short-length). Expression sites included telencephalic vesicle wall, basal plate of the mesencephalic vesicle (arrowhead), trigeminal ganglion (V), facio-acoustic (VII-VIII) ganglion complex, otic vesicle (ov), neural tube (nt), forelimb bud (bu), and the first branchial arch (b1), but not the second branchial arch (b2).

4.3.2 Panx1 mRNA expression at E10.5

The E10.5 embryo shows an obvious differentiation in the cephalic region. The primitive forebrain (prosencephalon) becomes subdivided into the telencephalon, which will later form cerebral hemispheres, and the diencephalon, which will form thalamic and hypothalamic regions of the brain (Rao and Jacobson, 2005). The two telencephalic vesicles appear anterior on either side of the third ventricle. Panx1 expression was observed in the wall of the two telencephalic vesicles (Figure 25). In the midbrain region, the mesencephalic basal plate and the vesicle wall show a noticeable Panx1 expression in lateral and dorsal view, respectively.
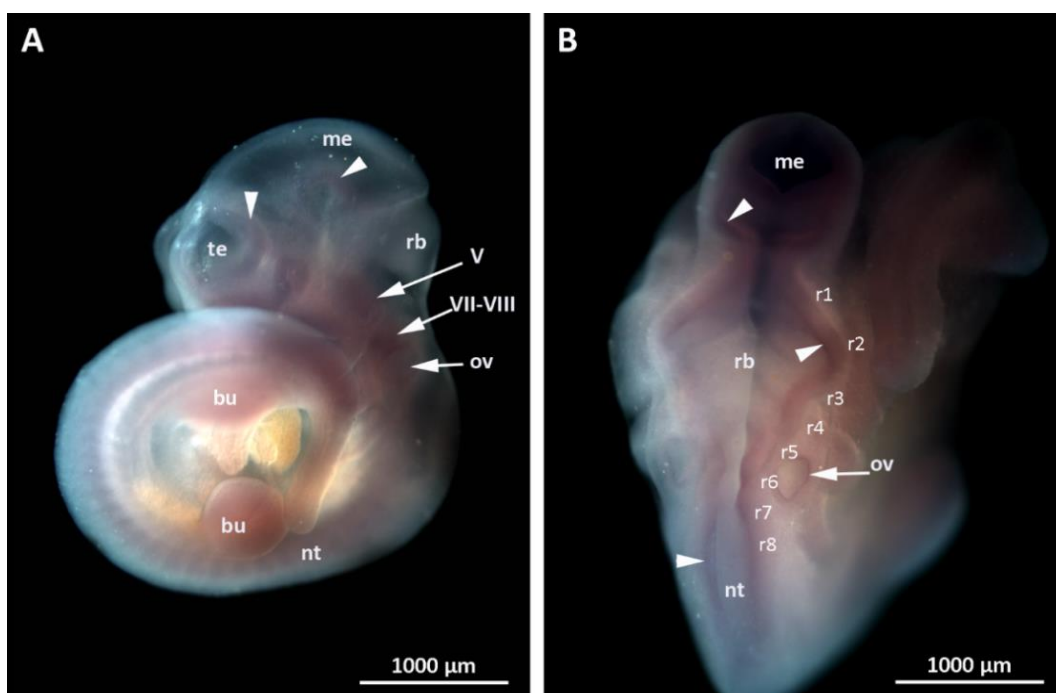

Figure 25. Panx1 mRNA expression in E10.5 embryo
(A) Lateral view *of* an E10.5 embryo showing Panx1 expression (arrowheads), in the telencephalic vesicle (te) and in the basal plate of the mesencephalic vesicle (me). More intense labeling appeared in the trigeminal ganglion (V), facio-acoustic ganglion complex (VII-VIII), and otic vesicle (ov). Panx1 is also present in neural tube (nt) and fore-/hindlimb buds (bu). (B) Dorsal view of E10.5 showing Panx1 expression (arrowhead) in the mesencephalic vesicle wall (me), the rhombencephalic vesicle wall (rb), and in the neural ridge of neural tube (nt) in the occipito-cervical region. Rhombomeres (r1–r8) were numbered as described by Cordes (2001).

At this stage of development, the hindbrain is subdivided into eight segments called rhombomeres (r1-r8) (Cordes, 2001). Panx1 exhibited a homogenous staining in all rhombomere segments (r1–r8). Some cranial ganglia in particular the trigeminal ganglion and the facio-acoustic ganglion complex exhibited a higher expression level than other cephalic regions. At this stage, the facial ganglion (VII) can hardly

be distinguished from the acoustic component (VIII) in the facio-acoustic ganglion complex. However, it appears that the whole complex, and thereby both ganglia, are Panx1-positive. Further expression sites were observed in the otic vesicle, forelimb and hindlimb buds. In the neural tube, the expression is clearly present in the truncal region. Expression was also observed in the neural ridge of the occipito-cervical region (Figure 25).

4.3.3   Panx1 mRNA expression at E11.5

Many morphological changes are observable in E11.5 embryos: the telencephalic vesicles increases dramatically in volume, and the lens vesicle becomes differentiated and separated from the ectoderm. The three branchial arches show an increasing volume, and the forelimb becomes subdivided into proximal and distal regions. Best results of whole-mount *in situ* hybridization were observed at this stage; the purple staining was more clearly visible than in previous stages (Figure 26).

The observed Panx1 signal in the walls of telencephalic vesicles (Figure 26, A and B), as well as in the alar plate of the mesencephalon (Figure 26 B) was more intense than at earlier stages. The mesencephalon showed fewer changes than other regions of the brain during development, it does not become subdivided into more parts and gives later rise to the midbrain, which connects the hindbrain (pons and cerebellum) with the forebrain (cerebral hemispheres, thalamic and hypothalamic regions). Panx1 expression was clearly visible also in the mesencephalic basal plate (tegmentum) (Figure 27 A). Interestingly, motor neurons of the oculomotor cranial nerve (III) develop from the mesencephalic basal plate between E10 and E12 (Wurst and Bally-Cuif, 2001). The developed oculomotor nucleus (III) keeps the localization in the midbrain (Guthrie, 2007).

The rhombencephalon is located posterior to the mesencephalon, which becomes subdivided into anterior region named the metencephalon (it gives rise to cerebellum), and posterior region is the myelencephalon (it will form the medulla oblongata). The basal plate of the metencephalon, which gives rise to motor neurons of the trochlear nucleus (IV) (Wurst and Bally-Cuif, 2001), exhibited Panx1 mRNA expression (Figure 27, A). Panx1 expression was also observed at this stage on the whole lip of rhombencephalon as well as in the roof plate of fourth ventricle (ventricular zone) (Figure 26 C). Some cranial ganglia, the trigeminal ganglion (V) and the facio-acoustic ganglion complex (VII-VIII), exhibited very clearly Panx1 expression. At this stage, it is possible to distinguish the acoustic ganglion component (VIII) from the facial ganglion (VII) (Figure 27, A). The otic vesicle is still located caudal to the facio-acoustic ganglion complex and Panx1 expression was detected in the wall of the vesicle

(Figure 27, A) as well as the maxillary component of first branchial arch. Spinal cord displays a continuous Panx1 expression signal in all spinal cord segments (Figure 27 B).
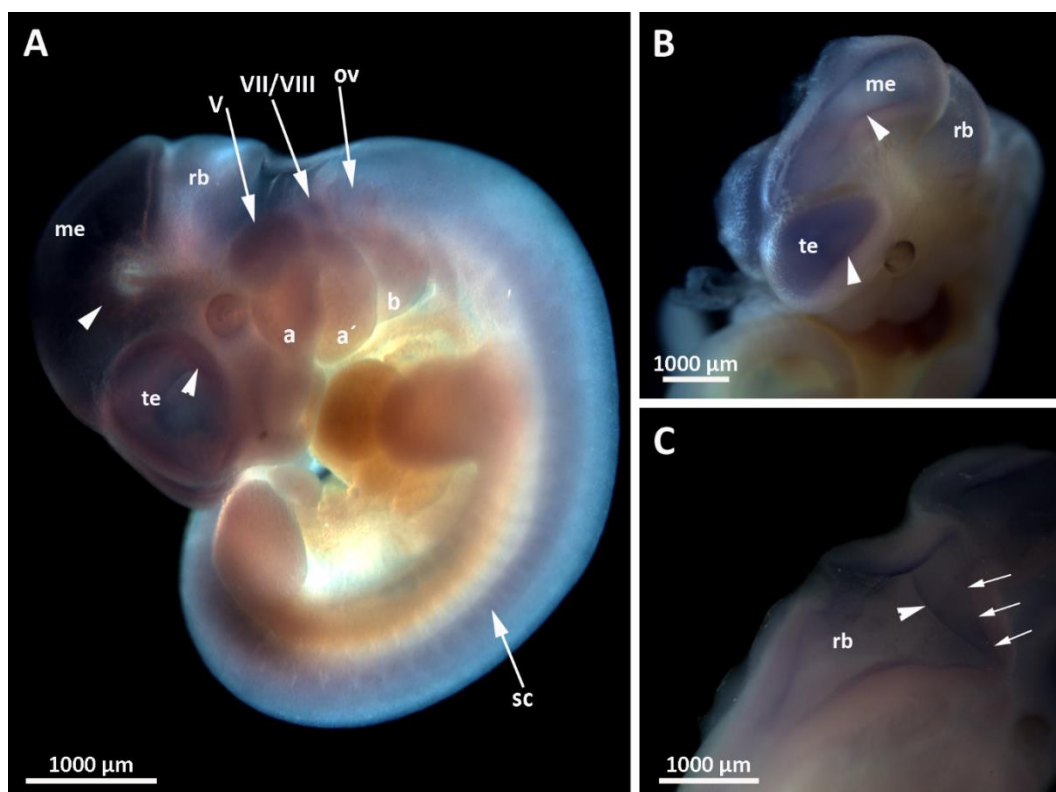

Figure 26. Panx1 mRNA expression in E11.5 embryo
Different views of E11.5 mouse embryos show Panx1 mRNA expression sites using DIG-labeled probes of antisense Panx1 Ct (short-length). (A) Lateral view shows expression sites (arrowheads) in the telencephalic vesicle wall (te) and the basal plate of the mesencephalic vesicle (me). Other expression sites were observed in trigeminal ganglion (V), facio-acoustic (VII/VIII) ganglion complex, otic vesicle (ov), spinal cord (sc) as well as in DRGs (not labeled). (B) Top view of cephalic region shows expression sites (arrowheads) at the wall of telencephalon vesicles (te) and the alar plate of the mesencephalon (me). (C) Posterior view of the cephalic region represents expression sites at the whole lip of rhombencephalon region (rb) (arrowhead) and in the ventricular layer of the fourth ventricle (arrows). (a) the maxillary component of first branchial arch, (a') mandibular component of the first branchial arch, (b) the second branchial arch.

Whole-mount *in situ* hybridization revealed that Panx1 is expressed mainly in the nervous system in all studied stages. To confirm the results obtained from whole-mount *in situ* hybridization and to reveal more details about the expression, vibratome sectioning was performed on embryos after the whole-mount *in situ* hybridization procedure.
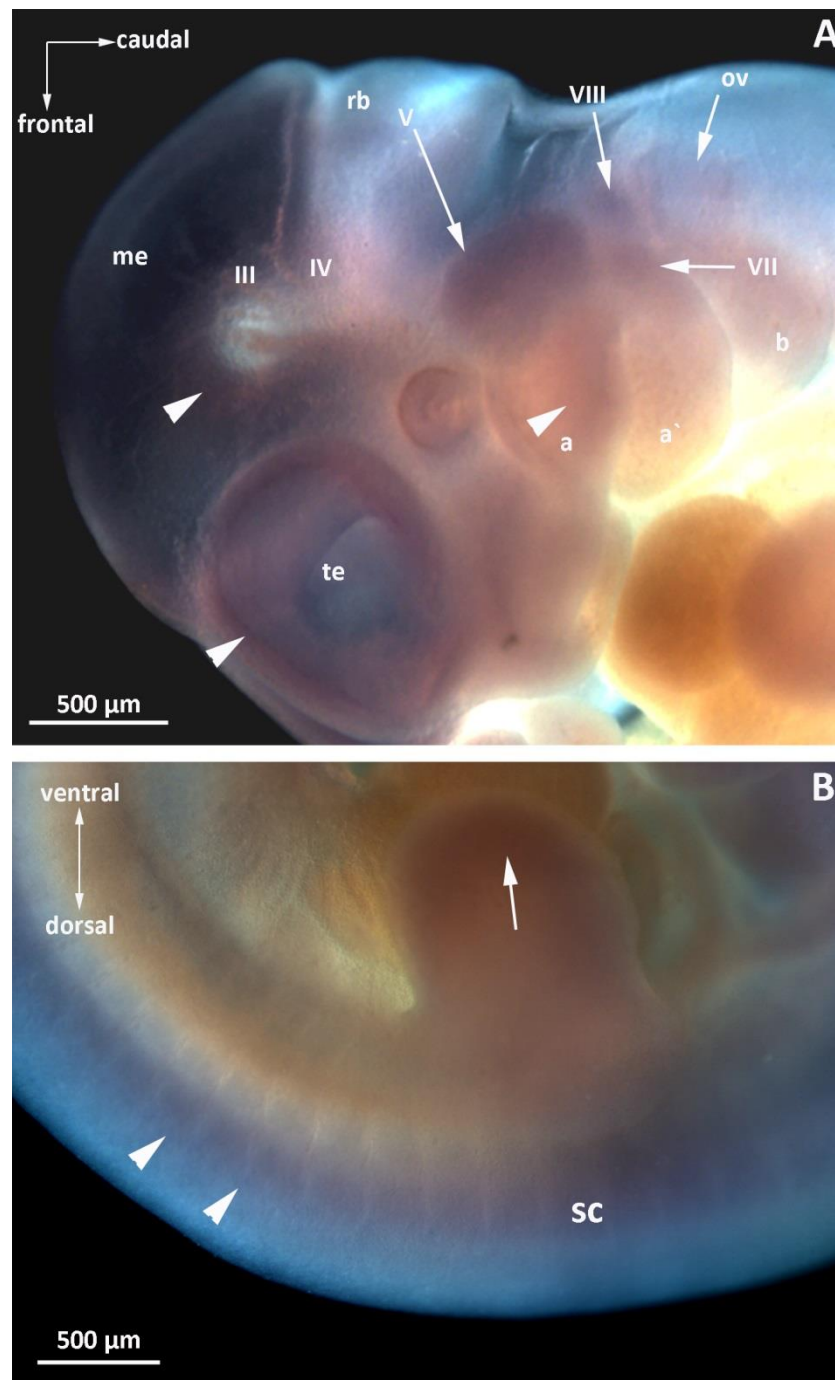
Figure 27. Panx1 mRNA expression in the head and the body of an E11.5 embryo
High magnification views of the head and the truncal part of spinal cord hybridized with the antisense Panx1 Ct (short-length) probe (whole-mount *in situ* hybridization). (A) Panx1 expression (arrowheads) was observed in the walls of telencephalic vesicles (te) and in the basal plate of mesencephalon (me). Characters III and IV indicate the origin of oculomotor and trochlear cranial nerves from the basal plate, respectively. Panx1 expression was clearly present in cranial ganglia, i.e. in trigeminal ganglion (V), facial ganglion (VII), and acoustic ganglion component (VIII). The wall of the otic vesicle (ov) exhibited also Panx1 expression as well as the maxillary component of the first branchial arch (a). (B) Panx1 expression was also detectable in all spinal cord segments (sc) (arrowheads) and in the apical region of the forelimb plate (arrow). (a') points to the mandibular component of the first branchial arch, (b) the second branchial arch, (rb) rhombencephalon.

4.3.4 Vibratome sectioning post WM-ISH

Embryos from E11.5 revealed best results by whole-mount *in situ* hybridization analysis as compared to other early stages of embryonic development. The purple staining was more abundant at this stage. Therefore, vibratome sectioning of E11.5 embryos was performed after the whole-mount *in situ* hybridization to obtain more details of expression sites. Hybridized embryos with antisense Panx1 Ct probe were sectioned and compared to the negative control of embryos hybridized with sense Panx1 Ct probe.

In a transversal section of the head region, the purple staining was observed only on the inner side of telencephalic vesicle wall (apical surface) (Figure 28). The embryonic cortex at this stage consists of two components, the ventricular zone (VZ) at the apical surface and the subventricular zone (SVZ) at the basal side. The VZ is made up of progenitor cells, which divide constantly at the apical surface; some cells exit the cell cycle and migrate into the SVZ (Dehay and Kennedy, 2007). This suggests that Panx1 is expressed in progenitor cells of VZ at this stage.

Another region of the section, the trigeminal ganglion, showed a clear staining in the whole tissue of the ganglion (Figure 28). The facial ganglion (VII) and acoustic ganglion component (VIII) were also Panx1-positive. These two ganglia were separated from each other and located ventral to the otic vesicle. An additional expression site was observed in the inferior ganglion of vagus nerve (not shown). This ganglion was invisible in whole-mount samples.

The inner side of the otic vesicle wall showed a hybridization signal in form of a dark line of purple staining. Moreover, a very light staining was observed in a section of the maxillary component of the first branchial arch, which develops to form later the face including the upper jaw. No staining was observed at any of these described sites in the sense negative control (Figure 28).

By whole-mount *in situ* hybridization, Panx1 expression was observed in the whole lip of rhombencephalon. This expression site was confirmed in a transversal section at the caudal level of the rhombencephalon. Panx1 expression was observed in the alar plate of the cranial myelencephalic part. A transversal section at the truncal level of the spinal cord showed a very light staining in the mantle layer of the developing spinal cord and in dorsal root ganglia (DRGs). The expression in DRGs was also observed in a sagittal section of tail region (Figure 29 F).
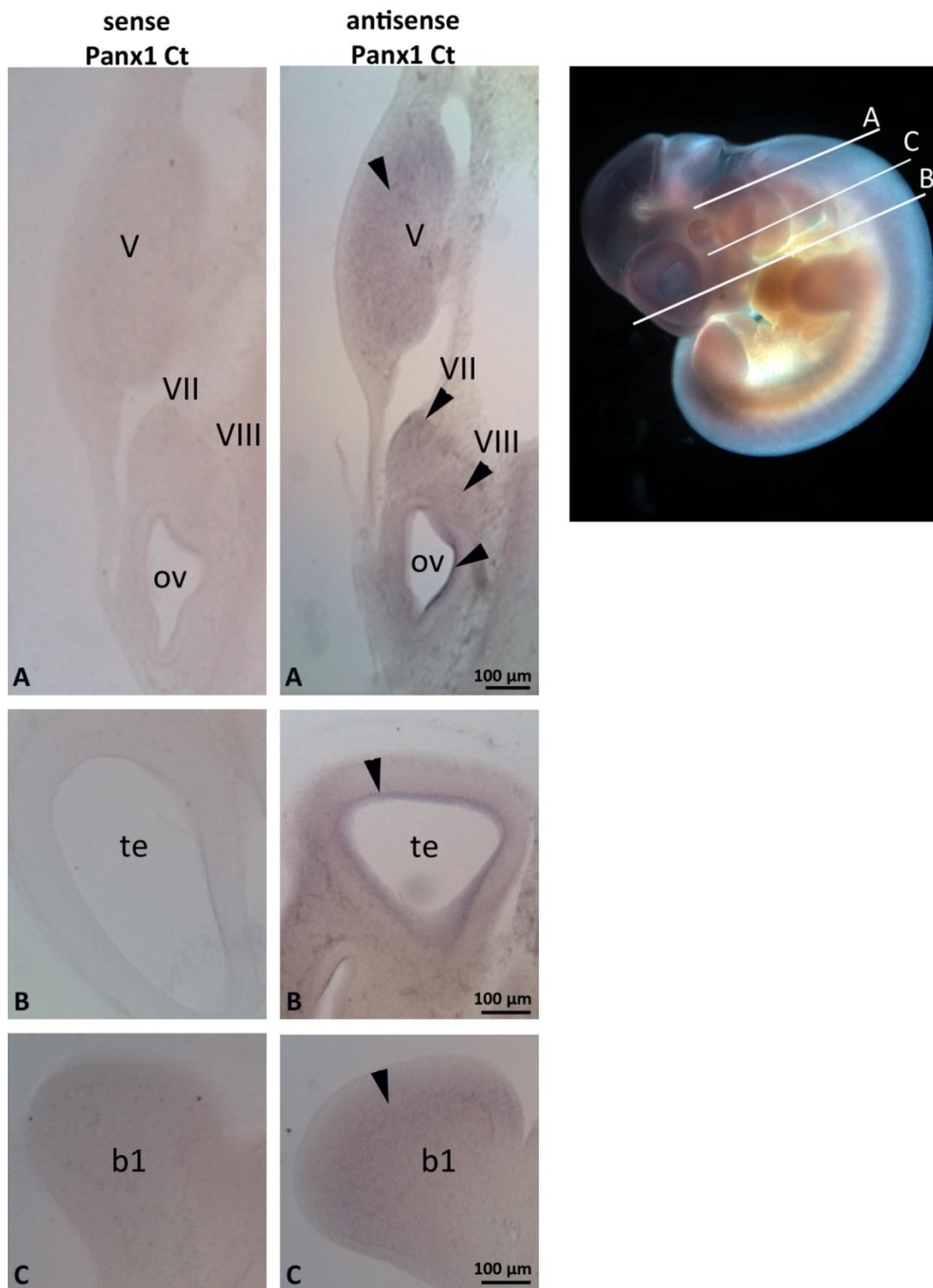
Figure 28. Cephalic transverse vibratome sections of an E11.5 embryo
Vibratome sections of an E11.5 embryo post whole-mount *in situ* hybridization. Section levels (A, B and C) are shown on the right. The middle column shows expression sites, which were observed using antisense Panx1 Ct (short-length). The left column shows the negative control of each region using sense Panx1 CT. (A) Panx1 expression (arrowheads) was observed in trigeminal ganglion (V), facial ganglion (VII), acoustic ganglion component (VIII), and in the wall of the otic vesicle (ov). (B) The wall of the telencephalon vesicle (te) exhibited also Panx1 expression (arrowhead). (**C**) The first branchial arch (b1) showed Panx1 expression (arrowhead) in the apical part.
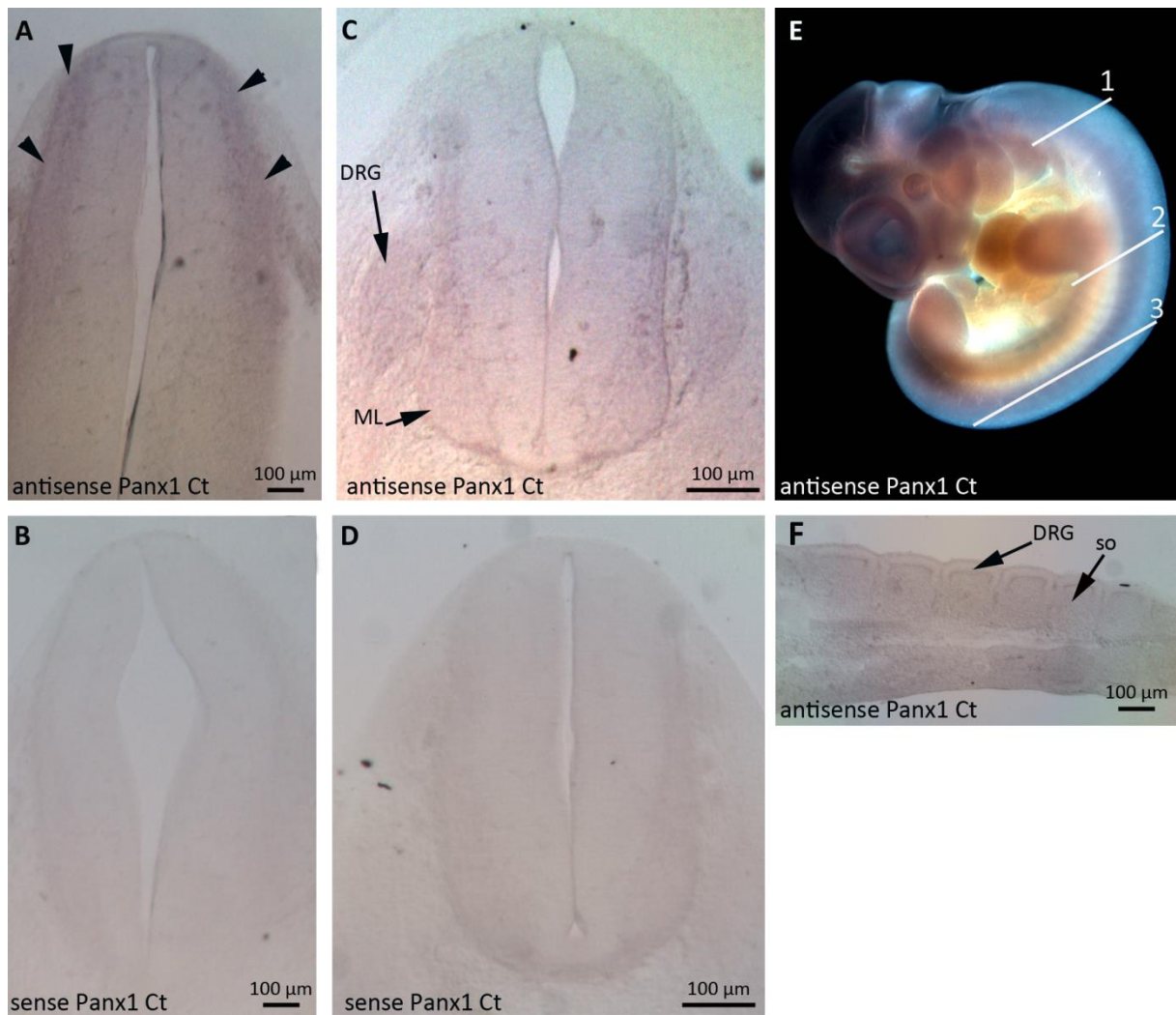
Figure 29. Truncal transverse vibratome sections of an E11.5 embryo

Vibratome sections of an E11.5 embryo post whole-mount *in situ* hybridization showing the dorsal region. (A and B) Transversal sections at the caudal level of the rhombencephalon (1). Panx1 (arrowhead) was detected in the alar plate of the myelencephalon, cranial part (A). Transversal (C and D) and sagittal (F) sections of spinal cord (2, 3), Panx1 was detectable in the mantle layer (mt) and dorsal root ganglia (DRGs) (C and F). No expression was detected in the negative control (B and D). Somites (so).

Table 12. Embryo structures expressing Panx1 mRNA

Labeled embryo structures	E9.5	E10.5	E11.5
Telencephalon vesicle	+	+	++
Mesencephalon			
Alar lamina	+	+	++
Basal plate	+	+	++
Rhombencephalon (r1–r8)			
Metencephalon	-	++	+++
Myelencephalon	-	++	+++
Cranial ganglia			
Oculomotor motor neurons (III)	-	+	++
Trochlear motor neurons (IV)	-	+	++
Trigeminal ganglion (V)	+	++	+++
Facial ganglion (VII)	+	++	+++
Acoustic ganglion (VIII)	+	++	+++
Vagus ganglion (X)	n.d.	n.d.	+++
Otic vesicle	+	++	++
Spinal cord	+	++	+++
Dorsal root ganglia	n.d.	n.d.	++
Branchial arch 1	+	+	+
Forelimb plate	+	+	+

(+) indicates the intensity of *in situ* hybridization staining in whole-mount embryos or in vibratome sections of studied stages. The intensity was determined according to the optical observation. (-) indicates the absence of the staining. In DRG, Panx1 was observed only in vibratome sections of E11.5 embryo. No vibratome sections were made of E9.5 and E10.5 embryos. n.d. not determined.

4.4   Panx1-β-Gal expression in transgenic embryos

The bacterial gene *LacZ* encodes β-galactosidase in *Escherichia coli* in order to cleave the disaccarid lactose into two monosaccharides, glucose and galactose. Histochemical staining (β-Gal staining) uses the fact that β-galactosidase hydrolyzes X-Gal molecules to release indole molecules and galactose. Two indole molecules dimerize and produce a visible blue/green staining (Juers et al., 2012). Thus, cells or tissues producing this staining reveal an endogenous or exogenous expression of beta-galactosidase (β-Gal) in active form.

β-Gal is, in addition to bacteria, also expressed in different mammalian cells at low level. To avoid the detection of endogenous expression of β-Gal, pH dependency of staining was investigated. Weiss et al. (1999) revealed that the endogenous β-Gal was active in acidic pH and that endogenous β-Gal detection can therefore be avoided using an alkaline pH for β-Gal staining. In this study, no endogenous β-Gal signal was detected in wildtype mice using a pH of 7.4 (Figure 30). In Panx1 transgenic mice (Panx1$^{tg/tg}$), the *LacZ* gene is inserted into the *Panx1* gene to be under the control of the *Panx1* promoter. Hence, the β-Gal staining can be used to evaluate Panx1 expression indirectly in whole-mount embryo.
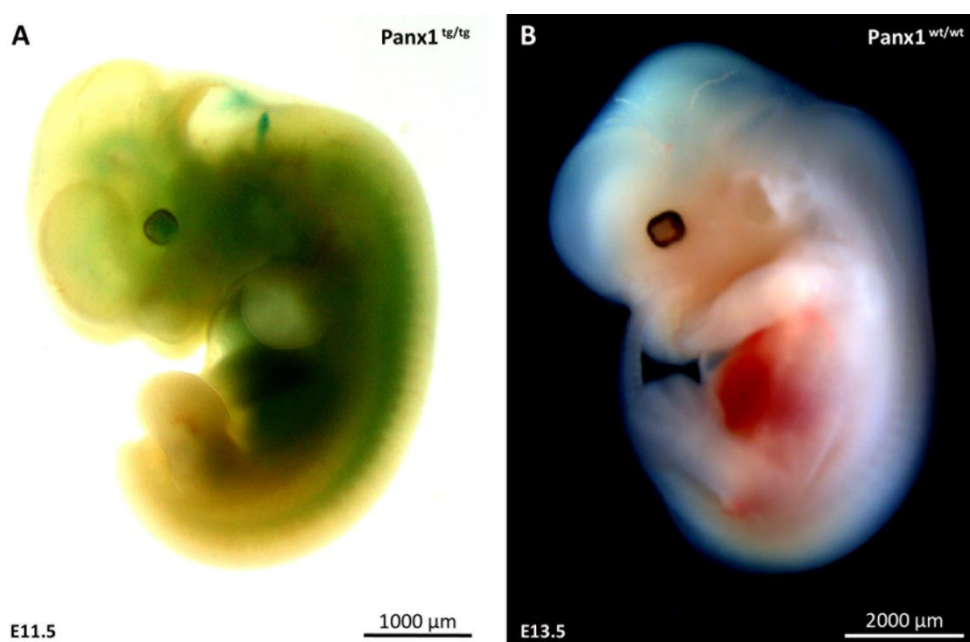

Figure 30. Signal specificity of β-Gal staining
Whole-mount β-Gal staining of Panx1$^{tg/tg}$ (A) and Panx1$^{wt/wt}$ (B) embryos at E11.5 and E13.5, respectively. No staining was visible in the wildtype embryo (B) compared to the transgenic embryo (A) under similar conditions.

4.4.1 Panx1-β-Gal expression in E11.5 Panx1$^{tg/tg}$ mice

Whole-mount β-Gal staining was used to detect β-Gal expression in the whole embryo, in order to evaluate sites expressing Panx1 indirectly. This method allowed comparing reporter gene expression of β-Gal with Panx1 mRNA expression by WM-ISH.

Many expression sites observed by WM-ISH were confirmed with β-Gal staining (Figure 31). The expression of β-Gal was observed in telencephalon and mesencephalon with lower expression in the basal plate of the mesencephalon. In the rhombencephalon, β-Gal expression was absent from the whole lip of the rhombencephalon. However, the roof plate of the metencephalon exhibited a strong signal. On the other hand, β-Gal staining in cranial ganglia (V, VII, and VIII) was very weak and hardly allowed identification of ganglia. A very strong signal was detected in the head behind the otic vesicle, likely to be the primary head vein. The expression of β-Gal in spinal cord was continuous in all segments. β-Gal staining in the abdominal region appeared non-specific.
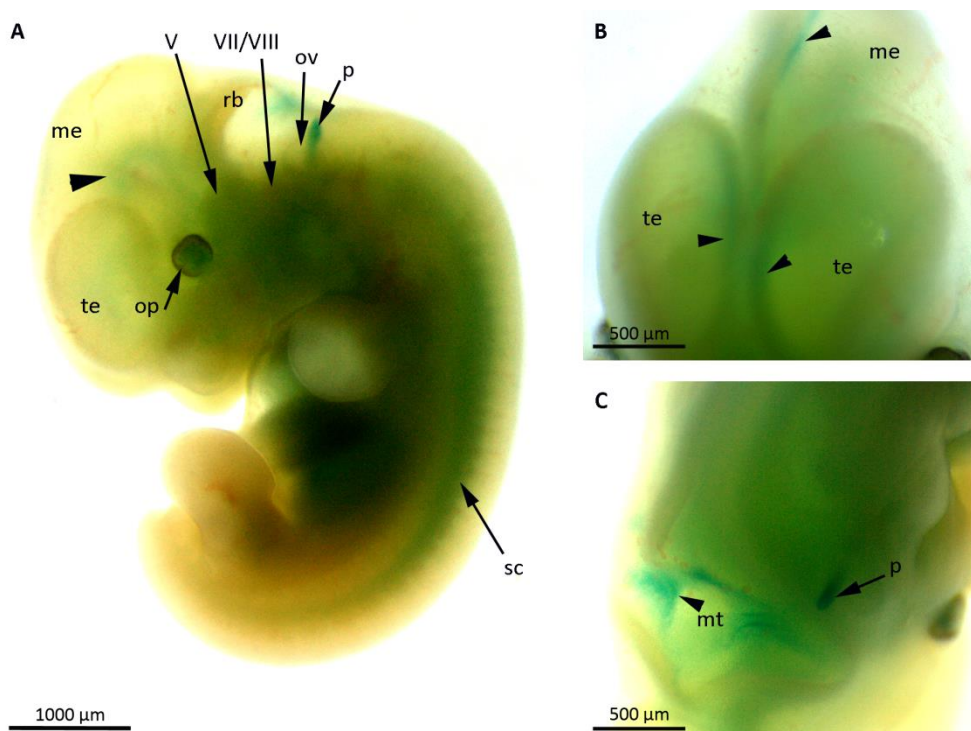

Figure 31. Whole-mount β-Gal staining of a Panx1$^{tg/tg}$ embryo at E11.5
(A) A lateral view of an E11.5 embryo shows β-Gal expression in different regions, in the basal plate of mesencephalon (arrowhead), in the trigeminal ganglion (V), in the facio-acoustic (VII/VIII) ganglion complex, in the optic cup (op), and in spinal cord (sc). Primary head vein (p) (B) Top view of the cephalic region shows the β-Gal staining (arrowheads) in the wall of telencephalic (te) and mesencephalic vesicles (me). (C) Dorsal-top view of the hindbrain region shows β-Gal expression in the roof plate of the metencephalon (mt).

For detailed analysis of whole-mount β-Gal staining, paraffin sectioning was carried out. Unfortunately, the remainder of the staining was not sufficient for microscopy. Hence, paraffin block photography was performed at different levels to show an overview of β-Gal expression sites. A block sectioned at the level of the cephalic region showed β-Gal staining in the roof plate of mesencephalic vesicle (Figure 32). Another block sectioned at the level of the rhombencephalon, shows the staining in the roof and floor plate of the caudal myelencephalic part. In spinal cord, the staining was visible in the mantle layer of the developing spinal cord and a very low level in DRGs (Figure 32 C).
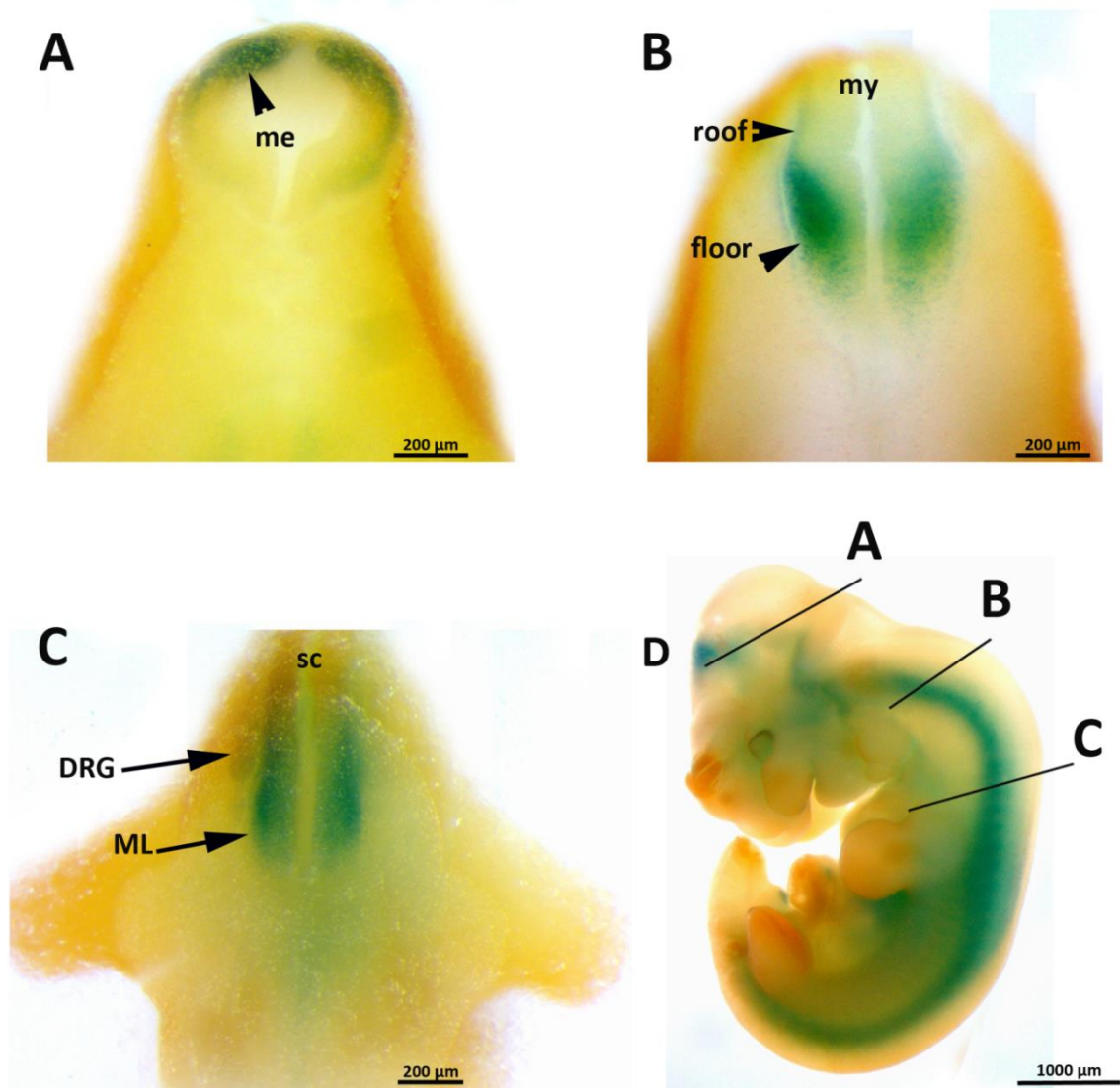
Figure 32. Overview of paraffin blocks post β-Gal staining of E11.5 Panx1$^{tg/tg}$ embryo
(A) Overview of paraffin blocks at the level of mesencephalon (me) shows β-Gal staining (arrowhead) in the roof plate. (B) At the caudal level of the myelencephalon (my), the staining is visible in roof and floor plates. (C) At spinal cord level, the mantle layer (m) of the developing spinal cord and dorsal root ganglia (DRGs) are β-Gal-positive. Block sections were obtained from the embryo in (D) at labeled levels.

4.5 Panx1 protein expression in mouse development

As described above, Panx1 expression was investigated in early stages of mouse development. This was based on PCR, whole-mount *in situ* hybridization, and β-Gal staining results. All these techniques revealed that the *Panx1* gene is expressed in early mouse development, in the head and the body with abundant expression during development of the nervous system. To date, there are limited data illustrating Panx1 protein distribution in mouse development. The aim of this part of the study was therefore to analyze the distribution of Panx1 protein during mouse development, as a key to understand its function during development.

The detection of a protein in a tissue requires protein-specific antibodies. In this study, different commercial antibodies against Panx1 were used for immunoblotting and immunofluorescence analyses. Many antibodies, however, either gave no signal or reacted unspecifically. Therefore, polyclonal antibodies were generated using immunization peptides according to the sequence described by Penuela et al. (2007).

4.5.1 Panx1 antibody generation

In this study, a polyclonal antibody was generated in rabbit using synthetic immunization peptides corresponding to amino acids 395 to 409 (QRVEFKDLDLSSEAA), located in the carboxy-terminus of the mouse Panx1 protein (Penuela et al., 2007). The pre-immune serum was collected from the animal prior to immunization and served as negative control. The antiserum was used without further purification. The antibody titer was determined using ELISA assay, and the specificity was characterized using immunolabeling and immunoblotting analyses. In parallel, analyses were performed using the pre-immune serum and preabsorbed antibodies with synthetic peptides as negative controls.

4.5.2 Panx1 antiserum reactivity determined by ELISA

The amount of the specific antibody in the antiserum was defined as the antibody titer. The antibody titer was determined at the highest dilution of the first antiserum, at which the absorbance ratio (absorbance of an antiserum sample to absorbance of PIS) was greater than 2.1 (Liu, 2009). Equal quantities (80 ng) of peptides were coated to wells. Serial dilutions (1:1,000 – 1:128,000) of the first antiserum and of PIS were allowed to bind to coated peptides. After the enzymatic detection of peptide-antibody complex via HRP antibodies, the produced color was measured. The absorbance value of antiserum dilutions was reduced in high dilution samples. PIS samples exhibited a constant

absorbance value. In all antiserum dilutions, the absorbance ratio was greater than 2.1 (Figure 33). The highest dilution (1:128,000) was defined as the antibody titer. These data are represented without statistical analysis, as this experiment was performed only once (n = 1).
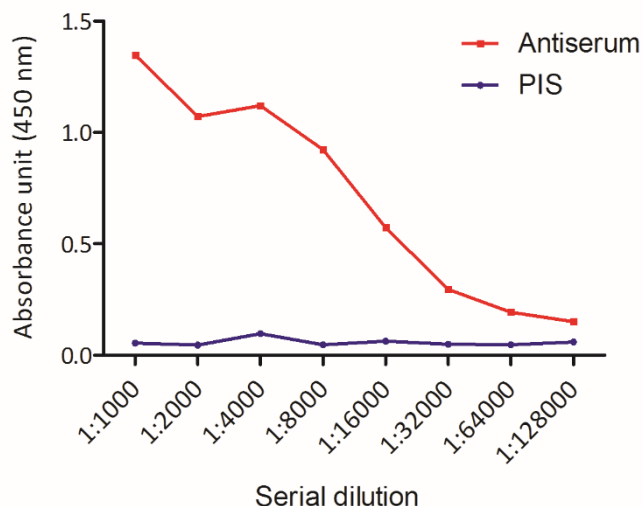

Figure 33. Antiserum titer determination by ELISA
Serial dilutions (1:1,000 – 1:128,000) of the first antiserum and PIS were applied to 80 ng of synthetic peptides. All diluted samples of the antiserum were taken as positive, as the absorbance ratio was greater than 2.1. The antibody titer was determined at the highest dilution of 1:128,000.

4.5.3   Panx1 antibody specificity determined by peptide competition assay

Polyclonal antibodies can react unspecific and exhibit unspecific signals. The peptide competition assay was used to determine the specific signal of the generated antibody. Prior to use in an immunoblot, the first antiserum was incubated with Panx1 synthetic peptides used for antibody generation. These peptides were used to bind Panx1 specific antibodies in the antiserum. Thus, peptide pre-incubation should result in the absence of any specific signal and all detected signals remaining were considered non-specific.

In this experiment, the antibody was preabsorbed with serial dilutions of Panx1 peptides to determine the optimum dilution for a complete peptide blocking. The experiment was performed using a brain protein lysate, as Panx1 expression had been reported in brain previously (Ray et al., 2005, Zappala et al., 2006). In the absence of peptides, the protein was detected at a molecular weight of 50 kDa corresponding to the molecular weight of Panx1. Samples, which were detected using the preabsorbed antiserum, showed a reduction in the intensity of the immunoreaction with increasing peptide quantities until 40x. No complete disappearance of the immunoreactivity was observed at these

dilutions (Figure 34). On the other hand, the negative control serum (PIS) did not detect any protein on the membrane.

In this experiment, peptides were incubated with the antiserum at 4°C only for two hours. However, a complete blocking was obtained by incubating the antiserum with peptides for 48 hours as described in the next section.
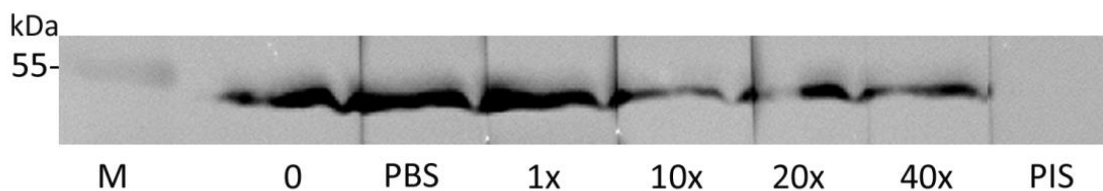

Figure 34. Panx1 antibody specificity as determined by peptide competition assay
The peptide competition assay was performed on brain protein lysate. The antiserum detected a protein at 50 kDa corresponding to the molecular weight of Panx1. The first antiserum in a dilution of 1:1,000 was preabsorbed with serial dilutions of Panx1 peptides (1x, 10x, 20x, and 40x). The preabsorbed antiserum showed reduced labeling intensity without complete elimination compared to not preabsorbed antiserum (0) or in PBS diluted antiserum. No protein was detectable with PIS.

4.5.4   Temporal expression of Panx1 protein in mouse development

As described above, Panx1 mRNA was expressed in early stages of mouse embryonic development, in both the head and the body (see Chapter 4.1). To analyze whether Panx1 mRNA was translated into protein at these stages, immunoblotting analysis was performed using the same developmental stages as in RT-PCR experiments. Ten embryos of E9.5 were pooled and proteins were isolated from whole embryos. Embryos of E10.5, E11.5 and E12.5 (six, six, and one embryos, respectively) were analyzed in samples of pooled heads or bodies separately. For each sample, the first antiserum was applied in addition to controls: of PIS and neutralized serum with 10x peptides. This experiment was performed only once (n = 1).

Panx1 antiserum reacted in all stages and exhibited multiple immunoreactive proteins. A protein was detected at a molecular weight of 55 kDa in addition to other proteins in most samples. Immunoreactivity at 46 and 55 kDa disappeared completely in E12.5 samples and partly in E9.5, E10.5, and E11.5 samples after peptide preabsorption (Figure 35).
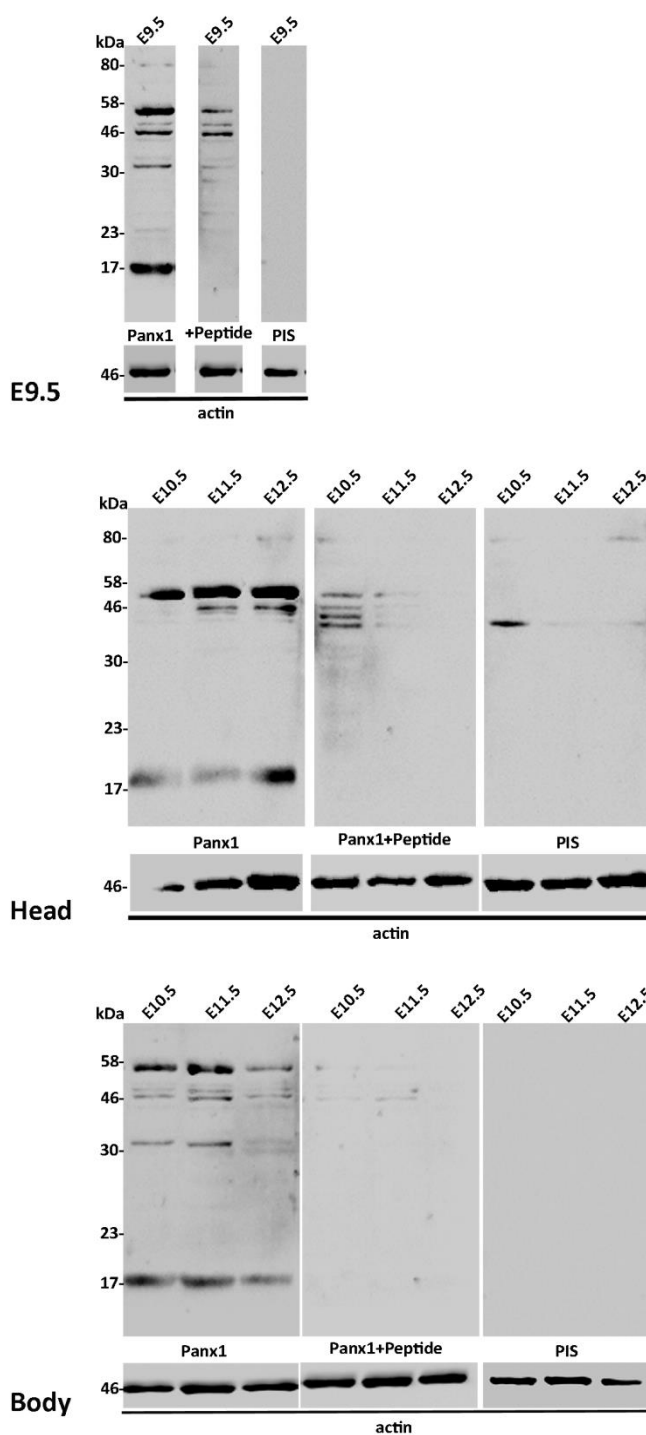
Figure 35. Temporal expression of Panx1 protein in mouse development
Protein lysates of whole-mount E9.5, heads and bodies of E10.5, E11.5 and E12.5 were examined using Panx1 antiserum, preabsorbed serum with 10x peptides, and PIS. Panx1 antiserum detected multiple immunoreactive proteins at 55, 46 and 32 kDa. Intensity of immunoreactions was decreased or absent using preabsorbed antiserum. Immunoreactivty was present at a molecular weight of 17 kDa in E9.5 and body samples or at 20 kDa in head samples incubated with Panx1 antiserum. This protein disappeared completely using the neutralized serum. No proteins were detected using the pre-immune serum (PIS) except an unspecific detection in the head of E10.5. The loading control of actin appeared at 46 kDa in all samples.

The immunoreactivity at a molecular weight of 32 kDa was restricted to E9.5 (whole embryo) and to body samples of all stages. Immunoreaction to this protein disappeared completely after peptide preabsorption. Further immunoreactivity was clearly present in all samples at a molecular weight of 17 kDa in E9.5 and body samples or at 20 kDa in head samples. This signal disappeared completely in all samples after peptide preabsorption. In the head of E10.5, an immunoreactive protein was visible using PIS, thus, it was considered non-specific. All other samples were negative using PIS. These results indicate that Panx1 protein is present in all studied stages in both the head and the body and exhibits multiple immunoreactive proteins.

4.5.5 Specificity of Panx1 antibody in the retina and cerebellum

The localization of Panx1 protein in tissues was determined using indirect immunolabeling detection. Firstly, the antiserum specificity was tested on tissues of cerebellum and retina, for which Panx1 expression had been reported previously. In the cerebellum, Panx1 expression was detected in Purkinje cells and in the granule cell layer. Additional immunopositive cells were also detected in the molecular cell layer (Figure 36). In the retina, Panx1 was observed in the ganglion cell layer (GCL), the inner nuclear layer (INL), and at the outer border of the outer nuclear layer (ONL). Some immunepositive cells appeared also in the outer plexiform layer (OPL) adjacent to the INL (Figure 36). In both regions investigated, no signal was observed in the negative control using PIS except an unspecific signal within the GCL.
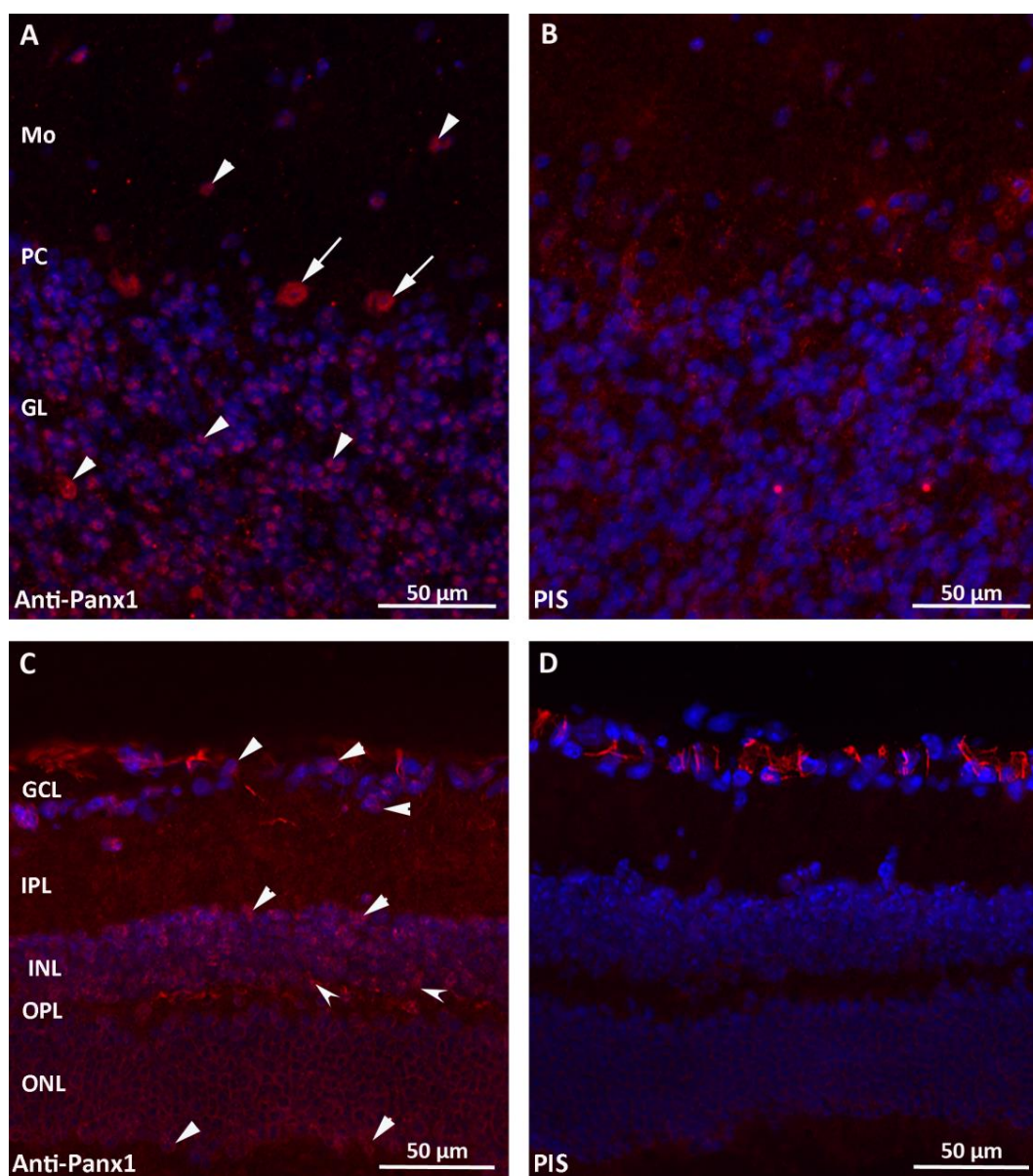
Figure 36. Panx1 antiserum specificity in the retina and cerebellum
(A) In the cerebellum, Panx1 immunoreactivity (red) was present in cerebellar Purkinje cells layer (PC) (arrows) and in the granule cell layer (GL) (arrowhead). Some immunepositive cells were present in the molecular layer (Mo) (arrowheads). (B) No labeling was detectable in the cerebellum using PIS. (C) In the retina, Panx1 immunopositive cells (arrowheads) were present in ganglion cells (arrowheads in GCL), in the inner nuclear layer (INL) and at the outer border of the outer nuclear layer (ONL). Barbed arrowheads indicate immunepositive cells in the outer plexiform layer (OPL) adjacent to the INL. (D) The staining observed in the GCL using PIS was considered non-specific. DAPI was used as nuclear dye (blue).

4.5.6   Panx1 protein distribution in spinal cord and sensory ganglia of E11.5

As described above, Panx1 mRNA expression was observed in early stages of mouse development. Immunoblotting analysis showed also the protein expression in all of these stages. To determine the localization of Panx1 protein in early stages, immunolabeling analysis was performed on E11.5 embryos. At this stage, Panx1 mRNA was more abundantly expressed than in other early stages and especially observed in trigeminal ganglion and spinal cord (see Chapter *4.3.3*).

Panx1 was detected using the antiserum, in addition, negative controls using PIS and neutralized serum (preabsorbed with 60x peptides) were performed (see Chapter *3.8.2*). An abundant expression of Panx1 was observed in the trigeminal ganglion, dorsal root ganglia, as well as in the mantle layer of the spinal cord (Figure 37). No expression was detectable in the dorsal horn and in the ventricular zone as well as in the floor plate. Labeling was considered specific, since no labeling was observed in negative controls using the neutralized serum or PIS.

For further determination of the cell types expressing Panx1 in DRGs and spinal cord, double immunolabeling was performed using Panx1 antiserum and NeuN antibody on spinal cord cryosections of E11.5 embryos. The neuronal marker NeuN (neuron-specific nuclear protein) is firstly detectable when neurons become post-mitotic and initiate the neuronal differentiation (Mullen et al., 1992). At E11.5, NeuN was expressed in the mantle layer but not in the ventricular zone or the floor plate. Panx1-immunopositive cells, which were found at the site of developing motor neurons in the mantle layer, were also NeuN-positive. However, the number of NeuN-positive cells in the mantle layer and DRGs exceeded the number of Panx1-positive cells (Figure 38).
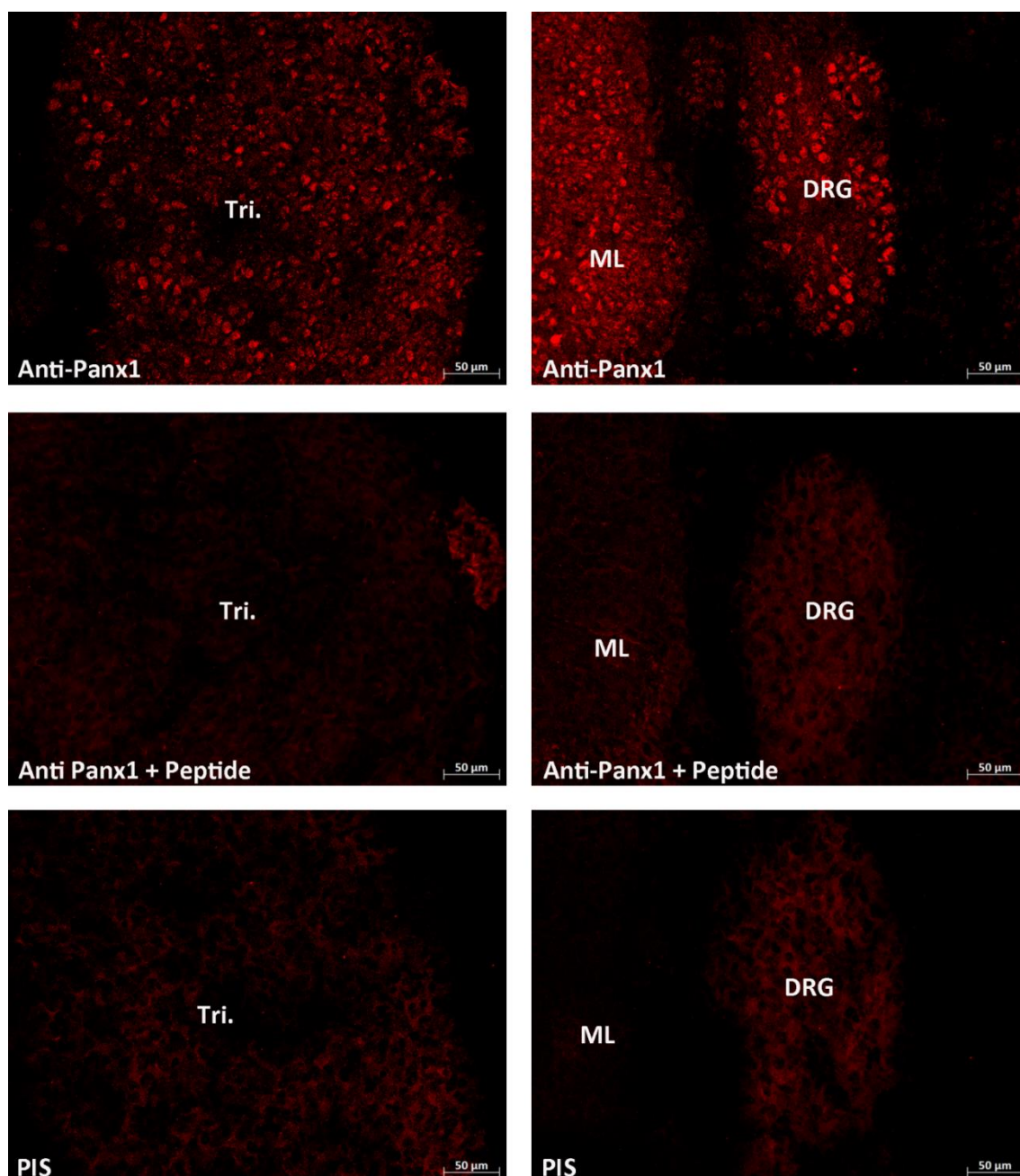
Figure 37. Panx1 expression in spinal cord and sensory ganglia at E11.5
Transversal sections of E11.5 embryos, located at the level of trigeminal ganglion and spinal cord, respectively, were used for immunofluorescence. Many positive cells were visible using the antiserum of Panx1. The signal was visible in trigeminal ganglion (Tri), dorsal root ganglion (DRG) and in the mantle layer of the neural tube (ML). No labeling was observed in these regions using neutralized serum (+ 60x peptide) or PIS (pre-immune serum).
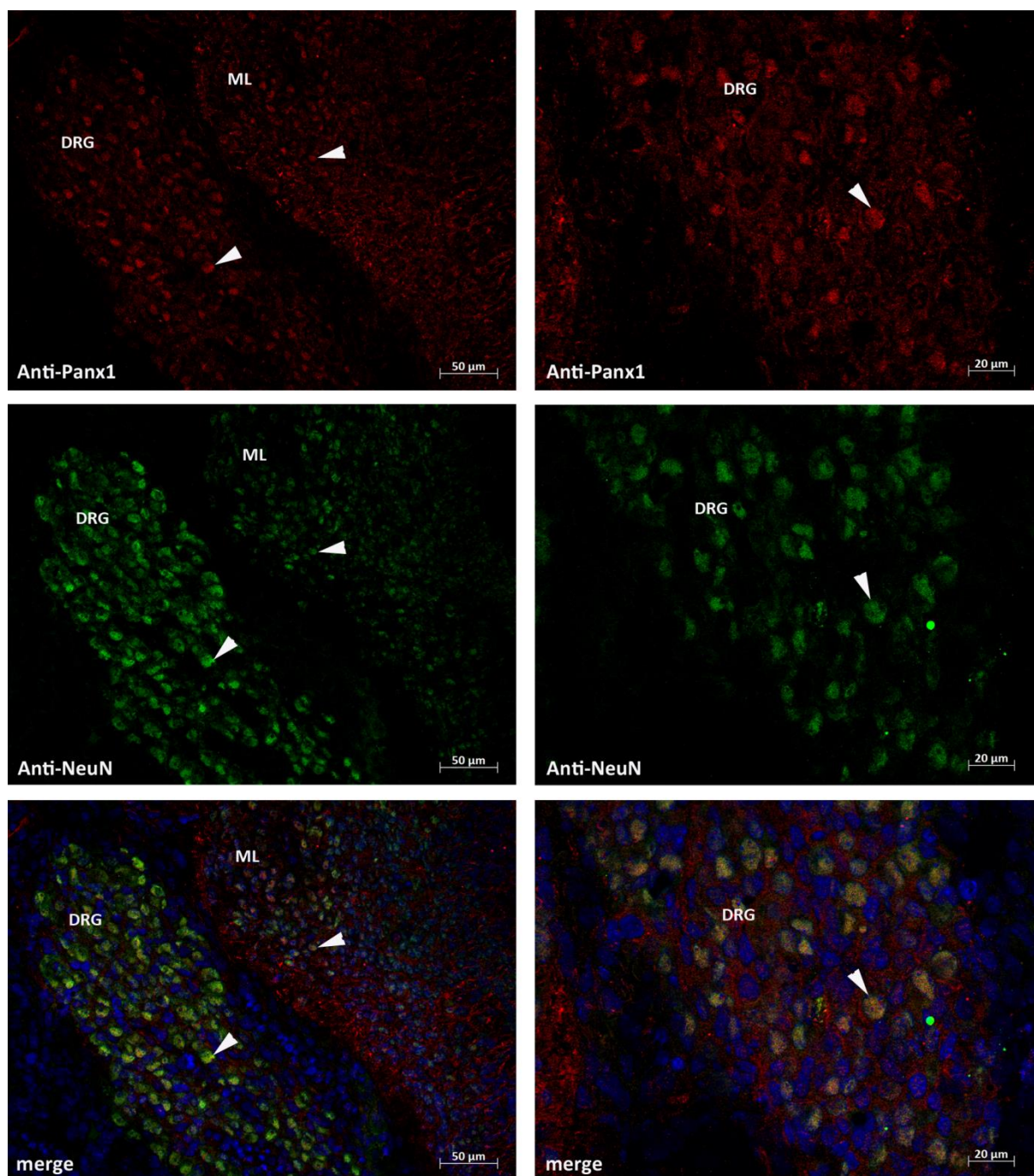
Figure 38. Co-localization of Panx1 and NeuN in an E11.5 embryo
Double immunolabeling using Panx1 antiserum and NeuN antibody was performed on cryosections of E11.5 embryos. Transversal spinal cord cryosection at low (left planel) and high (right panel) magnification showing Panx1 and NeuN expression (arrowheads) in the mantle layer (ML) and in DRG. (left). At high magnification, DRGs labeled with anti-Panx1 and anti-NeuN antibodies revealed the co-localization of Panx1 and NeuN (arrowheads). DAPI was used as nuclear dye (blue).

4.5.7 Panx1 mRNA and protein expression investigated in transgenic mice

To validate that primers used for further analysis did not detect any transcript in Panx1- or Panx2-transgenic mice, RT-PCR analysis was performed. The experiment was performed using tissues from wildtype animals and transgenic animals of Panx1$^{tg/tg}$, Panx2$^{tg/tg}$, and Panx1$^{wt/tg}$ / Panx2$^{tg/tg}$. Primers were tested on a total RNA extract of cerebellum and brainstem. An internal control was applied using the reference gene 18S rRNA.

Panx1 and Panx2 expression in cerebellum and brainstem was previously described in many reports (Baranova et al., 2004, Ray et al., 2006, Zappala et al., 2006). Samples of wildtype and heterozygous Panx1-transgenic animals (Panx1$^{wt/tg}$) showed a specific PCR product at the predicted size (Figure 39). No detectable products were visible in samples of homozygote transgenic mice Panx1$^{tg/tg}$ and Panx2$^{tg/tg}$ or in the absence of reverse transcriptase (NR) during cDNA syntheses.
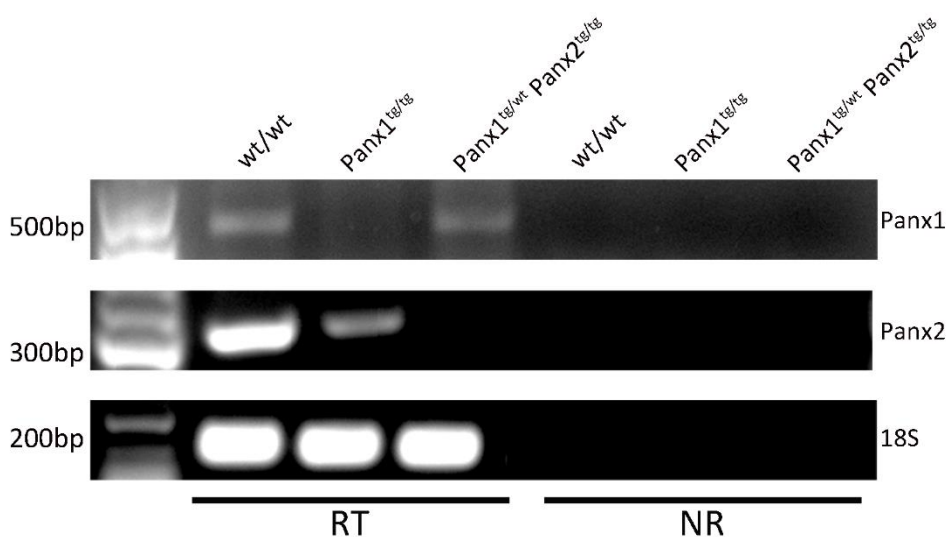

Figure 39. Panx mRNAs expression in transgenic mice
PCR analysis of wildtype and Panx1 / Panx2 transgenic tissues cerebellum and brainstem using primers amplifying Panx1, Panx2 or 18S. PCR product were present in both wildtype and heterozygous animal of Panx1$^{tg/wt}$ in the present of reverse transcriptase (RT) at the predicted size (443 bp Panx1, 266 bp Panx2 and 155 bp 18S). No PCR products were detectable in samples of homozygote transgenic animals and in the negative control without reverse transcriptase (NR). 18S rRNA amplification served as a reference for equal cDNA template.

This experiment revealed that the primers used were specific and that Panx1 and Panx2 were not present in the particular homozygote transgenic animals. This also allowed to use transgenic animals to examine the specificity of Panx1 antiserum using immunolabeling and immunoblotting analyses.

Immunohistochemically, Panx1 antiserum labeled cells in the ganglion cell layer and in the inner nuclear layer of wildtype animals (Figure 40). No labeling was detected in the inner plexiform layer. On the other hand, Panx1 antiserum did not exhibit any signal in transgenic animals. This revealed that Panx1 antiserum detected Panx1 protein specifically.
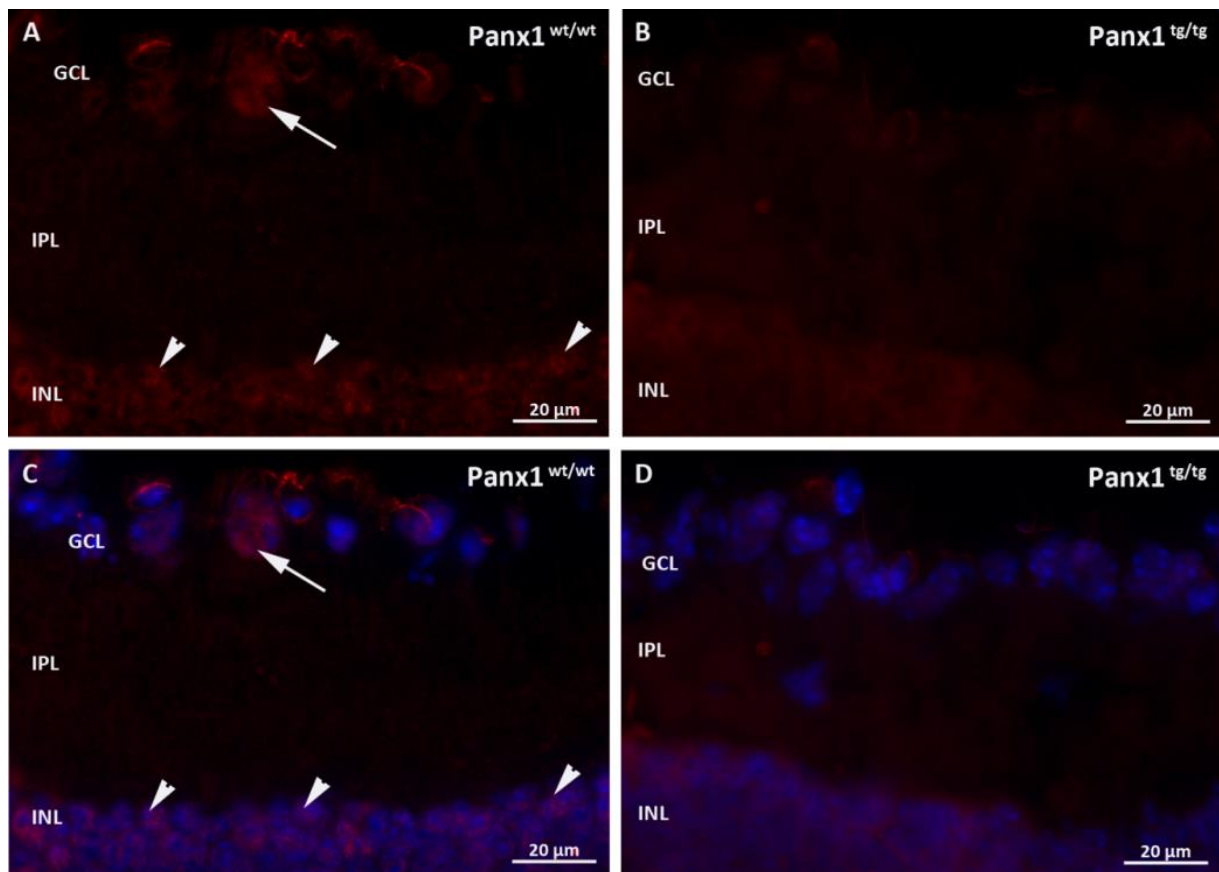

Figure 40. Panx1 expression in the retina of transgenic mice
Cryosections of the retina from Panx1$^{wt/wt}$ and Panx1$^{tg/tg}$ mice were labeled using Panx1 antiserum (red). (A) In the wildtype, Panx1 antiserum detected positive cells in ganglion cell layer (GCL) (arrow) and in the inner nuclear layer (INL) (arrowheads). No positive cells were detected in the inner plexiform layer (IPL). (B) In transgenic animal Panx1$^{tg/tg}$, no labeling was detected in the retina. (C and D) Same images as in A and B, respectively, are represented including the nuclear dye DAPI (blue).

For further determination, the antiserum was tested using immunoblotting analysis on brain and cerebellum protein lysates of wildtype and transgenic animals. Using Panx1 antiserum, immunoreactive proteins were detected in the wildtype as well as in transgenic tissues, in both brain and cerebellum samples (Figure 41 A). Two immunoreactive proteins at 32 kDa and 35 kDa were present in transgenic animals whereas only one protein was detectable in wildtype tissues. An additional protein was detected at a molecular weight of 14 kDa in all samples. This experiment was

performed using the first antiserum; the same antiserum was used on embryonic lysates in previously described experiments (see Chapter 4.5.4).

Furthermore, three commercial antibodies were tested by immunoblotting. The monoclonal Panx1 antibody (ab124969) detected an immunoreactive protein at 48 kDa in wildtype as well as in transgenic animals using a dilution of 1:10,000. The polyclonal Panx1 antibody (ab139715) displayed two immunoreactive proteins at a molecular weight of 34 and 40 kDa; labeling was more intense in transgenic animals than in wildtype tissues. The monoclonal Panx1 antibody (MAB7097, R&D) detected a protein at 46 kDa in all samples with similar intensity (Figure 41). Immunoblotting analysis of each antibody was performed only once by investigating protein lysates of two organs, i.e. brain and cerebellum.
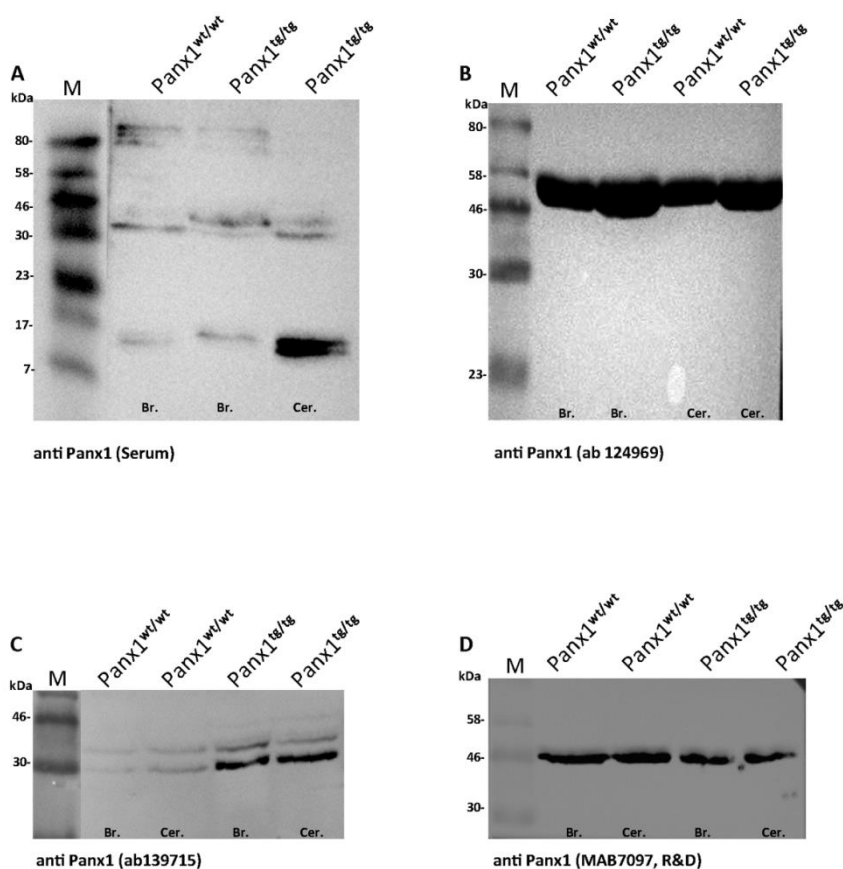
Figure 41. Panx1 protein expression in transgenic tissues
Panx1 antibodies were analyzed by Immunoblotting using protein lysates of brain (Br.) and cerebellum (Cer.) from Panx1$^{wt/wt}$ and Panx1$^{tg/tg}$ animals. (A) Panx1 antiserum showed two proteins at 32 and 35 kDa in transgenic animal Panx1$^{tg/tg}$ whereas only one protein was detectable in the wildtype Panx1$^{wt/wt}$. An additional protein was also visible at 14 kDa in all samples. (B) Anti Panx1 (ab124969) detected a protein at 48 kDa in both Panx1$^{wt/wt}$ and Panx1$^{tg/tg}$ of Br. and Cer. (C) A protein was detected very weakly at 40 kDa using anti Panx1 (ab139715) in both Panx1$^{wt/wt}$ and Panx1$^{tg/tg}$. An additional protein was strongly apparent in Panx1$^{tg/tg}$ and very weakly in Panx1$^{wt/wt}$ at 34 kDa. (D) No difference was apparent between Panx1$^{wt/wt}$ and Panx1$^{tg/tg}$ using anti Panx1 (MAB7097, R&D). This antibody detected a protein at 46 kDa in all samples.

The polyclonal Panx2 antibody (ARP42778_T100, AVIVA) was also tested on protein lysates of brain and cerebellum. The antibody detected a protein at 66 kDa corresponding to the molecular weight of Panx2. This detection was similar in wildtype and Panx2$^{tg/tg}$ transgenic animal (Figure 42).
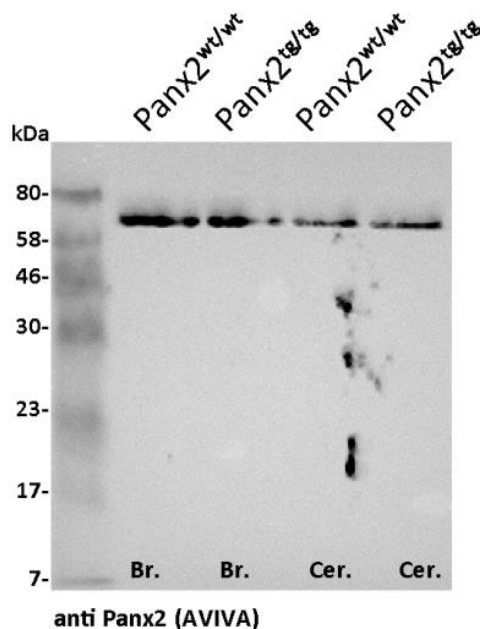
Figure 42. Panx2 protein expression in transgenic tissues
The specificity of the Panx2 antibody (AVIVA) was examined by immunoblotting using protein lysates of brain (Br.) and cerebellum (Cer.) from Panx2$^{wt/wt}$ and Panx2$^{tg/tg}$ animals. The antibody detected a protein at 66 kDa in both Panx2$^{wt/wt}$ and Panx2$^{tg/tg}$ tissues.

In immunoblot analysis, Panx1 and Panx2 antibodies employed in this study revealed similar immunoreactivities in both wildtype and transgenic Panx1$^{tg/tg}$ or Panx2$^{tg/tg}$ animals, respectively. The analysis of Panx protein expression therefore requires further analysis and the use of additional antibodies. In the course of this project, alternative methods were used for the detection of Panx1 expression with focus on spinal cord and sensory ganglia.

4.6 Panx1 expression in spinal cord and sensory ganglia

In situ hybridization and PCR analysis revealed that Panx1 mRNA is expressed in spinal cord and sensory ganglia during development. To investigate the cellular and regional distribution further, expression was investigated in adult spinal cord and sensory ganglia using β-Gal staining. This analysis was quantifiable from E18.5 onwards. To obtain an overview about Panx1 expression in spinal cord, whole-mount β-Gal staining was performed on spinal cord and sensory ganglia from a 4-week-old Panx1^tg/tg mouse (Figure 43). The β-Gal staining was observed in all spinal segments of the posterolateral tract. No staining was observed in the dorsal funiculus or in the ventral funiculus. On the other hand, all DRGs and trigeminal ganglia exhibited clearly the β-Gal staining. This experiment revealed that Panx1 is expressed in all spinal segments as well as in DRGs and trigeminal ganglion. For further determination of signals, β-Gal staining was performed on cryosections of these regions.
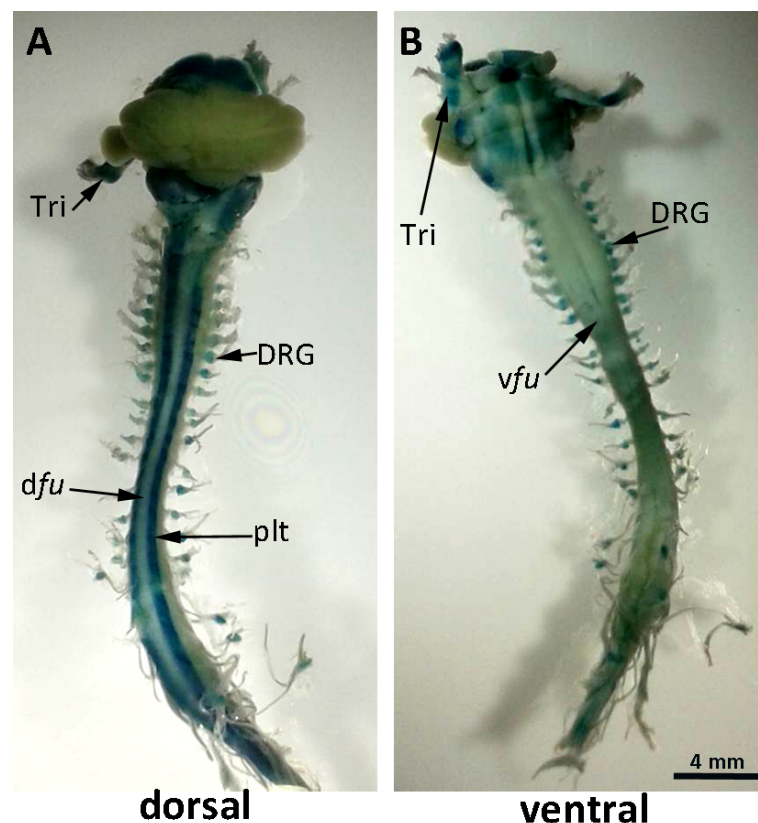
Figure 43. Whole-mount β-Gal staining of spinal cord and sensory ganglia
The whole-mount spinal cord attached to the dorsal root ganglia (DRGs) and sensory trigeminal ganglia was prepared from a 4-week-old Panx1^tg/tg mouse. The preparation was stained whole mount with β-Gal. (A) A dorsal view shows the positive β-Gal staining at all segments of the posterolateral tract (plt) in spinal cord and brain stem. No staining was observed in the dorsal funiculus (d*fu*) and in the ventral funiculus (v*fu*). Trigeminal ganglion (Tri) and DRGs were stained also with β-Gal. (B) The ventral region of spinal cord did not show the staining product.

4.6.1   β-Gal staining on cryosections

In Panx1-transgenic animals, the reporter gene *LacZ* is under control of the *Panx1* promoter. *Panx1* promoter activity was evaluated indirectly using β-Gal staining. This method indirectly allows the determination of cells expressing Panx1 in tissues. On cryosections, best results were observed by fixation of the tissue prior to staining with 0.2 % glutardialdehyde. The signal was absent when using acetone or 4 % formaldehyde, and very light after ethanol fixation (not shown). Therefore, glutardialdehyde fixation was used in all β-Gal staining experiments on sections. The specificity of this staining was tested in studied tissues by comparing the positive signal in transgenic tissues with tissues of wildtype animals as negative control. No staining was observed in the negative control (Figure 44).
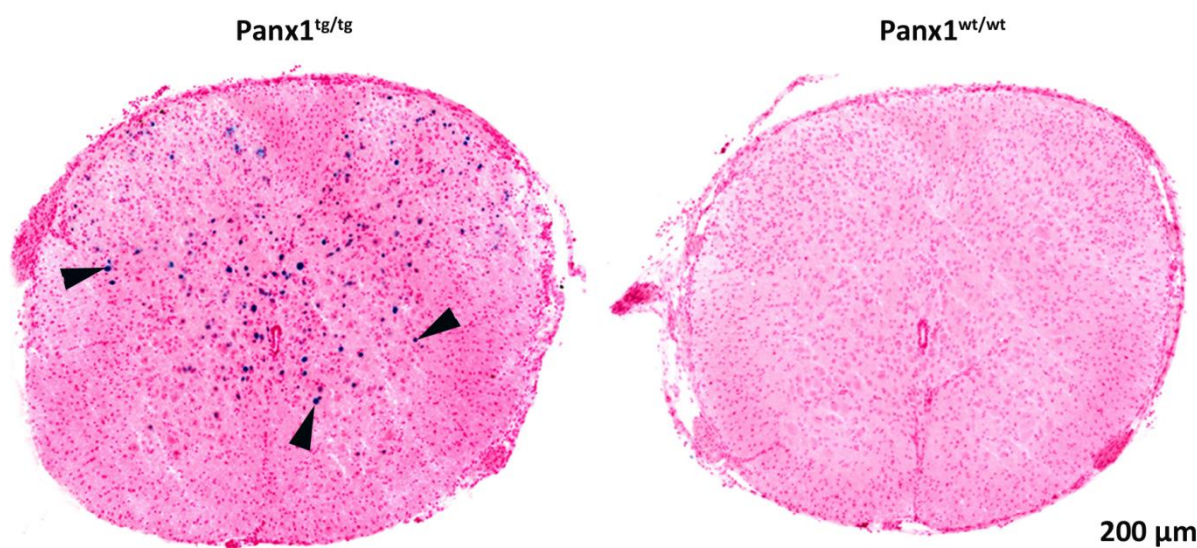
Figure 44. The specificity of β-Gal staining on cryosections
Cryosections of spinal cords from 9-day-old mice (P9) were stained with β-Gal staining. The staining (blue; arrowheads) was present in transgenic animals Panx1$^{tg/tg}$ (left) and absent in the wildtype Panx1$^{wt/wt}$ (right). Fast red staining (red) was used as nuclear stain.

4.6.2   Panx1-β-Gal expression in spinal cord development

Panx1 mRNA expression in spinal cord is already described using RT-PCR analysis but little is known about its distribution. Panx1 protein distribution has been described only in adult mice using immunolabeling (Zappala et al., 2006). The observed β-Gal signal on cryosections allowed studying the distribution of Panx1 during the development of spinal cord. An overview of spinal cord sections showed a variation in the distribution of β-Gal-positive cells during the development (Figure 46).

To determine how numbers of Panx1-positive cells changed during the development, a direct optical quantitative analysis was performed by counting β-Gal-positive cells. The quantification was performed on sections of thoracic spinal segments. β-Gal-positive cells were generally observed in the gray matter of spinal cord. The density of positive cells was determined at E18.5, P9, P12 and adult stages. A higher density of positive cells was observed in embryonic and postnatal stages than in adult animals (Figure 45). During early postnatal stages, the density increased significantly from P9 to P12. This increase was followed by a significant reduction in adult animals. This result revealed that Panx1 expression is temporally regulated in spinal cord development.
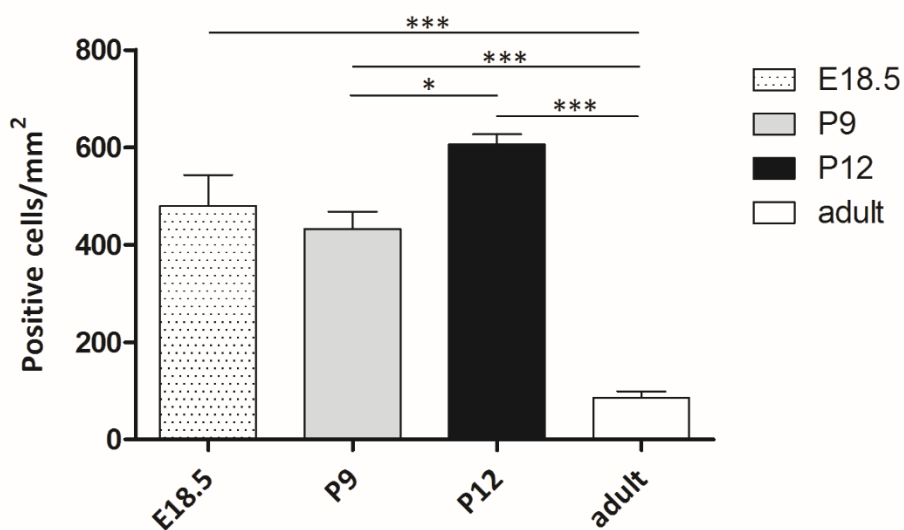
Figure 45. Panx1 expression in spinal cord development
This diagram shows the density of β-Gal-positive cells in spinal cord gray matter. The quantification was performed on sections of Panx1tg/tg animals from different stages (E18.5, P9, P12, and adult). The number of β-Gal-positive cells increased significantly at postnatal stage P12 and decreased largely in the adult. Asterisks indicate a significant difference between groups (*p <0.05, ***p <0.001). Shown are mean values ± SEM.
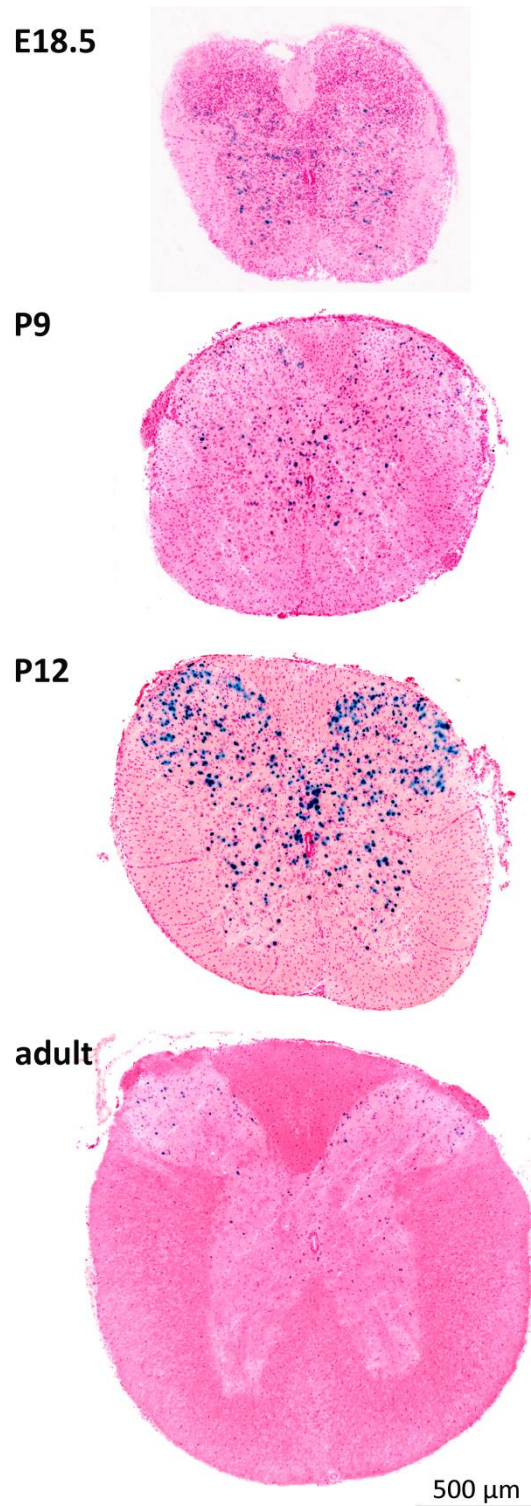
Figure 46. Panx1 distribution in spinal cord development
Cryosections of thoracic spinal segments were stained with β-Gal staining (blue). Sections were obtained from different stages E18.5, P9, P12, and adult. Fast red staining (red) was used as nuclear stain. In all stages, β-Gal-positive cells were restricted to the gray matter. The highest number of positive cells was observed at P12. A gradational distribution appears from dorsal to ventral within most stages. The apparently inverse distribution (ventral to dorsal) at E18.5 was not confirmed by quantification (see Figure 47).

β-Gal-positive cells did not appear to show a homogeneous distribution in the gray matter. Optical observation of the overview revealed a graded distribution of positive cells from dorsal to ventral in most stages, however, at E18.5 it seemed inverse from ventral to dorsal (Figure 46). To examine this observation quantitatively, it was necessary to differentiate between the dorsal region (laminae I-V) and the ventral region (laminae VII-X) of the spinal cord at all stages. Determination of the density of β-Gal-positive revealed that the dorsal region exhibited more positive cells per area than the ventral region at all stages investigated (Figure 47). Within each stage, only P12 spinal cord showed a significant reduction from the dorsal region to the ventral region. The dorsal region of P12 spinal cord exhibited a significant increase in the number of β-Gal-positive cells compared to other regions and stages. On the other hand, both dorsal and ventral regions of adult spinal cord showed the lowest number of positive cells compared to all other regions and stages. In contrast, no significant difference in cell number was observed within E18.5 and P9 spinal cord or between these two stages.
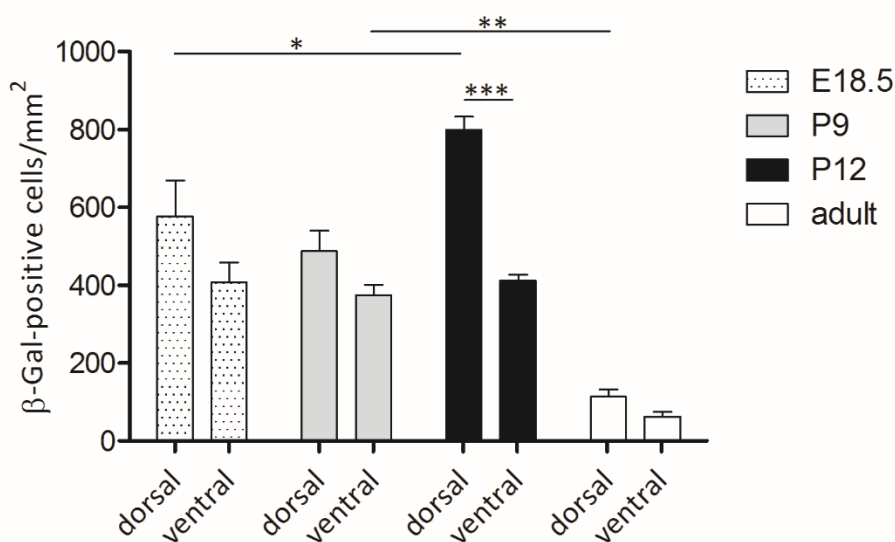
Figure 47. Gradational distribution of Panx1 in spinal cord
The density of β-Gal-positive cells was compared between the dorsal region (laminae I-V) and the ventral region (laminae VII-X) of spinal cord. P12 spinal cord exhibited a significant difference between dorsal and ventral regions. The number of β-Gal-positive cells was significantly increased in the dorsal region of P12 spinal cord compared to all regions of other stages. In contrast, a significant reduction of β-Gal-positive cells was exhibited in regions of adult spinal cord. Number of positive cells was not significantly different at E18.5 and P9 spinal cord. Asterisks indicate a significant difference between groups (*p < 0.05, **p < 0.01, and ***p < 0.001). Shown are mean values ± SEM.

The difference between dorsal and ventral regions was determined from the areal density of β-Gal-positive cells. Nevertheless, it is unknown whether the areas investigated (dorsal and ventral) have the same density of cells. Therefore, the ratio of β-Gal-positive cells to the total number of cells was

determined in these regions. This determination was performed on sections of P12 animals, as this stage exhibited a significant difference in the density of β-Gal-positive cells between dorsal and ventral regions.

β-Gal staining was performed to determine lacZ expressing cells and nuclear fast red stain was used to identify other cells. All cells were counted and the ratio of β-Gal-positive cells was calculated. This quantification revealed that the percentage of β-Gal-positive cells was reduced in the ventral area v1 compared to the dorsal area d1. Only the ventral area v2 (laminae VIII and IX) showed a significantly reduction in the percentage of β-Gal-positive cells comparing to other areas (Figure 48, B). For a more detailed analysis, the gray matter of P12 spinal cord was subdivided into four areas d1 (laminae I-II), d2 (laminae III-V), v1 (laminae VII, and X), and v2 (laminae VIII and IX). The percentage of β-Gal-positive cells in the dorsal region (laminae I-V) was significantly higher than in the ventral region (laminae VII-X) (Figure 48, A). This confirmed the results that the number of β-Gal-positive cells per area was higher in the dorsal region than in the ventral part of the spinal cord.

These results demonstrate that Panx1 expression in spinal cord displays a graded distribution from dorsal to ventral at P12. The dorsal region, d1, of lamina (I-III) had the highest number of Panx1-positive cells. In contrast, the ventral region, v2, of lamina (VIII and IX) had the lowest number of positive cells.

Figure 48. The ratio of β-Gal-positive cells in the gray matter of P12 spinal cord
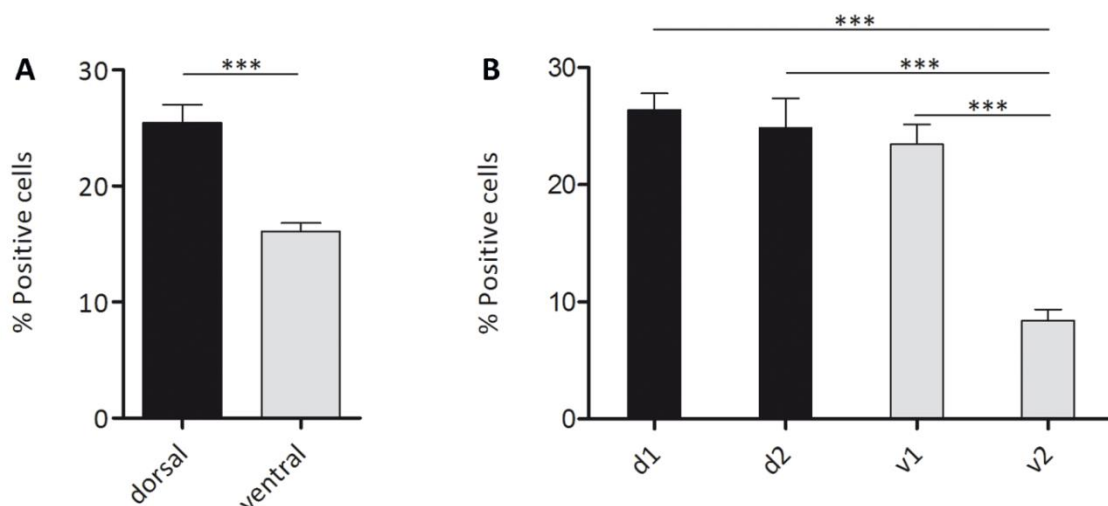
(A) The ratio of β-Gal-positive cells in the dorsal region (laminae I-V) was significantly higher than the ventral region (laminae VII-X). (B) Within spinal cord laminae, the percentage of β-Gal-positive cells significantly declined from dorsal to ventral. d1 (laminae I-II), d2 (laminae III-V), v1 (laminae VII, and X), v2 (laminae VIII and IX). Asterisks indicate a significant difference between groups (***p <0.001). Shown are mean values ± SEM.

4.6.3   Relative gene expression in adult spinal cord

The graded distribution of Panx1 protein was analyzed by light microscopy based on β-Gal staining as described in the previous section. Another quantitative analysis was performed to compare the relative expression of Panx1 mRNA between the dorsal and the ventral region of adult spinal cord. Given that Panx1 can associate with several purinergic receptors (Li et al., 2011), the relative gene expression of the receptors P2X3R and P2X7R was also analyzed in spinal cord samples. Based on the evidence that Panx2 showed co-expression with Panx1 in several regions of adult rat brain (Vogt et al., 2005), the association of Panx1 with Panx2 expression was also investigated in studied regions of spinal cord. The reference gene 18S rRNA was used as an internal calibrator.

The cranial thoracic region of spinal cord was sagittally divided into two parts, the dorsal region (lamina I-V) and the ventral region (lamina VII-X). As described above, lamina VI is absent in the thoracic region of mouse spinal cord. RNA was extracted from these parts. This experiment was performed using samples of three adult animals (n=3). Samples were analyzed at the same time using a 96-well PCR plate.

In terms of Panx1 expression, results were different from the quantitative results of β-Gal-positive cells as described above. Panx1 expression in the dorsal region was significantly lower than in the ventral region (Figure 49). This expression pattern was also reflected by purinergic receptors P2X3R and P2X7R. In contrast, Panx2 expression in the dorsal region was significantly higher than in the ventral region.
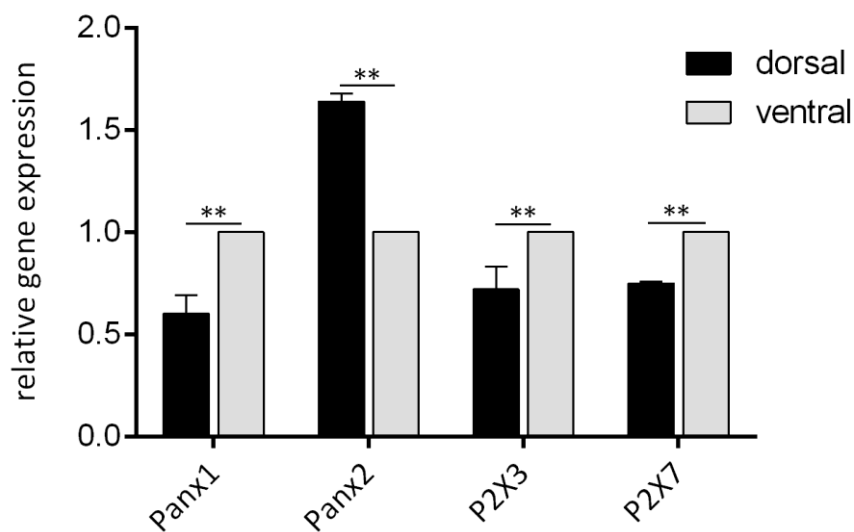
Figure 49. Relative gene expression in adult spinal cord
In the thoracic region of adult spinal cord, the relative mRNA expression of Panx1, Panx2, P2X3R, and P2X7R in the dorsal region was compared with the ventral region using real time qPCR analysis. Panx1 mRNA expression level in the ventral region was significantly higher than in the dorsal region. P2X3R mRNA and P2X7R mRNA exhibited a similar expression pattern; mRNA expression in the dorsal region shows significantly lower expression than in the ventral region. In contrast, the highest expression level of Panx2 mRNA was in the dorsal region. 18S rRNA was used as reference gene. The asterisk indicated a significant difference between groups (**$p < 0.01$). Shown are mean values ± SEM.

4.6.4   Histological analysis of transgenic spinal cord

Panx1 expression during development of the spinal cord led to examine whether the lack of Panx1 also caused a phenotypic change. As quantitative analyses of β-Gal staining showed the highest number of Panx1-positive cells in postnatal stage P12, the thoracic region of this stage was histologically analyzed. This analysis was performed on two groups of animals: wildtype and Panx1[tg/tg]. Each group included samples of three P12 animals (n=3). Paraffin sections of spinal cord were stained using Masson Goldner staining which allows a differentiated visualization of tissues. Nuclei were stained dark brown, cytoplasm and muscle fibers were stained red, and connective tissue appeared in green (Figure 50).

Using light microscopic analysis on sections of three animals from each group, no morphologic alterations were observed in transgenic animals compared to wildtype animals. In all sections, cells exhibited similar distribution in the gray and white matter. Cytoplasm appeared more dark red in the gray matter than in the white matter. The spinal cord was surrounded by a connective tissue shown in green. This analysis did not give any indication of a morphological changes in spinal cord caused by Panx1 deficiency.
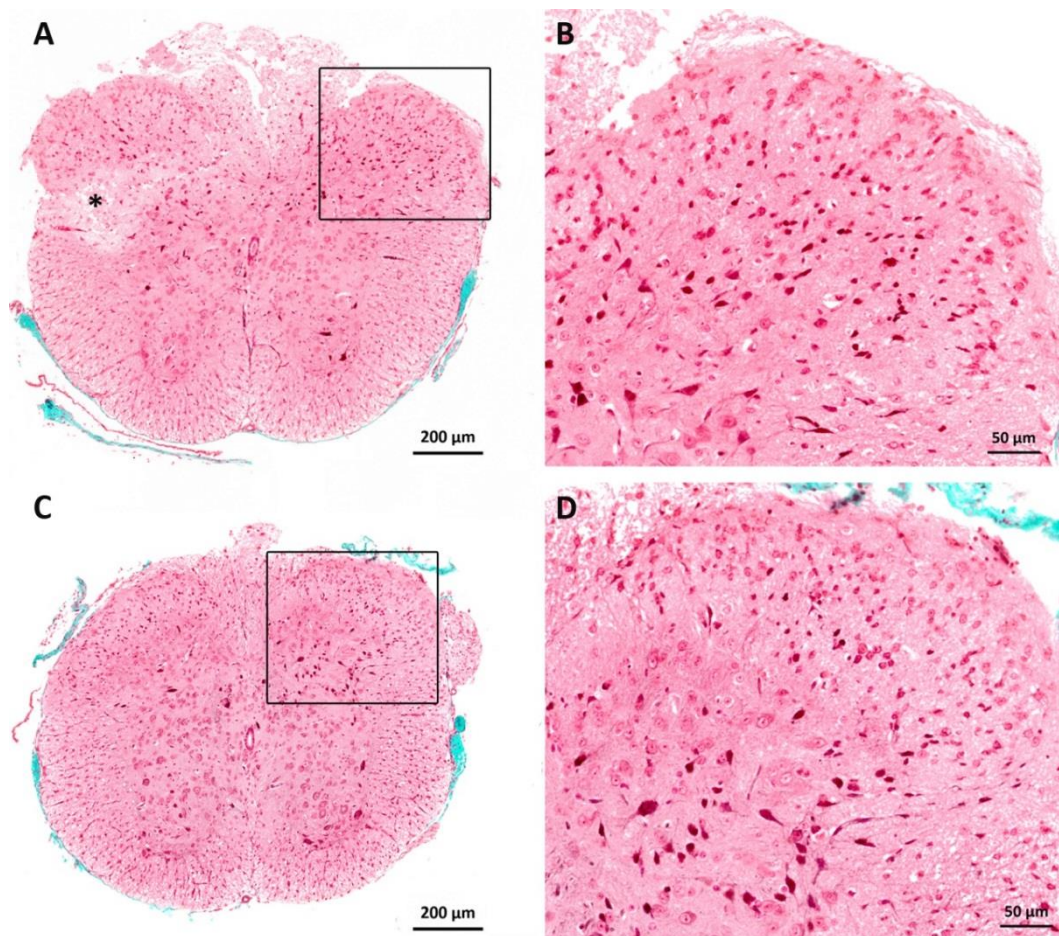
Figure 50. Histological analysis of transgenic spinal cord
Paraffin sections of the thoracic region of spinal cord were obtained from P12 animals: Panx1$^{wt/wt}$ (A) and Panx1$^{tg/tg}$ (C). Insets in A and C are shown at higher magnification in B and D, respectively. Sections were stained using Masson Goldner staining. The microscopic analysis did not show any obvious morphologic changes in transgenic animals compared to wildtype tissues. *The asterisk indicated a sectioning artifact. Nuclei (dark brown), cytoplasm (red) and connective tissue (green).

4.6.5 Panx1 expression in dorsal root ganglia

Panx1 expression in DRGs has not been described previously. In this study, Panx1 in DRGs was firstly observed in sections of E11.5 embryos; vibratome sections post whole-mount *in situ* hybridization showed a very light signal. β-Gal staining confirmed Panx1 expression in DRGs from this stage. Sections of paraffin blocks after whole mount β-Gal staining exhibited β-Gal signal in DRGs. For further determination of Panx1 expression in DRGs, a quantitative analysis was performed on stained cryosections of DRGs. Analyzed ganglia were obtained from the thoracic region of P9 transgenic animals Panx1$^{tg/tg}$ (Figure 51). Cryosections were stained with β-Gal staining. The size of β-Gal-positive

and -negative neurons was measured in all neurons whose nuclei were visible in the section. Positive neurons were sorted and grouped by size in increments of 50 μm. The same was done for all neurons (positive and negative neurons). The number of neurons in each group was determined. β-Gal-positive neurons were observed in all groups (Figure 52). This made 40 % of all neurons in each group (± 10 %) (not shown). In most sections, some satellite glia cells (3 ± 1) were identified as β-Gal-positive. Panx1 was expressed in all types of neurons in DRGs. The percentage of Panx1-positive cells was similar in all neuronal cell types.
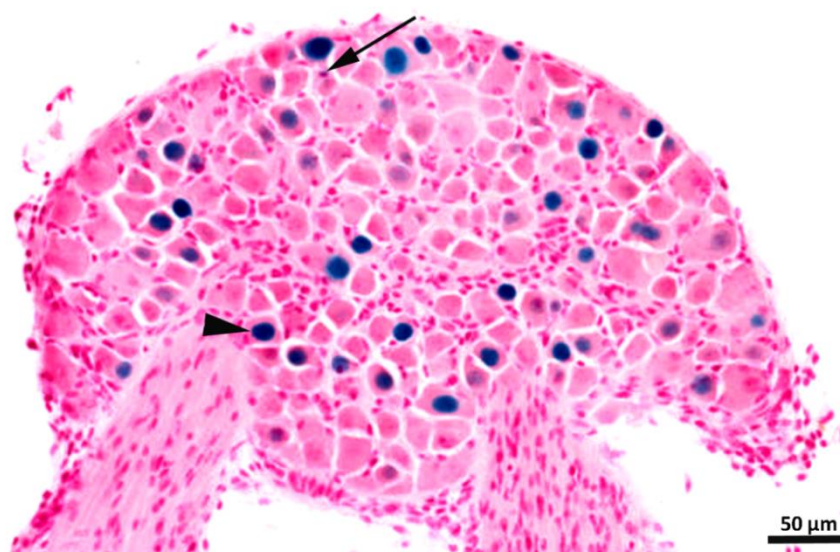

Figure 51. Panx1 expression in DRG of P9 mice
β-Gal staining was performed on cryosections of DRG from P9 Panx1$^{tg/tg}$ animals. β-Gal staining (blue) was observed in many neuronal cells (arrowhead) and some satellite glia cells (arrow). Three glia cells (± 1) were β-Gal-positive per section. Positive neurons showed different signal intensity.
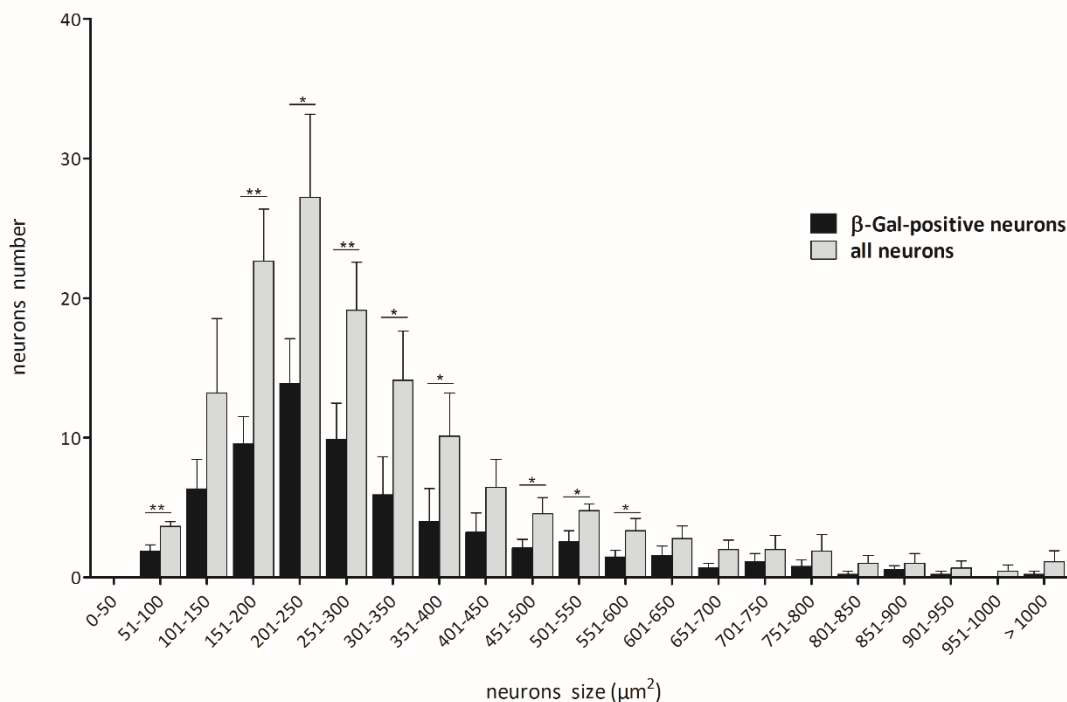
Figure 52. Size-frequency distribution of Panx1-positive neurons in DRGs of P9 mice
A diagram shows β-Gal-positive neurons and their size-frequency distributions comparing to all neurons in DRG of P9 transgenic animals Panx1[tg/tg]. β-Gal-positive cells were present in all groups of neurons except one group (951-1000). Asterisks indicated a significant difference between β-Gal-positive neurons (black columns) and all neurons (gray columns) within a group (*p < 0.05 and **p < 0.01). Shown are mean values ± SEM.

4.6.6   Relative Panx1 expression in sensory ganglia

As described above, Panx1 was observed in trigeminal ganglion and in all DRGs using whole mount β-Gal staining. Based on the fact that neurons in each sensory ganglia relay information from a discrete dermatome, the relative gene expression of Panx1 was compared between sensory ganglia of different regions. This included the trigeminal ganglion and dorsal root ganglia of cervical, thoracic and lumbar regions. Nine mice were used for this experiment. Ganglia of each region were pooled from three mice to obtain enough RNA. These groups were used to replicate experiments three times (n=3). Using an equal quantity of RNA, cDNA syntheses of all regions were performed in one preparation for all samples. The relative expression of Panx1 was determined in all regions of ganglia at one time. 18S rRNA expression was used as reference gene in all experiments.

Panx1 showed different expression levels within sensory ganglia of different spinal cord regions (Figure 53). Cervical and thoracic ganglia exhibited significantly higher expression levels than trigeminal ganglia. Within DRGs, the expression level increased in cervical and thoracic ganglia and was reduced in lumbar ganglia.
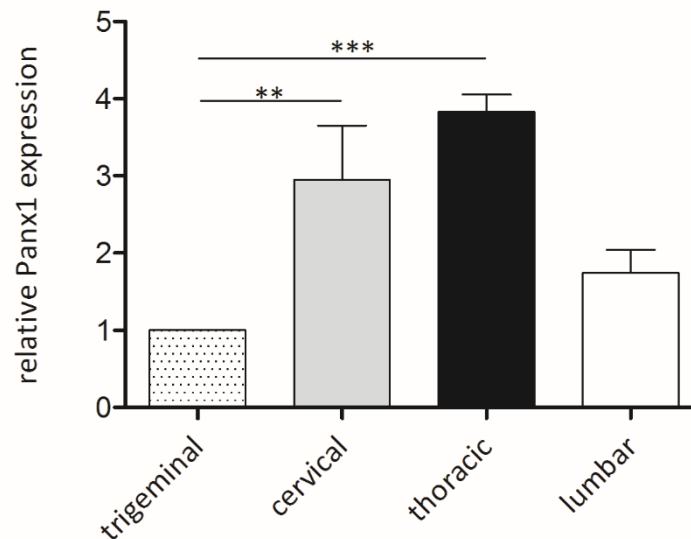
Figure 53. The relative expression of Panx1 in sensory ganglia
Panx1 expression increased significantly in cervical and thoracic ganglia and a reduced thereafter in the lumbar ganglia. The lowest expression level appeared in trigeminal ganglia. 18S rRNA was used as reference gene. Asterisks indicate a significant difference between groups (**$p < 0.01$, and ***$p < 0.001$). Shown are mean values ± SEM.

4.6.7 Relative P2X3R expression in sensory ganglia

Panx1 can associate with several purinergic receptors (Li et al., 2011). P2X3R is the major purinergic receptor expressed in the soma of sensory ganglia (Huang, Gu and Chen 2013). It has higher expression levels in trigeminal ganglia and DRGs than other purinergic family members (Xiang et al., 1998). P2X3R immunoreactivity exhibits more intensity in small-diameter than large- diameter neurons (Xiang et al., 1998). In this context, the relative expression of P2X3R was investigated in studied regions (see Chapter 4.6.6) of sensory ganglia to compare its expression with that of Panx1. P2X3R showed diverse expression levels within sensory ganglia. A significantly lower expression level of P2X3R was observed in trigeminal ganglia compared to cervical and thoracic DRGs (Figure 54). Within DRGs, the thoracic region exhibited the highest expression level of P2X3R, which was decreased significantly in the lumbar region. These results revealed that relative expression levels of Panx1 and P2X3R are very similar within

sensory ganglia of different spinal areas. This provided hints that these genes might be associated in sensory ganglia.
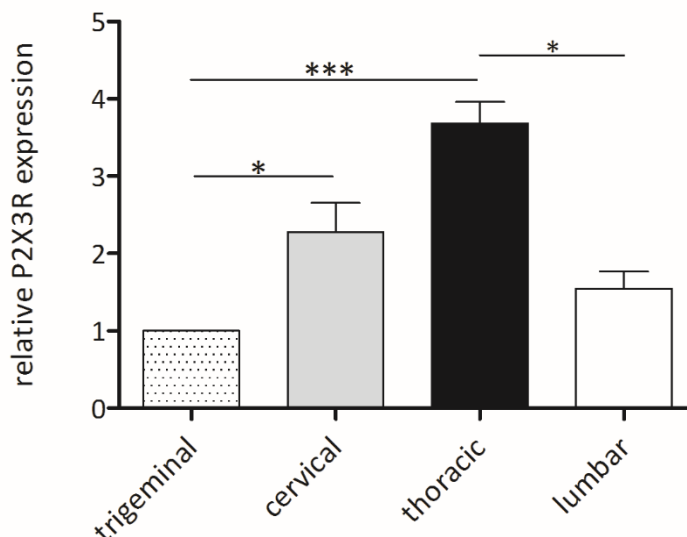
Figure 54. The relative expression of P2X3R in sensory ganglia
P2X3R exhibited the lowest expression level in trigeminal ganglia. This expression level increased significantly in cervical and thoracic ganglia and reduced significantly in lumbar ganglia. 18S rRNA was used as reference gene. Asterisks indicate a significant difference between groups (*p < 0.05, and ***p < 0.001). Shown are mean values ± SEM.

4.6.8   Relative P2X7R expression in sensory ganglia

In contrast to P2X3R, the purinergic receptor P2X7 was abundantly expressed in satellite glia cells (Figure 55), whereas a limited P2X7R expression was found in neurons (Chen et al., 2008). As described above, Panx1 can be associated with P2X7R and activated by ATP stimulation of P2X7R. Therefore, P2X7R expression in sensory ganglia was investigated to determine its expression, as it was done for Panx1 and P2X3R. Within studied regions of sensory ganglia, P2X7R showed a different expression pattern than Panx1 and P2X3R. The highest expression level of P2X7R was observed in trigeminal ganglion, followed by decreasing expression in cervical, thoracic and lumbar ganglia (Figure 56). Lumbar ganglia exhibited a significantly lower expression level than other ganglia. This experiment revealed that P2X7R showed reduced expression compared to P2X3R and Panx1 in sensory ganglia.
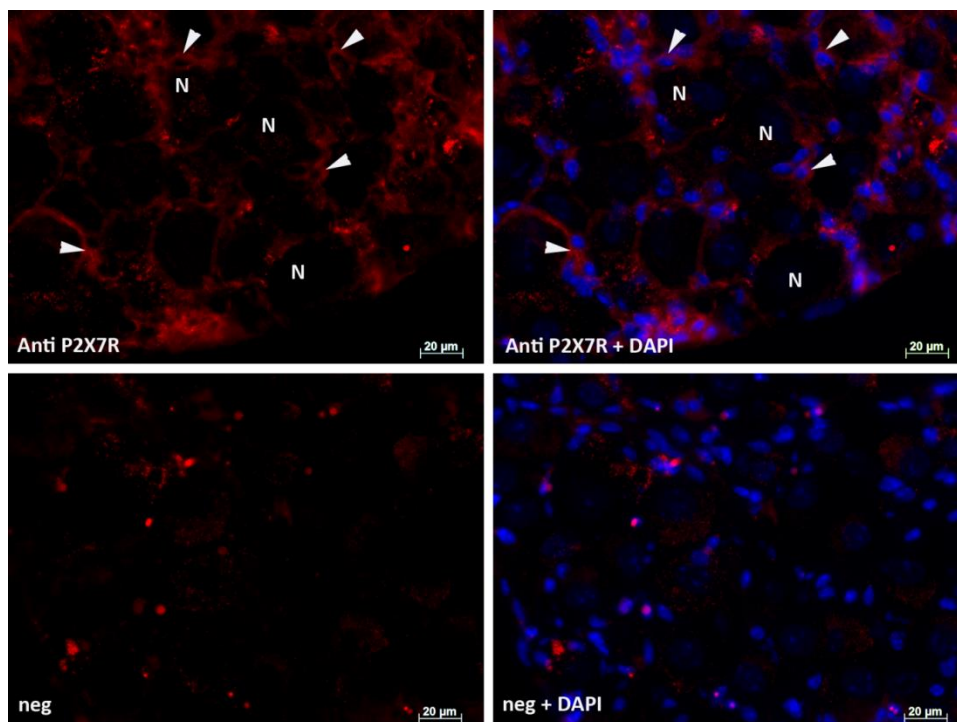
Figure 55. P2X7R expression in sensory ganglia
Immunolabeling of P2X7R in DRGs of an adult mouse showed a specific signal (red staining) in satellite glia cells (arrowheads). Neurons (N) did not exhibit P2X7R immunoreactivity. The erd staining observed in the the negative control without the primary antibody was considered non-specific. DAPI was used as nuclear dye (blue).
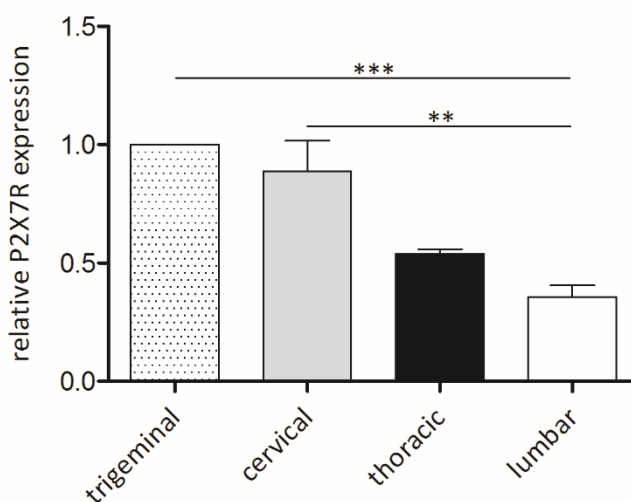
Figure 56. The relative expression of P2X7R in sensory ganglia
The relative expression of P2X7R was higher in trigeminal ganglia than in DRGs. Within DRGs, the expression level declined significantly from cervical to lumbar ganglia. 18S rRNA was used as reference gene. Asterisks indicate a significant difference between groups (**$p < 0.01$, and ***$p < 0.001$). Shown are mean values ± SEM.

5   Discussion

Panx1, one member of the gap junction protein family, forms transmembrane channels. Panx1 protein has a similar topology as connexins and innexins (Ambrosi et al., 2010) by forming four transmembrane domains and by oligomerization into hexameric channels (Boassa et al., 2007). Topologically, Panx1 channels differ from connexins and innexins by possessing N-glycosylation sites on the second extracellular loop (Boassa et al., 2007, Penuela et al., 2007). Panx1 channels can also be pharmacologically distinguished from connexin hemichannels using probenecid (Silverman et al., 2008), a Panx1 inhibitor, or the connexin and Panx1 blocker carbenoxolone (Bruzzone et al., 2005)

Panx1 channels, however, allow the passage of ions and small molecules between the cytoplasm and the extracellular space (Dahl and Keane, 2012). The purine nucleotide (ATP) is the major molecule released via Panx1 channels (Dahl et al., 2013). This molecule was found to be released from neural progenitor cells of mouse fetal neurospheres in episodic burst events (Lin et al., 2007). ATP mediates purinergic signaling, which regulates neural progenitor cells expansion and neurogenesis (Lin et al., 2007). Extracellular ATP, on the other hand, showed a mitotic effect on cells of the subventricular zone after ATP infusion into the lateral ventricle of an adult mouse brain (Suyama et al., 2012).

These data have led to the suggestion that Panx1 might be implicated in the neurogenesis by ATP releases. In this context, Panx1 protein was found to be expressed in a variety of tissues including the nervous system, for instance, in the subventricular zone of the lateral ventricles during postnatal (Wicki-Stordeur et al., 2012) and adult neurogenesis (Wicki-Stordeur and Swayne, 2013). During postnatal neurogenesis, Panx1 showed regulation in the proliferation of neural stem and progenitor cells (Wicki-Stordeur et al., 2012). Panx1 was also involved in cell migration and neurite extension during adult neurogenesis (Wicki-Stordeur and Swayne, 2013).

In mouse development, Panx1 mRNA expression has been described in late stages (from E13.5 onwards), whereas no description of Panx1 expression has been reported in early stages of neurogenesis (up to E12.5). To determine the role of Panx1 in early development, Panx1 mRNA expression was investigated in this study in early embryonic stages (E9.5, E10.5, E11.5 and E12.5) using RT-PCR and whole-mount *in situ* hybridization. These methods revealed that Panx1 was particularly expressed in the developing nervous system. This finding has brought attention to investigate the temporal and the spatial expression of Panx1 protein. Analysis of Panx1 protein distribution showed Panx1 expression in post-mitotic neurons of developing spinal cord and sensory ganglia. In addition, Panx1 expression was examined using Panx1-transgenic mice (Panx1$^{tg/tg}$).

In the second part of the study, the profile of Panx1 expression in spinal cord and dorsal root ganglia was investigated using the activity of the reporter gene *LacZ* in Panx1$^{tg/tg}$ transgenic mice. Panx1 showed a graded distribution in the gray matter of the spinal cord. All sizes of neurons exhibited Panx1 expression in DRGs. Furthermore, the relative mRNA expression of Panx1 and purinergic receptors of P2X3 and P2X7 was comparatively analyzed in spinal cord and sensory ganglia to determine Panx1 expression in studied regions selected questions were also addressed for Panx2.

5.1 The temporal expression of pannexin mRNA in mouse development

Panx1 mRNA expression in mouse development has previously been described in late stages (from E13.5 onwards) (Baranova et al., 2004, Ray et al., 2005). Quantitative analysis showed an increase in the expression level from E14 to E18 in the cortex, cerebellum and eye (Ray et al., 2005). On the other hand, pannexin expression has not yet been described in early stages (up to E12.5) of mouse development. Thus, the first aim of this study was the analysis of the expression of Panx1 and Panx2 mRNA in early stages (E9.5, E10.5, E11.5 and E12.5) of mouse development. At E9.5, whole embryos were used for analysis, whereas at later stages (E10.5, E11.5 and E12.5), head and body were analyzed separately. RT-PCR results revealed that Panx1 and Panx2 are expressed in early stages of mouse development. An equal quantity of cDNA was used of all samples for PCR analysis. This was confirmed through detection of the reference gene 18S rRNA. As head and the body still resulted in different amplification product intensities, both samples might express Panx1 and Panx2 at different level. These results provide the first evidence that Panx1 and Panx2 expression occurs as early as E9.5 and, thus, provides hints that pannexins might be involved in early neurogenesis of the nervous system. Based on these results, the next aim was to investigate the spatial distribution of Panx1 mRNA.

5.2 The spatial expression of Panx1 mRNA in mouse development

In previous studies, the earliest description of Panx1 mRNA was in the brain of E13.5 embryos (Baranova et al., 2004); *in situ* hybridization signal was stronger in the CNS than in other tissues. In the brain of an E18 mouse embryo, *in situ* hybridization analysis revealed that Panx1 was strongly expressed in the cortical plate and subplate as well as in the hippocampus (Ray et al., 2005). In rat

embryo at E14 and E17, radioactive *in situ* hybridization analysis revealed Panx1 expression in the brain and spinal cord (Vogt et al., 2005).

In this study, the distribution of Panx1 mRNA is described in detail in earlier stages of mouse development, particularly at E9.5, E10.5, and E11.5. At these stages, whole mount *in situ* hybridization was successful. However, no hybridization signal was obtained in an E12.5 embryo, although a specific signal was observed in the positive control detecting MyoD mRNA at the same age. The purple staining of the Panx1 cRNA probe was restricted to cephalic ventricles, whereas no staining was observed in the body. This observation did not confirm RT-PCR results, detecting Panx1 expression also in the body. In view of the increasing size of the embryo, these results suggest that the Panx1 cRNA probe might not have reached its target because of longer diffusion distances. The MyoD probe, in turn, might have reached its target within surface muscles more easily. In contrast, the target of Panx1 cRNA probe is located inside the embryo and is protected through recently developed tissues which might hinder the passage of cRNA probe its target in late stages (from E12.5 onwards).

On the other hand, the staining obtained with the antisense Panx1 Ct probe was in general much lower than that of the antisense MyoD probe. This might either indicate a lower diffusion or binding efficiency of the probe, or indicate that the expression level of Panx1 might be lower than the MyoD expression. This can be determined by comparing the expression of both genes using quantitative analyses e.g. real time qPCR.

WM-ISH experiments confirmed RT-PCR results in that Panx1 mRNA is expressed in the head and the body of most studied stages. The expression level increased clearly during development, based on the intensity of the stain. In studied stages, Panx1 is expressed generally in the nervous system as well as in regions outside of the nervous system, which will be discussed in detail (see below).

5.2.1 Panx1 mRNA expression in the telencephalon

The cerebral hemispheres develop from the wall of the telencephalic vesicle during cortical neurogenesis, which occurs from E11 to E17 during mouse development (Vitalis et al., 2013). At E9.5, the telencephalic wall consists initially of bipolar neuroepithelial cells, which proliferate intensely without entering neurogenesis. Some neuroepithelial cells switch from proliferation to neuron-generation at E10.5 of mouse development (Iacopetti et al., 1999). At these stages, particularly E9.5, a very light hybridization staining was observed in the wall of the telencephalic vesicle. The expression became stronger in the E10.5 embryo and the most intense staining of this region appeared in the

E11.5 embryo. At this stage, cortical neurogenesis begins in the ventricular zone (VZ) by generating radial glial cells and post-mitotic neurons. Newly generated neurons migrate along radial glial cells through the subventricular zone to reach their target in the cortical laminae (Sanes et al., 2011). In this study, the purple staining of hybridization was observed in vibratome sections on the apical site of the ventricle wall, suggesting that Panx1 is expressed in the ventricular zone at the beginning of neurogenesis.

Panx1 expression in the wall of telencephalic vesicle in these stages suggests that Panx1 expression is present at the onset of the cortical neurogenesis. Bearing in mind that Panx1 remains expressed in the cortex throughout development and reaches the highest level at E18 (Ray et al., 2005), Panx1 is present during the whole period of cortical neurogenesis. This suggests that Panx1 might play a role in the development of the cortex.

5.2.2 Panx1 mRNA expression in the mesencephalon

Panx1 expression has previously been described in many regions of the adult mesencephalon, i.e. in the superior and inferior colliculus, substantia nigra as well as in the nucleus of the oculomotor nerve (Ray et al., 2005, Zappala et al., 2006). In this study, Panx1 was observed in the roof plate as well as in the basal plate of the mesencephalon at E11.5. The expression increases during development and appears most clearly in E11.5 embryos. Motor neurons in the oculomotor nucleus (III) originate from the basal plate and differentiate between E10 and E12 of mouse development (Wurst and Bally-Cuif, 2001). This suggests that Panx1 in the mesencephalic basal plate might be expressed in motor neurons of cranial nerve (III) at this stage. Therefore, Panx1 might play a role in the development of midbrain.

5.2.3 Panx1 mRNA expression in the metencephalon

The cerebellum develops in the anterior part of the hindbrain (metencephalon) from two regions, the roof plate of the fourth ventricle (ventricular zone) and the rhombic lip of the first rhombomere. The ventricular zone gives rise to all GABAergic inhibitory neurons, including Purkinje cells, Golgi cells, stellate cells, and basket cells, as well as Bergmann glia cells. The rhombic lip, in turn, gives rise to all excitatory glutamatergic neurons, including progenitor cells of granule cells (Basson and Wingate, 2013). At E11.5, these progenitor cells migrate tangentially from the rhombic lip over the ventricular zone to accumulate in a layer named the external granule cell layer (egl) (Figure 57) (Martinez et al., 2013). During postnatal cerebellar development, generated granule cells migrate radially inwards along fibers of Bergmann glia cells to form the internal granule layer (Xu et al., 2013). On the other

hand, cells in the ventricular zone, e.g. Purkinje cells, become post-mitotic between E10 and E13 (Namba et al., 2011, Hawkes, 2012) and migrate along radial glia cells toward the pial surface.
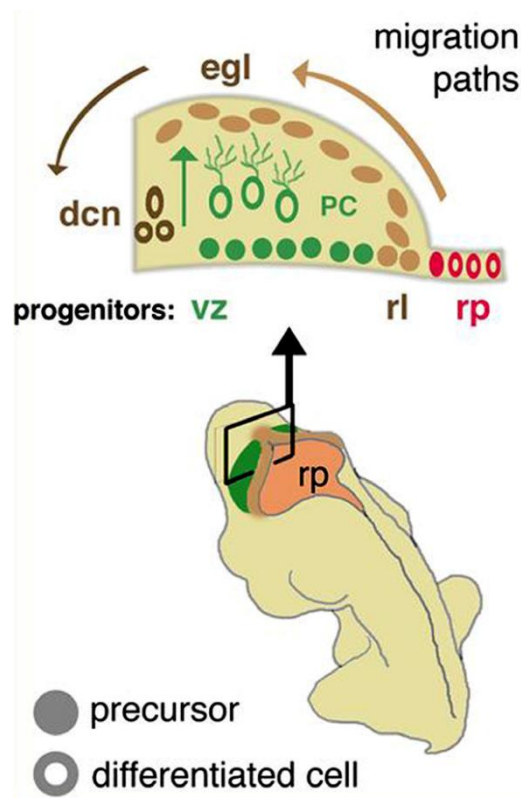
Figure 57. Schematic representation of cerebellum development
The cerebellum originates from two regions: the ventricular zone and the rhombic lip. The ventricular zone (vz) gives rise to all GABAergic neurons including Purkinje cells (pc), which migrate radially outward. The rhombic lip (rl) gives rise to glutamatergic neurons of granule cell precursors and neurons of the deep cerebellar nucleus (dcn), which migrate tangentially from rl over the vz to form the external germinal layer (egl). Postnatal, cells in the egl migrate radially inwards to the internal granule layer (igl). Taken from Basson and Wingate (2013) .

Quantitative analysis showed a high expression level of Panx1 in the cerebellum of E16 and E18 embryos compared to postnatal stages (Ray et al., 2005, Ray et al., 2006). There are, however, no data showing the cellular Panx1 distribution in embryonic stages. In the mature cerebellum, Panx1 is expressed in Purkinje neurons and Bergmann glia cells as well as in Golgi neurons of the granular cell layer (Ray et al., 2006, Zappala et al., 2006, Cone et al., 2013).

In this study, Panx1 mRNA expression was observed on the lip of the rhombencephalon in E10.5 embryos. The expression was more clearly visible in E11.5 embryos, not only in the rhombic lip but also in the ventricular zone, anterior to the first rhombomere. This suggests that Panx1 is expressed in

the early cerebellar neurogenesis in progenitors of both GABAergic and glutamatergic neurons. It appears that Panx1 expression in progenitors of glutamatergic neurons is restricted to the progenitors of granule cells during embryogenesis, as Panx1 is not observed in mature granule cells (Ray et al., 2006, Zappala et al., 2006). On the other hand, Panx1 is still expressed in mature GABAergic neurons.

From the basal plate of the metencephalon originate motor neurons of the trochlear nucleus (IV) (Wurst and Bally-Cuif, 2001). Panx1 expression in the basal plate of the metencephalon suggests that Panx1 might be expressed in motor neurons of the cranial nerve IV at early stages. Panx1 might play a role in the development of this cranial nerve nucleus.

5.2.4 Panx1 mRNA expression in the myelencephalon

The segmentation of rhombomeres appears in early hindbrain development (see Chapter 4.3.2). Each rhombomere gives rise to motor neurons, which belong to a defined cranial nerve, e.g., progenitor cells in rhombomeres r2 and r3 give rise to motor neurons of the trigeminal nerve V, which innervates radially muscles (Sanes et al., 2011).

For various connexin isoforms, characteristic spatiotemporal expression patterns were described in hindbrain development. Connexin 31 was the first connexin discovered in hindbrain development (Dahl et al., 1997). Cx31 shows a segment-specific expression in a very short developmental window between E8 and E11. The expression is restricted to two rhombomeres (r3 and r5) only (Jungbluth et al., 2002). Cx43 is also expressed in hindbrain development from E9.5 onward, visible as longitudinal stripes in the medial hindbrain from rhombomere 1 onwards. On the other hand, Cx36 expression starts later, from E10.5 onwards, and is visible as continuous columns posterior to rhombomere 4 (Jungbluth et al., 2002).

In this study, Panx1 was not detectable in the rhombencephalon of E9.5 embryos. Expression was firstly detected at E10.5. The spatial expression of Panx1 was very similar to that of Cx36 expression in the lip of rhombomeres. However, Panx1 showed a homogenous expression in all rhombomeres of E11.5 embryos, not only in posterior rhombomeres as described for Cx36. Interestingly, Cx36 has been found to regulate neuronal differentiation of neural progenitor cells *in vitro* (Hartfield et al., 2011). Because of the similar spatial and temporal expression of Cx36 and Panx1, one might hypothesize a comparable role in myelencephalic neurogenesis.

5.2.5 Panx1 mRNA expression in the spinal cord

In spinal cord development, spinal progenitor cells in the ependymal layer proliferate and give rise to post-mitotic neurons (Arber, 2012). Neurons, which are derived from different progenitor cells, migrate radially to their target destination in the mantle layer. Migrated neurons create laminal subpopulations in the gray matter of spinal cord. Many connexin isoforms are expressed during spinal cord development. Cx36, Cx37, Cx40, Cx43, and Cx45 expression was observed in E15 and E18 rat embryos (Chang et al., 1999). These connexins exhibit a different spatial distribution within the dorsal and ventral horn. On the other hand, there is to date only one publication stating Panx1 mRNA expression in embryonic spinal cord: Panx1 was observed in sagittal sections of E14 and E17 rat embryos using radioactive *in situ* hybridization (Vogt et al., 2005).

In this study, Panx1 expression was detected firstly in the truncal region of E9.5 embryos. The expression increased and spread towards the caudal region of the E10.5 embryo. In E11.5 embryos, Panx1 was observed in all spinal segments. Transverse vibratome sections of E11.5 embryos post WM-ISH showed a very light Panx1 signal in the mantle layer of the ventral horn. No labeling was detectable in the ependymal layer. These results were confirmed by β-Gal staining, which appeared in the mantle layer of all spinal segments. The absence of Panx1 expression in the ependymal layer gives a hint that Panx1 might be not implicated in cell proliferation during spinal cord development, as most cells in the mantle layer are already post-mitotic.

5.2.6 Panx1 mRNA expression in sensory ganglia

Panx1 expression in sensory ganglia has been firstly noted by Baranova et al. (2004) . Panx1 was observed in trigeminal ganglia and DRGs in a sagittal section of an E13.5 embryo using *in situ* hybridization. There are no further descriptions about Panx1 expression in embryonic stages of sensory ganglia development. As mentioned above (see Chapter 1.3.1), neural progenitors of trigeminal, geniculate, spiral and vestibular ganglia start migrating from their placodes and neural crest at the beginning of neurogenesis between E8.5 and E9 to form an accumulation of ganglion tissues.

In this study, Panx1 mRNA expression was observed in cranial ganglia immediately after the beginning of neurogenesis, i.e. in trigeminal ganglion and in the facio-acoustic ganglion complex (VII-VIII) of E9.5 embryos. The expression increased during development within studied stages, the highest expression was observed in E11.5 embryos. This observation was confirmed in vibratome sections, which also revealed an additional expression site at the inferior ganglion of the vagus nerve (not shown). This ganglion had previously not been observed by photographing whole-mount embryos. Even the

expression in DRGs was observed for the first time in vibratome sections as a very light staining of *in situ* hybridization. This signal was also confirmed in paraffin-blocks after β-Gal staining. These results are in concordance with other recent studies, showing Panx1 expression in many cranial ganglia of adult rodents, e.g. in trigeminal ganglion (Hanstein et al., 2013), in the nodose-petrosal-jugular complex (Retamal et al., 2014), in spiral and vestibular ganglia (Tang et al., 2008).

This study, however, also revealed that Panx1 mRNA is expressed in most sensory ganglia, including cranial nerve sensory ganglia and dorsal root ganglia, immediately after the beginning of the neurogenesis, and that its expression increases during development.

5.2.7 Panx1 mRNA expression in the developing eye and ear

Panx1 showed, in previous studies, a stable expression during cochlea development from E16.5 to P45 using RT-PCR (Tang et al., 2008). In E16.5 embryos, Panx1 was observed in epithelial cells of the developing organ of Corti (Tang et al., 2008). In this present study, Panx1 expression appeared in the inner side of the otic vesicle at E11.5. The otic vesicle gives rise to the cochlear duct (Phippard et al., 1999), suggesting that Panx1 might play a role in the development of the cochlear duct. In adult cochlea, Panx1 is also expressed in the organ of Corti and in further regions e.g. in the spiral limbus as well as in inner and outer sulcus cells (Tang et al., 2008, Wang et al., 2009). It is well known, on the other hand, that mutations in connexins can cause the deafness in human patients and animal models (Sanchez and Verselis, 2014). In the human genome, the location of nonsyndromic sensorineural deafness DFNA11 region on loci 11q12.3–q21 overlaps with the *Panx1* gene location on chromomsome 11q14.3 (Wang et al., 2009). Panx1 was shown to be expressed in the inner ear (Wang et al., 2009). However, calcium signals showed identical propagation in organotypic cochlear cultures of wildtype and Panx1-deficient mice (Anselmi et al., 2008). Thus, the functional role of Panx1 in hearing physiology still needs to be elucidated.

In the optic cup, it was difficult to distinguish the purple staining in WM-ISH from the retinal pigment. In contrast, β-Gal staining was easily distinguishable in E11.5 embryos. This staining revealed that Panx1 is expressed in the eye of E11.5 embryos. In a previous study, quantitative analysis of Panx1 expression in the eye showed that Panx1 expression increased during mouse development from E14 to E18 and declined thereafter sharply in postnatal and adult stages (Ray et al., 2005). The β-Gal signal observed in the optic cup indicates Panx1 expression in the retina at early stages. Thereby, Panx1 might be involved in the development of the retina. Its function might be comparable to that of Cx43 in retinal development (Cook and Becker, 2009). Cx43 has been found to regulate the proliferation of

retinal neuronal progenitors in the retinal pigment epithelium of chicken embryos at E5 (Pearson et al., 2005).

5.2.8 Panx1 mRNA expression in the branchial arch and forelimb plate

Panx1 is clearly expressed in the surface ectoderm of the first branchial arch and in the apical ectodermal ridge (AER) of the developing forelimb in E11.5 embryos. Panx1 expression in embryonic skin was previously reported in dermis and epidermis of E13.5 mouse embryos (Celetti et al., 2010). The expression level of Panx1 was reduced in the adult skin compared to postnatal stages (Celetti et al., 2010). In neonatal skin, keratinocytes, fibroblasts and hair follicles exhibit a high expression level of Panx1. Panx1 regulates keratinocyte migration and dermal fibroblast proliferation (Penuela et al., 2014a). Panx1 deletion resulted in dysregulation of keratinocyte migration and increasing proliferation of dermal fibroblasts (Penuela et al., 2014a). Moreover, Panx1 was expressed in the AER which directs outgrowth of the limb along the proximal axis (Casanova et al., 2011). This expression at the ectodermal ridge might provide hints that Panx1 is involved in skin development or that it might guide the outgrowth of the apical ridge through the interaction between Panx1 and cytoskeletal proteins β-actin and arp3 (actin related protein 3) (Wicki-Stordeur and Swayne, 2013).

5.3 Panx1 protein expression in mouse development

Panx1 mRNA expression was temporally and spatially investigated in mouse development. To date, Panx1 protein expression had not been reported at these early stages (E9.5 – E12.5). A polyclonal antibody against Panx1 (antiserum) was generated in the rabbit and used to detect Panx1 protein.

The antiserum detected multiple protein bands using the method of immunoblotting. The intensity of the immunoreactive products was reduced using antiserum pre-absorbed with Panx1-synthetic peptides used to generate the antibody. The antiserum required a long pre-incubation time for a complete blocking. A forty-times excess of peptides did not block the antiserum completely after a short pre-incubation time of two hours, whereas a tenfold excess of peptides was able to block binding completely after a prolonged incubation time of 48 hours. However, immunolabeling required more peptides (60x) for complete blocking than immunoblotting (10x peptides), as antibody concentrations for immunolabeling are generally chosen higher than for immunolabeling.

The antiserum showed specific detection on cryosections of defined tissues. In the cerebellum, the antiserum detected Panx1 protein in Purkinje cells and in cells of the granule cell layer. This confirms

the description by Ray et al. (2005) and Zappala et al. (2006). Additional positive cells were also detected in the molecular cell layer. These positive cells were also observed using the Mo503 antibody (Cone et al., 2011) as recently described by Cone et al. (2013). The antiserum detected Panx1-immunopositive cells in most retinal layers, which is in agreement with the results published by Ray et al. (2005) and Kranz et al. (2013).

In summary, immunoblotting and immunolabeling analyses demonstrated the specificity of the antiserum as based on the comparison to negative controls of preabsorbed antiserum and to PIS.

5.3.1　The temporal expression of Panx1 protein in mouse development

Panx1 protein has a molecular mass of 48.07 kDa, but multiple protein bands were exhibited on immunoblots of studied stages. Posttranslational modification of Panx1, e.g. glycosylation, can cause multiple protein bands on the immunoblot (Boassa et al., 2007, Penuela et al., 2007). This might explain the presence of multiple immunoreactive proteins between 46 and 55 kDa observed in the immunoblot using the Panx1 antiserum. These proteins were not visible in the negative controls, using PIS or preabsorbed antiserum, of body samples, but were visible in all head samples and in the E9.5 embryo.

The E9.5 embryo and all body samples exhibited also an immunoreactive product at 32 kDa. This product was not detected in the negative control of PIS or by preabsorbed antiserum. It has been recently reported that Panx1 can be expressed in three splice variants; Panx1a (48 kDa), Panx1c (40 kDa), and Panx1d (34 kDa) (Li et al., 2011). However, the protein detected at 32 kDa in the present study cannot be the isoform Panx1d (Table 2). This isoform lacks most of the C-terminus (Li et al., 2011), including the epitope sequence of the peptide used for immunization. Other studies showed that the Panx1 sequence includes two caspase cleavage sites (A and B) (Chekeni et al., 2010). Different products can be predicted from these two caspase cleavage sites, i.e. proteins of 6, 19, 24, 30, and 42 kDa (Figure 58). Only the protein products of 6 and 30 kDa can theoretically be detected with the Panx1 antiserum, as these products include the peptide sequence used for immunization. This suggests that the immunoreactive product of 32 kDa might be a cleavage product. No protein product of 6 kDa, on the other hand, was detected in the present study.

On the immunoblot, an immunoraction product was observed at 17 kDa in E9.5 and body samples or at 20 kDa in head samples and was not visible in the negative control of PIS or preabsorbed antiserum.

This protein, however, is larger than the predicted cleavage product 6 kDa. Therefore, the nature of this product is still unknown although it shows Panx1 immunoreactivity.

Taken together, the data showed that Panx1 protein was expressed in all studied stages in both the head and the body. This was also confirmed by RT-PCR results, showing Panx1 mRNA expression in these stages. Panx1 protein might be present in different forms during mouse development, e.g. in glycosylated and un-glycosylated forms. Penuela et al. (2007) found that glycosylation of Panx1 was required for trafficking of the protein from the endoplasmic reticulum into the plasma membrane. This suggested that Panx1 might exhibit different subcellular localization, for instance in the cytoplasm and in the cell membrane, and these might possibly be associated with different functions during development.

Given that one observed immunoractive product of 32 kDa could present a cleavage product of caspase-3, Panx1 might be activated by caspase cleavage (Sandilos et al., 2012). This interaction between Panx1 and caspase-3 might also be required during development. Caspase-3 was found to play a nonapoptotic function in development (D'Amelio et al., 2010), mediated through regulation of neural stem cell differentiation and neurite extention (Fernando et al., 2005). Furthermore, caspase-3 deficient mice (CPP32^{-/-}) showed a strongly affected nervous system (D'Amelio et al., 2010); E11.5 embryos of CPP32^{-/-} showed obvious brain aberrations, which were caused by cell number increase. These results suggest, that Panx1 might also interact with caspase-3 in nervous system development. This hypothesis needs further evaluation. The determination of Panx1 protein distribution in studied stages will help understanding Panx1 function during development.
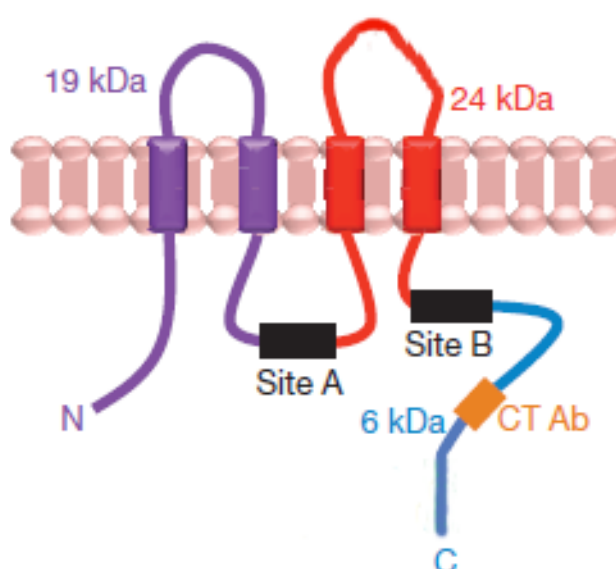

Figure 58. Predicted caspase cleavage sites in Panx1 protein

An illustration of Panx1 indicates the predicted caspase cleavage sites (sites A and B). The predicted product of each fragment is shown. CT indicates the epitope of Panx1 antiserum. Modified from Chekeni et al. (2010).

5.3.2   The spatial distribution of Panx1 protein in mouse development

The spatial distribution of Panx1 protein was investigated in regions of the head and the body of E11.5 embryos, as Panx1 mRNA was more abundantly expressed at this stage than at E9.5 or E10.5. The antiserum detected Panx1 in trigeminal ganglion and in the mantle layer of spinal cord as well as in DRGs. No expression was detectable in the dorsal horn and in the ventricular zone as well as in the floor plate of spinal cord. This confirmed the distribution of Panx1 mRNA in these regions, and also immunoblotting results showing Panx1 protein expression in the head and the body of E11.5 embryos. Panx1-positive cells in the mantle layer and in DRGs were co-labeled with the neuronal marker NeuN. However, not all NeuN-positive cells in these regions were Panx1-positive. This suggested that Panx1 protein expression was restricted to a defined cell subpopulation in these regions. The colocalization of Panx1 with NeuN indicated that Panx1 is expressed in post-mitotic neurons, which start to differentiate into mature neurons. NeuN is expressed in the nucleus and the cytoplasm of neurons at the post-mitotic stage (Mullen et al., 1992, Lavezzi et al., 2013). On the other hand, at this stage, the ventricular zone represents mitotically active cells, which express the cell cycle protein Ki67 (Battiste et al., 2007). In contrast, cells of the mantle layer do not express this protein. This confirmed that Panx1 is expressed in the region of post-mitotic neurons and is absent in the area of mitotic cells (ventricular zone). This is in contrast to the description of Panx1 expression in the developing rat cerebellum. Both, proliferating neurons (Ki67-positive cells) and non-proliferating neurons exhibit Panx1 mRNA expression (Vogt et al., 2005). This suggests that the role of Panx1 might vary within regions of the nervous system during neurogenesis.

On the other hand, Panx1 might play a role in post-mitotic events of neurogenesis e.g. migration, differentiation, or neurite outgrowth. Interestingly, Panx1 shows an influence on cellular behaviors of cell migration and neurite extension (Wicki-Stordeur and Swayne, 2013). During postnatal neurogenesis, Panx1 regulates negatively neurite outgrowth. Knockdown of Panx1 induces the extension of neurites, while Panx1 overexpression inhibits the outgrowth of neurites (Wicki-Stordeur and Swayne, 2013). In Neuro-2a cells, Panx1 knockdown reduced cell migration (Wicki-Stordeur and Swayne, 2013). This suggests that Panx1 expression in neurons of spinal cord or DRGs during early embryogenesis might regulate the extension of neurites or induce migration of neurons to the target destination. Other studies showed that connexin hemichannels are involved in spontaneous electrical activity, which affects a variety of developmental processes (Moore et al., 2014). The hemichannel

blocker carbenoxolone showed a significantly blocked spontaneous activity in the human fetal cortex (Moore et al., 2014). Thus, it is of interest to know if Panx1 in post-mitotic neurons contributes also to spontaneous electrical activity in spinal cord, which was identified in the motor neuron region at early stages of mouse spinal cord development (E11) (Hanson and Landmesser, 2003). This finding requires, however, further physiological analysis using a Panx1 blocker, i.e. probenecid.

5.4   Panx1 expression in transgenic mice

As described in Chapter 3.2.2, Panx1-transgenic mice (Panx1[tg/tg]) (Anselmi et al., 2008) and Panx2-transgenic mice (Panx2[tg/tg]) (Bargiotas et al., 2011) were generated by inserting the bacterial gene *LacZ* into exon1 of *Panx1* and of *Panx2* genes via homologous recombination. This insertion is detectable by PCR analysis and by β-Gal staining of transgenic tissues. Due to the insertion, mRNA transcription of Panx1 and Panx2 is prevented through the insertion of an off-frame stop codon, and, consequently, Panx1 mRNA and Panx2 mRNA were not present in Panx1[tg/tg] and Panx2[tg/tg] mice, respectively. These results confirm the description of Bargiotas et al. (2011) that Panx1[tg/tg] and Panx2[tg/tg] express no Panx1 or Panx2 mRNA, respectively, as determined by real time qPCR and *in situ* hybridization analyses.

Panx1 protein expression was not detectable in the retina of Panx1[tg/tg] mice using immunolabeling analysis. This finding confirms that transgenic animals lack Panx1, as immunopositive cells were clearly visible in the ganglion cell layer and in the inner nuclear layer of wildtype animals. Thus, these results also indicate that the antiserum exhibits a specific signal.

Using immunoblotting analysis, however, the Panx1 antiserum detected proteins in tissues of transgenic animals similar to those observed in wildtype tissues. Proteins with a molecular weight of 35 and 32 kDa were present in brain and cerebellum lysates of Panx1[tg/tg] mice, in addition to a protein at 14 kDa. Commercial antibodies (Table 2) also detected proteins in Panx1[tg/tg] similar to those in the wildtype. It is difficult to bring these results in line with RT-PCR results of this study or with immunoblotting analysis of Bargiotas et al. (2011).

The sequence of peptides, which were used to generate the Panx1 antiserum, was used in several studies (Penuela et al., 2007, Penuela et al., 2009, Bargiotas et al., 2011, Cone et al., 2013, Penuela et al., 2014a). Some of these studies used Panx1-deficient animals to examine the specificity of purified antibodies. Bargiotas et al. (2011) did not observe immunoractive proteins in brain tissue lysate of Panx1[tg/tg], using the same animals as in the present study. In other Panx1-deficient animals, described by Qu et al. (2011), this purified antibody did not detect any immunoractive proteins in thymus or

spleen lysates as described by Penuela et al. (2014a), whereas small protein bands were still detectable using brain lysates of these animals (Cone et al., 2013).

In the study of Cone et al. (2013), the immunoreactivity of several Panx1 antibodies was compared. Whereas used antibodies reacted similar by immunolabeling and immunoblotting of cultured cells, different immunoreactivities were observed by immunoblotting of brain lysates of knockout and control mice. Immunolabeling also showed different subcellular localizations. Dendrites were preferably labeled using the antibody against the N-terminus of Panx1, whereas the cell body was labeled using antibodies against the C-terminus or the intracellular loop. These differences might be due to different subcellular localizations of modified or non-modified Panx1-protein.

Interestingly, similar results were obtained for Panx2$^{tg/tg}$ animals. Panx2 antibodies displayed a similar pattern of immunoreactivity in wildtype and transgenic animals, whereas Panx2 mRNA was not present in Panx2$^{tg/tg}$. These results reflect the finding by Bargiotas et al. (2011), who also found that only one generated and purified antibody against Panx2 reacted specifically in transgenic mice, whereas two other commercial antibodies reacted unspecifically (Bargiotas et al., 2011).

Similar data were obtained for Panx1: Numerous antibodies against Panx1 had previously been investigated using these transgenic mice (Bargiotas et al., 2011). Six antibodies did not pass the immunoblotting test; four of them were commercial antibodies. Only one purified antibody reacted specifically. This antibody was directed against the same peptide epitope, which was used for immunization in this study. Therefore, it is preferable to purify the antiserum, e.g. using antigen-specific affinity purification, and analyze the specificity on different tissues from the CNS and other organs, e.g. liver or spleen.

5.4.1 Phenotypic analysis of transgenic spinal cord

Pannexin mutant animals were used in several studies to determine the role of pannexin in organs or diseases. For instance, Panx1 was shown to modulate wound repair upon injury in the neonatal mouse skin (Penuela et al., 2014a). Panx1 knockout mice delayed wound healing from dorsal skin (Penuela et al., 2014a). In other study, Panx1 appeared to have a pathological role in ischemic retina (Dvoriantchikova et al., 2012). Panx1 deletion suppressed the inflammasome and IL-1b production *in vivo* in post-ischemic retinal ganglion cells. Thereby, the loss of retinal ganglion cells was also protected by Panx1 deletion (Dvoriantchikova 2012). On the other hand, the role of Panx1 in brain ischemia is still not clear (Bargiotas et al., 2011, Cisneros-Mejorado et al., 2015). The propagation of cortical

spreading depolarization, which relies on hemichannels or gap junction, was not affected in the absence of Panx1 and Panx2 (Bargiotas et al., 2011). In a model of MCAO, however, inhibition or deletion of Panx1 significantly decreased the infarct volume and reduced motor symptoms, suggesting Panx1 to be a major player in brain damage after ischemia (Cisneros-Mejorado et al., 2015).

However, Panx1 mutant animals were generally described as viable, and fertile and they did not show any obvious developmental or behavioral abnormalities. Histological analyses of neonatal mouse skin did not reveal any obvious skin phenotype in Panx1-deficient mice (Penuela et al., 2014a) other than changes in the thickness of skin layers. The thickness of epidermal and dermal layers was reduced whereas the thickness of hypodermal adipose tissue was increased in Panx1-deficient mice (Penuela et al., 2014a).

Phenotypic analysis of the thoracic region of spinal cord was performed on histological sections. No obvious morphologic difference was observed using microscopic analysis on paraffin section after Masson Goldner staining. This suggested that in spinal cord, Panx1-deficiency did not result in any obvious morphologic phenotype, or that compensatory mechanisms took over, for instance by increasing expression of connexin hemichannels.

5.5 Panx1 gene expression in spinal cord

Panx1 gene expression in spinal cord was detected indirectly using β-Gal staining. Panx1 distribution in spinal cord showed a temporal regulation. The number of Panx1-positive cells was higher in postnatal stages (e.g. P12) than in embryonic stages (E18.5) or in adult mice. This expression pattern was not identical to the temporal expression of Panx1 mRNA described for cortex and cerebellum development (Ray et al., 2005), as the highest level of Panx1 mRNA in these two regions appeared at embryonic stage E18 and was reduced from postnatal to adult stages. The reduction of Panx1 expression from postnatal to adult has also been reported in other regions. In the skin, Panx1 protein expression was higher in up to 4-week-old mice than in adult mice (Penuela et al., 2014a). However, Panx1 expression was not constant during development and had the lowest level in adult animals. This is similar to Cx37 mRNA expression which showed a significant increase in the first two postnatal weeks and a reduction in following stages of rat neocortex development (Prime et al., 2000).

Panx1 was present in all spinal segments of 4-week-old Panx1$^{tg/tg}$ mice. The posterolateral tract exhibited intensively the β-Gal staining along the spinal cord. In contrast, Panx1 was not detectable in the dorsal funiculus or in the ventral funiculus.

Transverse spinal cord sections showed heterogeneous distribution of Panx1 gene expression. Panx1 showed a graded distribution within the gray matter of studied stages (E18.5, P9, P12, and adult). The density of Panx1-β-Gal-positive cells in the dorsal region (laminae I-V) was significantly higher than in the ventral region (laminae VII-X) of P12 spinal cord. This was confirmed by the ratio of Panx1-β-Gal-positive cells to negative cells in these regions. In contrast to the ventral region (lamina VIII and IX), the dorsal region (lamina I-III) showed the highest level of Panx1-β-Gal expression according to this optical analysis.

In a previous study, Panx1 protein distribution was immunohistochemically detected only in the ventral region of adult spinal cord, i.e. in laminae VII, VIII, and IX (Zappala et al., 2006). Performing β-Gal staining, however, in this study a positive signal was also detected in dorsal laminae of the spinal cord. These differences might be explained by the methodology used. Immunolabeling determines the localization of a protein within the cell, whereas β-Gal staining reports the activity of a gene promoter without pointing to the localization of the protein. β-Gal staining is generally observed in the cell body of positive cells. On the other hand, proteins in the nervous system can be located very distant from the cell body e.g. in the periphery of the axon or dendrite. Panx1, for example, exhibits a post-synaptic localization in neurons of cortex and hippocampus (Zoidl et al., 2007). This suggests that the Panx1 protein of dorsal horn neurons might be not located in the cell body but in the periphery outside of the spinal cord. This might explain the absence of Panx1 protein in the dorsal horn as reported by Zappala et al. (2006), whereas in the ventral horn, Panx1 protein showed a cytoplasmic localization in motor neurons (Zappala et al., 2006). Zappala et al. (2006) also provides an alternative explanation for the absence of Panx1 protein from the dorsal horn. Panx1 protein in this region might be modified so that epitopes for the antibody used are masked and cannot be detected. However, Panx1 protein expression in the dorsal horn has been recently reported in lumbar segments of rat spinal cord using immunoblotting analysis (Bravo et al., 2014). This finding confirms results in the present study that Panx1 is expressed in the dorsal horn of spinal cord.

Panx1 mRNA and protein are also expressed in non-neuronal cells of the spinal cord. Panx1 immunoreactivity was detected in cultured astrocytes, which were obtained from postnatal rat spinal cord (Garre et al., 2010). Isolated microglia from embryonic spinal cord at E13.5 also exhibited Panx1 expression (Rigato et al., 2012). In intact animals, microglia seem to be homogeneously distributed in both the white and gray matter of spinal cord (Zhang et al., 2008). In the present study, the signal of β-Gal staining was restricted to the gray matter; no expression was detected in the white matter of all studied stages. Therefore, Panx1 expression in microglia might be very low or absent so that these cells are not detectable by β-Gal staining. Generally, β-Gal staining was used for determination of Panx1

distribution in spinal cord without defining particular cell types expressing Panx1. As described in Chapter 4.6.1, best results of β-Gal staining were obtained using glutardialdehyde fixation. This fixation is unsuitable for immunochemical staining, as glutardialdehyde causes an excessive crosslinking of proteins and thus antigens will be masked (Renshaw, 2007). Therefore, further analyses of cell types expressing Panx1 by double labeling were limited.

The graded distribution of Panx1 gene expression in spinal cord revealed that the dorsal part of the spinal cord exhibited more Panx1-β-Gal-positive cells than the ventral part. This observation, however, was not confirmed by the quantitative method of real time qPCR, which revealed that Panx1 mRNA expression in the ventral region was significantly higher than in the dorsal region of adult mice. By PCR, neural cells of the ventral horn were shown to express more Panx1 mRNA than those of the dorsal horn. Thus, the relative expression of Panx1 mRNA is dissimilar to the number of β-Gal-positive cells, thereby not allowing the comparison between results.

In contrast to Panx1 expression, Panx2 exhibited clearly a higher expression in the dorsal region of spinal cord than in the ventral region as determined by qPCR analysis. This result revealed that Panx2 expression in spinal cord shows an expression complementary to Panx1.

5.5.1   Association of Panx1 and P2X3R and P2X7R in spinal cord

ATP release is one major role of Panx1 channels (Dahl et al., 2013), and ATP itself is a widespread intercellular signaling molecule in the nervous system. This molecule is involved in several mechanisms, for instance neurotransmission or regulation of proliferation (Cotrina and Nedergaard, 2009). On the other hand, Panx1 channels were found being activated via purinergic receptors after extracellular stimulation by ATP (Locovei et al., 2006b). P2X7R, a subtype of purinergic receptors, was found to be expressed in neurons of the dorsal and ventral horn of rat spinal cord using *in situ* hybridization (Deuchars et al., 2001). The protein of P2X7R showed localization in the presynaptic terminal of the intermediolateral cell column of spinal cord (Deuchars et al., 2001). Whereas P2X7R has been described to be associated with motor neurons pathways (Deuchars et al., 2001), P2X3R was described in association with sensory pathways (Nakatsuka and Gu, 2006). P2X3R protein was observed in the superficial laminae (I and II laminae) of the dorsal horn in spinal cord (Novakovic et al., 1999).

This led to investigate the association between Panx1 and purinergic receptors in spinal cord. In the present study, the relative mRNA expression of P2X3 and P2X7 was compared between the dorsal and

the ventral region of spinal cord. Similar patterns were found for the relative expression of both receptors P2X3 and P2X7. However, the dorsal region exhibited significantly lower expression levels than the ventral region. This expression was similar to the Panx1 mRNA expression pattern in adult spinal cord. Bearing in mind that Panx1 was found to be associated with P2X7 receptor in macrophages (Pelegrin and Surprenant, 2006), relative mRNA expression results provided hints that Panx1 might be also associated with the purinergic receptors P2X3 and P2X7 in adult spinal cord. This association might regulate ATP release, which is among other functions involved in peripheral and central nociceptive transmissions, including the mechanism of neuropathic pain (Ide et al., 2009).

In this context, it is of interest that P2X7 receptors were upregulated after peripheral nerve injury. P2X7R mRNA and protein were highly expressed in the dorsal horn of spinal cord after peripheral nerve injury obtained by transection of the tibial and common peroneal nerves (Kobayashi et al., 2011). The intrathecal blockade of P2X7R using a specific antagonist suppressed the development of mechanical hypersensitivity for 3 to 7 days after injury (Kobayashi et al., 2011). In a recent study, Panx1 was also shown to be involved in the mechanisms underlying central sensitization in neuropathic pain (Bravo et al., 2014). The blockade of Panx1 channels in spinal cord through intrathecal injection of 10Panx (a mimetic inhibitory peptide of the first extracellular loop blocking Panx1 channels (Pelegrin and Surprenant, 2006)), probenecid, or carbenoxolone reduced the spinal C-reflex wind-up reactivity in intact animals (Bravo et al., 2014). Furthermore, this blockage reduced also the mechanical hyperalgesia in the neuropathic rat for a short time (Bravo et al., 2014).

The present study revealed that Panx1 is expressed in spinal cord development, in both the dorsal and the ventral regions. Panx1 expression is temporally regulated, shows an increase in postnatal and a decrease in adult animals, and exhibits a heterogeneous distribution in the gray matter. Panx1 might be associated with purinergic receptors of P2X3 and P2X7 in adult spinal cord.

5.6   Panx1 expression in sensory ganglia

This study provides the first description of Panx1 distribution in DRGs using β-Gal staining. Panx1 was abundantly expressed in all neuronal cell types, i.e. small, intermediate, and large diameter neurons of P9 animals. Some satellite glia cells were also β-Gal-positive at this stage (P9). As 40 % ± 10 of all neurons were Panx1-positive in each of the neuronal cell types, Panx1 shows a universal expression in all cell types of P9 mice. It is unknown, whether Panx1 is still universally expressed or if there is a change to the restricted expression in a defined cell type in the adult. For the purinergic receptor

P2X3R, expression switches during postnatal development of mice from a universal expression to a restricted expression in 47.5 % ± 2.8 of neurons at P14 (Ruan et al., 2004). P2X3R is also expressed in small and intermediate neurons (Ruan et al., 2004). Both proteins, Panx1 and P2X3R, show a similar ratio of positive neurons in postnatal stages, in addition to their expression in small and intermediate neurons. This suggests that Panx1 and P2X3 might be coexpressed in DRGs. This suggestion needs further analyses, i.e. immunohistochemistry for both proteins.

Panx1 expression was observed in all DRGs and trigeminal ganglia of postnatal mice, and Panx1 was heterogeneously expressed within these ganglia. Whole mount β-Gal staining of spinal cord with attached sensory ganglia showed that all DRGs are β-Gal-positive, as well as the trigeminal ganglion. The expression level, however, was significantly higher in thoracic ganglia than in other ganglia. In contrast, the trigeminal ganglion showed the lowest expression of Panx1. This expression pattern was very similar to the expression pattern of the purinergic receptor P2X3. On the other hand, the purinergic receptor P2X7 showed a very different expression pattern within sensory ganglia. The expression level of P2X7R was significantly higher in trigeminal ganglion than in DRGs of all regions, which showed a graded reduction in P2X7R expression.

These results revealed that Panx1 is widely expressed is sensory ganglia. In DRGs, Panx1 was universally expressed in neurons and very few SGCs were found Panx1-positive. Whereas Panx1 shows an association with both purinergic receptors P2X3 and P2X7 in spinal cord, Panx1 in sensory ganglia might be associated with P2X3R but not with P2X7R. However, Panx1 expression in the soma provides a hint that Panx1 might be involved in the communication between neurons and SGCs, for instance through release of second messengers like ATP (Huang et al., 2013).

Neuronal somata in sensory ganglia are isolated from each other, they are warped completely with satellite glial cells (SGCs) forming a structural unit (Hanani, 2005). SGCs communicate with each other through gap junctions (Figure 59), which permit electrical and metabolic communication between glial cells. On the other hand, no gap junction formation was observed between SGCs and the soma surrounded by these cells (Huang et al., 2013). Sensory neurons communicate with associated SGCs via the release of transmitters. ATP is the major transmitter in sensory ganglia binding to purinergic receptors. P2X7R is the unique subtype of metabotropic receptors expressed in SGCs (Chen et al., 2012), whereas P2X3R is expressed in small and intermediate sensory neurons (Ruan et al., 2004).

Released ATP, which serves as a pain mediator (Hamilton and McMahon, 2000), activates P2X7 receptors in SGCs after painful injury (Zhang et al., 2007). This activation leads to release of tumor

necrosis factor-α (TNF-α) from SGCs (Zhang et al., 2007). TNF-α, in turn, binds on receptors on somata to increase the excitability of neurons (Ji et al., 2013). Thus, the present study provides hints that ATP might also be released from neuronal somata in DRGs via Panx1 channels.

Further analyses, however, are required to determine the physiological and pathology-associated functions of Panx1 in DRGs. It is of interest to determine if Panx1 channels are the main pathway for ATP release from neuronal somata in DRGs. If so, the use of Panx1 blockers or the ablation of Panx1 expression might modulate the neuropathic pain pathway as already demonstrated for the central perception of neuropathic pain at spinal cord level (Bravo et al., 2014). This modulation might offer an additional opportunity in pain therapy by targeting Panx1 channel activity in dorsal root ganglion neurons.
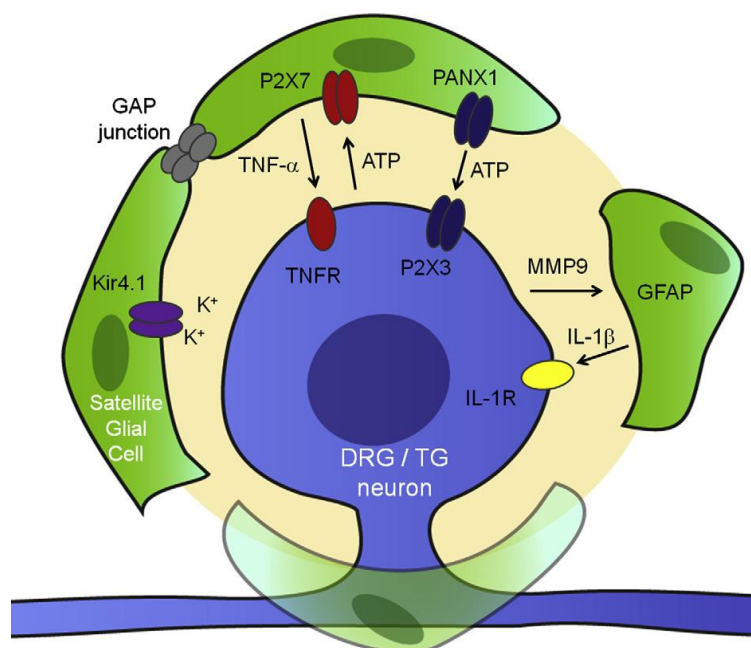

Figure 59. Schematic representation of neuronal-glial interaction in DRGs and trigeminal ganglia
Neuronal somata (blue) are completely surrounded by satellite glial cells (SGCs) (green) forming a structural unit. SGCs communicate with each other through gap junctions. There are no gap junctions mediating communication between somata and SGCs. ATP is critically involved in neuronal–glial communication. A painful injury results in ATP release from somata. ATP activates P2X7 in SGCs and leads to release of tumor necrosis factor-α (TNF-α). Persistent nociceptive activity results in matrix metalloproteinase-9 (MMP-9) release from primary sensory neurons, which leads to release of interleukin-1b (IL-1b) in SGCs. TNF-α and IL-1b bind to receptors on sensory neurons to elicit hyperexcitability. Taken from Ji et al. (2013).

6   Conclusion

The present study revealed that Panx1 mRNA and protein are expressed at early stages of mouse development (E9.5, E10.5, E11.5, E12.5). Panx1 mRNA expression increases during development and is abundantly distributed in the developing nervous system particularly in the wall of cephalic ventricles, cranial nerve ganglia, spinal cord, and dorsal root ganglia. Panx1 protein is mainly expressed in post-mitotic neurons of the developing spinal cord and sensory ganglia. This finding suggests that Panx1 expression at early stages might contribute to a variety of developmental processes.

In spinal cord, Panx1 expression is temporally regulated. The highest expression was observed at postnatal stages. Panx1 is expressed in all spinal segments and shows a gradational distribution within the gray matter. Panx1 mRNA expression is similar to that of purinergic receptors P2X3 and P2X7. An association between Panx1 and these purinergic receptors is thought to be of functional importance and might be required to induce pannexin channel activation.

In sensory ganglia, Panx1 mRNA is heterogeneously expressed within DRGs and trigeminal ganglia and shows similar expression to that of P2X3R expression but not to P2X7R expression. In postnatal DRGs, Panx1 is expressed in all cell types of neuronal somata. Panx1 might mediate purinergic signaling between neurons and SGCs by releasing ATP as a peripheral pain mediator. Thus, targeting Panx1 channels in DRG neurons might be considered in pain research.

In conclusion, Panx1 is widely expressed in the developing nervous system during early stages of embryogenesis. All segments of adult spinal cord show a graded distribution of Panx1 in the gray matter. The newly discovered expression of Panx1 in DRGs requires further functional analysis, including its putative involvement in sensory modulation and pain.

7   References

Abascal F, Zardoya R (2013) Evolutionary analyses of gap junction protein families. Biochimica et biophysica acta 1828:4-14.

Alexander DB, Goldberg GS (2003) Transfer of biologically important molecules between cells through gap junction channels. Current medicinal chemistry 10:2045-2058.

Ambrosi C, Gassmann O, Pranskevich JN, Boassa D, Smock A, Wang J, Dahl G, Steinem C, Sosinsky GE (2010) Pannexin1 and Pannexin2 channels show quaternary similarities to connexons and different oligomerization numbers from each other. The Journal of biological chemistry 285:24420-24431.

Anselmi F, Hernandez VH, Crispino G, Seydel A, Ortolano S, Roper SD, Kessaris N, Richardson W, Rickheit G, Filippov MA, Monyer H, Mammano F (2008) ATP release through connexin hemichannels and gap junction transfer of second messengers propagate Ca2+ signals across the inner ear. Proceedings of the National Academy of Sciences of the United States of America 105:18770-18775.

Arber S (2012) Motor Circuits in Action: Specification, Connectivity, and Function. Neuron 74:975-989.

Bao L, Locovei S, Dahl G (2004) Pannexin membrane channels are mechanosensitive conduits for ATP. FEBS letters 572:65-68.

Bao L, Samuels S, Locovei S, Macagno ER, Muller KJ, Dahl G (2007) Innexins form two types of channels. FEBS letters 581:5703-5708.

Baranova A, Ivanov D, Petrash N, Pestova A, Skoblov M, Kelmanson I, Shagin D, Nazarenko S, Geraymovych E, Litvin O, Tiunova A, Born TL, Usman N, Staroverov D, Lukyanov S, Panchin Y (2004) The mammalian pannexin family is homologous to the invertebrate innexin gap junction proteins. Genomics 83:706-716.

Barbe MT, Monyer H, Bruzzone R (2006) Cell-cell communication beyond connexins: the pannexin channels. Physiology (Bethesda, Md) 21:103-114.

Bargiotas P, Krenz A, Hormuzdi SG, Ridder DA, Herb A, Barakat W, Penuela S, von Engelhardt J, Monyer H, Schwaninger M (2011) Pannexins in ischemia-induced neurodegeneration. Proceedings of the National Academy of Sciences of the United States of America 108:20772-20777.

Barron DJ, Valdimarsson G, Paul DL, Kidder GM (1989) Connexin32, a gap junction protein, is a persistent oogenetic product through preimplantation development of the mouse. Developmental Genetics 10:318-323.

Basson MA, Wingate RJ (2013) Congenital hypoplasia of the cerebellum: developmental causes and behavioural consequences. Frontiers in Neuroanatomy 7.

Battiste J, Helms AW, Kim EJ, Savage TK, Lagace DC, Mandyam CD, Eisch AJ, Miyoshi G, Johnson JE (2007) Ascl1 defines sequentially generated lineage-restricted neuronal and oligodendrocyte precursor cells in the spinal cord. Development (Cambridge, England) 134:285-293.

Bauer R, Loer B, Ostrowski K, Martini J, Weimbs A, Lechner H, Hoch M (2005) Intercellular communication: the Drosophila innexin multiprotein family of gap junction proteins. Chemistry & biology 12:515-526.

Bennett MV, Zukin RS (2004) Electrical coupling and neuronal synchronization in the Mammalian brain. Neuron 41:495-511.

Bergoffen J, Scherer SS, Wang S, Scott MO, Bone LJ, Paul DL, Chen K, Lensch MW, Chance PF, Fischbeck KH (1993) Connexin mutations in X-linked Charcot-Marie-Tooth disease. Science 262:2039-2042.

Bhalla-Gehi R, Penuela S, Churko JM, Shao Q, Laird DW (2010) Pannexin1 and pannexin3 delivery, cell surface dynamics, and cytoskeletal interactions. The Journal of biological chemistry 285:9147-9160.

Blom N, Sicheritz-Pontén T, Gupta R, Gammeltoft S, Brunak S (2004) Prediction of post-translational glycosylation and phosphorylation of proteins from the amino acid sequence. PROTEOMICS 4:1633-1649.

Boassa D, Ambrosi C, Qiu F, Dahl G, Gaietta G, Sosinsky G (2007) Pannexin1 channels contain a glycosylation site that targets the hexamer to the plasma membrane. The Journal of biological chemistry 282:31733-31743.

Boassa D, Qiu F, Dahl G, Sosinsky G (2008) Trafficking dynamics of glycosylated pannexin 1 proteins.

Bosco D, Haefliger JA, Meda P (2011) Connexins: key mediators of endocrine function. Physiological reviews 91:1393-1445.

Bravo D, Ibarra P, Retamal J, Pelissier T, Laurido C, Hernandez A, Constandil L (2014) Pannexin 1: A novel participant in neuropathic pain signaling in the rat spinal cord. Pain.

Bruzzone R, Barbe MT, Jakob NJ, Monyer H (2005) Pharmacological properties of homomeric and heteromeric pannexin hemichannels expressed in Xenopus oocytes. J Neurochem 92:1033-1043.

Bruzzone R, Hormuzdi SG, Barbe MT, Herb A, Monyer H (2003) Pannexins, a family of gap junction proteins expressed in brain. Proceedings of the National Academy of Sciences of the United States of America 100:13644-13649.

Bruzzone R, White TW, Paul DL (1996) Connections with Connexins: the Molecular Basis of Direct Intercellular Signaling. European Journal of Biochemistry 238:1-27.

Bunse S, Schmidt M, Prochnow N, Zoidl G, Dermietzel R (2010) Intracellular cysteine 346 is essentially involved in regulating Panx1 channel activity. The Journal of biological chemistry 285:38444-38452.

Casanova JC, Uribe V, Badia-Careaga C, Giovinazzo G, Torres M, Sanz-Ezquerro JJ (2011) Apical ectodermal ridge morphogenesis in limb development is controlled by Arid3b-mediated regulation of cell movements. Development (Cambridge, England) 138:1195-1205.

Caspary T, Anderson KV (2003) Patterning cell types in the dorsal spinal cord: what the mouse mutants say. Nat Rev Neurosci 4:289-297.

Celetti SJ, Cowan KN, Penuela S, Shao Q, Churko J, Laird DW (2010) Implications of pannexin 1 and pannexin 3 for keratinocyte differentiation. Journal of cell science 123:1363-1372.

Chang Q, Gonzalez M, Pinter MJ, Balice-Gordon RJ (1999) Gap junctional coupling and patterns of connexin expression among neonatal rat lumbar spinal motor neurons. The Journal of neuroscience : the official journal of the Society for Neuroscience 19:10813-10828.

Chekeni FB, Elliott MR, Sandilos JK, Walk SF, Kinchen JM, Lazarowski ER, Armstrong AJ, Penuela S, Laird DW, Salvesen GS, Isakson BE, Bayliss DA, Ravichandran KS (2010) Pannexin 1 channels mediate 'find-me' signal release and membrane permeability during apoptosis. Nature 467:863-867.

Chen JCJ, Goldhamer DJ (2004) The core enhancer is essential for proper timing of MyoD activation in limb buds and branchial arches. Developmental Biology 265:502-512.

Chen Y, Li G, Huang LY (2012) P2X7 receptors in satellite glial cells mediate high functional expression of P2X3 receptors in immature dorsal root ganglion neurons. Molecular pain 8:9.

Chen Y, Zhang X, Wang C, Li G, Gu Y, Huang LY (2008) Activation of P2X7 receptors in glial satellite cells reduces pain through downregulation of P2X3 receptors in nociceptive neurons. Proceedings of the National Academy of Sciences of the United States of America 105:16773-16778.

Cisneros-Mejorado A, Gottlieb M, Cavaliere F, Magnus T, Koch-Nolte F, Scemes E, Perez-Samartin A, Matute C (2015) Blockade of P2X7 receptors or pannexin-1 channels similarly attenuates postischemic damage. J Cereb Blood Flow Metab.

Condorelli DF, Parenti R, Spinella F, Trovato Salinaro A, Belluardo N, Cardile V, Cicirata F (1998) Cloning of a new gap junction gene (Cx36) highly expressed in mammalian brain neurons. The European journal of neuroscience 10:1202-1208.

Cone A, Boassa D, Fuller K, Martone M, Sosinsky G (2011) Comparison of Pannexin1 ATP Channel Expression in Rat Brain Tissue. Microscopy and Microanalysis 17:336-337.

Cone AC, Ambrosi C, Scemes E, Martone ME, Sosinsky G (2013) A comparative antibody analysis of Pannexin1 expression in four rat brain regions reveals varying subcellular localizations. Frontiers in Pharmacology 4.

Cook JE, Becker DL (2009) Gap-junction proteins in retinal development: new roles for the "nexus". Physiology (Bethesda, Md) 24:219-230.

Cordes SP (2001) Molecular genetics of cranial nerve development in mouse. Nat Rev Neurosci 2:611-623.

Cotrina ML, Nedergaard M (2009) Physiological and pathological functions of P2X7 receptor in the spinal cord. Purinergic signalling 5:223-232.

D'Amelio M, Cavallucci V, Cecconi F (2010) Neuronal caspase-3 signaling: not only cell death. Cell death and differentiation 17:1104-1114.

D'Hondt C, Ponsaerts R, De Smedt H, Bultynck G, Himpens B (2009) Pannexins, distant relatives of the connexin family with specific cellular functions? BioEssays : news and reviews in molecular, cellular and developmental biology 31:953-974.

Dahl E, Willecke K, Balling R (1997) Segment-specific expression of the gap junction gene connexin31 during hindbrain development. Dev Gene Evol 207:359-361.

Dahl G, Keane RW (2012) Pannexin: from discovery to bedside in 11+/-4 years? Brain research 1487:150-159.

Dahl G, Locovei S (2006) Pannexin: to gap or not to gap, is that a question? IUBMB life 58:409-419.

Dahl G, Miller T, Paul D, Voellmy R, Werner R (1987) Expression of functional cell-cell channels from cloned rat liver gap junction complementary DNA. Science 236:1290-1293.

Dahl G, Qiu F, Wang J (2013) The bizarre pharmacology of the ATP release channel pannexin1. Neuropharmacology 75:583-593.

De Bellard ME, Ching W, Gossler A, Bronner-Fraser M (2002) Disruption of Segmental Neural Crest Migration and Ephrin Expression in Delta-1 Null Mice. Developmental Biology 249:121-130.

De Sousa PA, Valdimarsson G, Nicholson BJ, Kidder GM (1993) Connexin trafficking and the control of gap junction assembly in mouse preimplantation embryos. Development (Cambridge, England) 117:1355-1367.

Dehay C, Kennedy H (2007) Cell-cycle control and cortical development. Nat Rev Neurosci 8:438-450.

Deuchars SA, Atkinson L, Brooke RE, Musa H, Milligan CJ, Batten TF, Buckley NJ, Parson SH, Deuchars J (2001) Neuronal P2X7 receptors are targeted to presynaptic terminals in the central and peripheral nervous systems. The Journal of neuroscience : the official journal of the Society for Neuroscience 21:7143-7152.

Dvoriantchikova G, Ivanov D, Barakat D, Grinberg A, Wen R, Slepak VZ, Shestopalov VI (2012) Genetic ablation of Pannexin1 protects retinal neurons from ischemic injury. PloS one 7:e31991.

Dvoriantchikova G, Ivanov D, Panchin Y, Shestopalov VI (2006) Expression of pannexin family of proteins in the retina. FEBS letters 580:2178-2182.

Elliott MR, Chekeni FB, Trampont PC, Lazarowski ER, Kadl A, Walk SF, Park D, Woodson RI, Ostankovich M, Sharma P, Lysiak JJ, Harden TK, Leitinger N, Ravichandran KS (2009) Nucleotides released by apoptotic cells act as a find-me signal to promote phagocytic clearance. Nature 461:282-286.

Evans WH, De Vuyst E, Leybaert L (2006) The gap junction cellular internet: connexin hemichannels enter the signalling limelight. The Biochemical journal 397:1-14.

Fernando P, Brunette S, Megeney LA (2005) Neural stem cell differentiation is dependent upon endogenous caspase 3 activity. FASEB J 19:1671-1673.

Garre JM, Retamal MA, Cassina P, Barbeito L, Bukauskas FF, Saez JC, Bennett MV, Abudara V (2010) FGF-1 induces ATP release from spinal astrocytes in culture and opens pannexin and connexin hemichannels. Proceedings of the National Academy of Sciences of the United States of America 107:22659-22664.

Guthrie S (2007) Patterning and axon guidance of cranial motor neurons. Nat Rev Neurosci 8:859-871.

Hamilton SG, McMahon SB (2000) ATP as a peripheral mediator of pain. J Auton Nerv Syst 81:187-194.

Hanani M (2005) Satellite glial cells in sensory ganglia: from form to function. Brain research Brain research reviews 48:457-476.

Hanson MG, Landmesser LT (2003) Characterization of the circuits that generate spontaneous episodes of activity in the early embryonic mouse spinal cord. J Neurosci 23:587-600.

Hanstein R, Negoro H, Patel NK, Charollais A, Meda P, Spray DC, Suadicani SO, Scemes E (2013) Promises and pitfalls of a Pannexin1 transgenic mouse line. Frontiers in Pharmacology 4.

Harrison M, O'Brien A, Adams L, Cowin G, Ruitenberg MJ, Sengul G, Watson C (2013) Vertebral landmarks for the identification of spinal cord segments in the mouse. NeuroImage 68:22-29.

Hartfield EM, Rinaldi F, Glover CP, Wong LF, Caldwell MA, Uney JB (2011) Connexin 36 expression regulates neuronal differentiation from neural progenitor cells. PloS one 6:e14746.

Hawkes R (2012) Pattern formation during development of the embryonic cerebellum. Frontiers in Neuroanatomy 6.

Herve JC, Bourmeyster N, Sarrouilhe D (2004) Diversity in protein-protein interactions of connexins: emerging roles. Biochimica et biophysica acta 1662:22-41.

Hilario E, Mackay J (2007) Protocols for Nucleic Acid Analysis by Nonradioactive Probes: Humana Press.

Houghton FD (2005) Role of gap junctions during early embryo development. Reproduction (Cambridge, England) 129:129-135.

Huang EJ, Liu W, Fritzsch B, Bianchi LM, Reichardt LF, Xiang M (2001) Brn3a is a transcriptional regulator of soma size, target field innervation and axon pathfinding of inner ear sensory neurons. Development (Cambridge, England) 128:2421-2432.

Huang EJ, Wilkinson GA, Farinas I, Backus C, Zang K, Wong SL, Reichardt LF (1999) Expression of Trk receptors in the developing mouse trigeminal ganglion: in vivo evidence for NT-3 activation of TrkA and TrkB in addition to TrkC. Development (Cambridge, England) 126:2191-2203.

Huang LY, Gu Y, Chen Y (2013) Communication between neuronal somata and satellite glial cells in sensory ganglia. Glia 61:1571-1581.

Huang Y-J, Maruyama Y, Dvoryanchikov G, Pereira E, Chaudhari N, Roper SD (2007a) The role of pannexin 1 hemichannels in ATP release and cell–cell communication in mouse taste buds. Proceedings of the National Academy of Sciences 104:6436-6441.

Huang Y, Grinspan JB, Abrams CK, Scherer SS (2007b) Pannexin1 is expressed by neurons and glia but does not form functional gap junctions. Glia 55:46-56.

Iacopetti P, Michelini M, Stuckmann I, Oback B, Aaku-Saraste E, Huttner WB (1999) Expression of the antiproliferative gene TIS21 at the onset of neurogenesis identifies single neuroepithelial cells that switch from proliferative to neuron-generating division. Proceedings of the National Academy of Sciences of the United States of America 96:4639-4644.

Ide S, Minami M, Ikeda K (2009) [Gene polymorphisms in ATP (purinergic) receptors and pain sensitivity]. Masui The Japanese journal of anesthesiology 58:1122-1129.

Iglesias R, Dahl G, Qiu F, Spray DC, Scemes E (2009) Pannexin 1: The Molecular Substrate of Astrocyte "Hemichannels". The Journal of Neuroscience 29:7092-7097.

Ishibashi J, Perry RL, Asakura A, Rudnicki MA (2005) MyoD induces myogenic differentiation through cooperation of its NH2- and COOH-terminal regions. The Journal of cell biology 171:471-482.

Iwamoto T, Nakamura T, Doyle A, Ishikawa M, de Vega S, Fukumoto S, Yamada Y (2010) Pannexin 3 regulates intracellular ATP/cAMP levels and promotes chondrocyte differentiation. The Journal of biological chemistry 285:18948-18958.

Jessell TM (2000) Neuronal specification in the spinal cord: inductive signals and transcriptional codes. Nat Rev Genet 1:20-29.

Ji RR, Berta T, Nedergaard M (2013) Glia and pain: is chronic pain a gliopathy? Pain 154 Suppl 1:S10-28.

Juers DH, Matthews BW, Huber RE (2012) LacZ beta-galactosidase: structure and function of an enzyme of historical and molecular biological importance. Protein science : a publication of the Protein Society 21:1792-1807.

Jungbluth S, Willecke K, Champagnat J (2002) Segment-specific expression of connexin31 in the embryonic hindbrain is regulated by Krox20. Developmental Dynamics 223:544-551.

Kaufman MH (2003) The Atlas of Mouse Development: Academic Press.

Kobayashi K, Takahashi E, Miyagawa Y, Yamanaka H, Noguchi K (2011) Induction of the P2X7 receptor in spinal microglia in a neuropathic pain model. Neuroscience letters 504:57-61.

Kranz K, Dorgau B, Pottek M, Herrling R, Schultz K, Bolte P, Monyer H, Penuela S, Laird DW, Dedek K, Weiler R, Janssen-Bienhold U (2013) Expression of Pannexin1 in the outer plexiform layer of the mouse retina and physiological impact of its knockout. Journal of Comparative Neurology 521:1119-1135.

Kruger O, Plum A, Kim JS, Winterhager E, Maxeiner S, Hallas G, Kirchhoff S, Traub O, Lamers WH, Willecke K (2000) Defective vascular development in connexin 45-deficient mice. Development (Cambridge, England) 127:4179-4193.

Krysko DV, Leybaert L, Vandenabeele P, D'Herde K (2005) Gap junctions and the propagation of cell survival and cell death signals. Apoptosis : an international journal on programmed cell death 10:459-469.

Kumai M, Nishii K, Nakamura K, Takeda N, Suzuki M, Shibata Y (2000) Loss of connexin45 causes a cushion defect in early cardiogenesis. Development (Cambridge, England) 127:3501-3512.

Kumar NM, Gilula NB (1996) The gap junction communication channel. Cell 84:381-388.

Lavezzi AM, Corna MF, Matturri L (2013) Neuronal nuclear antigen (NeuN): a useful marker of neuronal immaturity in sudden unexplained perinatal death. Journal of the neurological sciences 329:45-50.

Li J, Habbes H-W, Eiberger J, Willecke K, Dermietzel R, Meier C (2007) Analysis of connexin expression during mouse Schwann cell development identifies Connexin29 as a novel marker for the transition of neural crest to precursor cells. Glia 55:93-103.

Li S, Tomic M, Stojilkovic SS (2011) Characterization of novel Pannexin 1 isoforms from rat pituitary cells and their association with ATP-gated P2X channels. General and comparative endocrinology 174:202-210.

Lin JH, Takano T, Arcuino G, Wang X, Hu F, Darzynkiewicz Z, Nunes M, Goldman SA, Nedergaard M (2007) Purinergic signaling regulates neural progenitor cell expansion and neurogenesis. Dev Biol 302:356-366.

Liu T, Li M, Zhang Y, Pang Z, Xiao W, Yang Y, Luo K (2013) A role for Innexin2 and Innexin3 proteins from Spodoptera litura in apoptosis. PloS one 8:e70456.

Liu X, Wu Y, Li M, Chen S, Zhou Y (2009) Production of polyclonal antibody against interleukin-33 and assessment of its distribution in murine liver and lung. Journal of biomedicine & biotechnology 2009:729197.

Lleras-Forero L, Streit A (2012) Development of the sensory nervous system in the vertebrate head: the importance of being on time. Current opinion in genetics & development 22:315-322.

Locovei S, Bao L, Dahl G (2006a) Pannexin 1 in erythrocytes: function without a gap. Proceedings of the National Academy of Sciences of the United States of America 103:7655-7659.

Locovei S, Scemes E, Qiu F, Spray DC, Dahl G (2007) Pannexin1 is part of the pore forming unit of the P2X(7) receptor death complex. FEBS letters 581:483-488.

Locovei S, Wang J, Dahl G (2006b) Activation of pannexin 1 channels by ATP through P2Y receptors and by cytoplasmic calcium. FEBS letters 580:239-244.

Lohman AW, Isakson BE (2014) Differentiating connexin hemichannels and pannexin channels in cellular ATP release. FEBS letters 588:1379-1388.

Luu B, Ellisor D, Zervas M (2011) The lineage contribution and role of Gbx2 in spinal cord development. PloS one 6:e20940.

Maes M, Decrock E, Cogliati B, Oliveira AG, Marques PE, Zaidan Dagli ML, Menezes GB, Mennecier G, Leybaert L, Vanhaecke T, Rogiers V, Vinken M (2014) Connexin and pannexin (hemi)channels in the liver. Frontiers in Physiology 4.

Malin SA, Davis BM, Molliver DC (2007) Production of dissociated sensory neuron cultures and considerations for their use in studying neuronal function and plasticity. Nat Protocols 2:152-160.

Marmigere F, Ernfors P (2007) Specification and connectivity of neuronal subtypes in the sensory lineage. Nat Rev Neurosci 8:114-127.

Maro GS, Vermeren M, Voiculescu O, Melton L, Cohen J, Charnay P, Topilko P (2004) Neural crest boundary cap cells constitute a source of neuronal and glial cells of the PNS. Nature neuroscience 7:930-938.

Martinez S, Andreu A, Mecklenburg N, Echevarria D (2013) Cellular and Molecular Basis of Cerebellar Development. Frontiers in Neuroanatomy 7.

Mesnil M, Crespin S, Avanzo JL, Zaidan-Dagli ML (2005) Defective gap junctional intercellular communication in the carcinogenic process. Biochimica et biophysica acta 1719:125-145.

Ming GL, Song H (2011) Adult neurogenesis in the mammalian brain: significant answers and significant questions. Neuron 70:687-702.

Montano JA, Perez-Pinera P, Garcia-Suarez O, Cobo J, Vega JA (2010) Development and neuronal dependence of cutaneous sensory nerve formations: Lessons from neurotrophins. Microscopy research and technique 73:513-529.

Moore AR, Zhou WL, Sirois CL, Belinsky GS, Zecevic N, Antic SD (2014) Connexin hemichannels contribute to spontaneous electrical activity in the human fetal cortex. Proc Natl Acad Sci U S A 111:E3919-3928.

Mullen RJ, Buck CR, Smith AM (1992) NeuN, a neuronal specific nuclear protein in vertebrates. Development (Cambridge, England) 116:201-211.

Nakatsuka T, Gu JG (2006) P2X purinoceptors and sensory transmission. Pflugers Arch 452:598-607.

Namba K, Sugihara I, Hashimoto M (2011) Close correlation between the birth date of Purkinje cells and the longitudinal compartmentalization of the mouse adult cerebellum. J Comp Neurol 519:2594-2614.

Nichols DH (1986) Mesenchyme formation from the trigeminal placodes of the mouse embryo. The American journal of anatomy 176:19-31.

Novakovic SD, Kassotakis LC, B. Oglesby I, Smith JAM, Eglen RM, Ford APDW, C. Hunter J (1999) Immunocytochemical localization of P2X3 purinoceptors in sensory neurons in naive rats and following neuropathic injury. Pain 80:273-282.

Ohbuchi T, Hohchi N, Ohkubo J, Hashida K, Koizumi H, Wakasugi T, Takenaga F, Suzuki H (2013) Identification of pannexins in rat nasal mucosa. Allergy & rhinology (Providence, RI) 4:e63-65.

Orthmann-Murphy JL, Enriquez AD, Abrams CK, Scherer SS (2007) Loss-of-function GJA12/Connexin47 mutations cause Pelizaeus-Merzbacher-like disease. Molecular and cellular neurosciences 34:629-641.

Panchin Y, Kelmanson I, Matz M, Lukyanov K, Usman N, Lukyanov S (2000) A ubiquitous family of putative gap junction molecules. Current biology : CB 10:R473-474.

Panchin YV (2005) Evolution of gap junction proteins--the pannexin alternative. The Journal of experimental biology 208:1415-1419.

Patel AV, Krimm RF (2010) BDNF is required for the survival of differentiated geniculate ganglion neurons. Dev Biol 340:419-429.

Pearson RA, Dale N, Llaudet E, Mobbs P (2005) ATP released via gap junction hemichannels from the pigment epithelium regulates neural retinal progenitor proliferation. Neuron 46:731-744.

Pelegrin P, Surprenant A (2006) Pannexin-1 mediates large pore formation and interleukin-1beta release by the ATP-gated P2X7 receptor. The EMBO journal 25:5071-5082.

Penuela S, Bhalla R, Gong XQ, Cowan KN, Celetti SJ, Cowan BJ, Bai D, Shao Q, Laird DW (2007) Pannexin 1 and pannexin 3 are glycoproteins that exhibit many distinct characteristics from the connexin family of gap junction proteins. Journal of cell science 120:3772-3783.

Penuela S, Bhalla R, Nag K, Laird DW (2009) Glycosylation regulates pannexin intermixing and cellular localization. Molecular biology of the cell 20:4313-4323.

Penuela S, Gehi R, Laird DW (2013) The biochemistry and function of pannexin channels. Biochimica et Biophysica Acta (BBA) - Biomembranes 1828:15-22.

Penuela S, Kelly JJ, Churko JM, Barr KJ, Berger AC, Laird DW (2014a) Panx1 regulates cellular properties of keratinocytes and dermal fibroblasts in skin development and wound healing. The Journal of investigative dermatology 134:2026-2035.

Penuela S, Simek J, Thompson RJ (2014b) Regulation of pannexin channels by post-translational modifications. FEBS letters 588:1411-1415.

Perkins G, Goodenough D, Sosinsky G (1997) Three-dimensional structure of the gap junction connexon. Biophysical journal 72:533-544.

Phelan P (2005) Innexins: members of an evolutionarily conserved family of gap-junction proteins. Biochimica et Biophysica Acta (BBA) - Biomembranes 1711:225-245.

Phelan P, Bacon JP, Davies JA, Stebbings LA, Todman MG, Avery L, Baines RA, Barnes TM, Ford C, Hekimi S, Lee R, Shaw JE, Starich TA, Curtin KD, Sun YA, Wyman RJ (1998) Innexins: a family of invertebrate gap-junction proteins. Trends in genetics : TIG 14:348-349.

Phelan P, Starich TA (2001) Innexins get into the gap. BioEssays : news and reviews in molecular, cellular and developmental biology 23:388-396.

Phippard D, Lu L, Lee D, Saunders JC, Crenshaw EB, 3rd (1999) Targeted mutagenesis of the POU-domain gene Brn4/Pou3f4 causes developmental defects in the inner ear. The Journal of neuroscience : the official journal of the Society for Neuroscience 19:5980-5989.

Piette D, Hendrickx M, Willems E, Kemp CR, Leyns L (2008) An optimized procedure for whole-mount in situ hybridization on mouse embryos and embryoid bodies. Nat Protocols 3:1194-1201.

Prime G, Horn G, Sutor B (2000) Time-related changes in connexin mRNA abundance in the rat neocortex during postnatal development. Developmental Brain Research 119:111-125.

Qu Y, Misaghi S, Newton K, Gilmour LL, Louie S, Cupp JE, Dubyak GR, Hackos D, Dixit VM (2011) Pannexin-1 is required for ATP release during apoptosis but not for inflammasome activation. Journal of immunology 186:6553-6561.

Rao MS, Jacobson M (2005) Developmental Neurobiology: Springer.

Ray A, Zoidl G, Wahle P, Dermietzel R (2006) Pannexin expression in the cerebellum. Cerebellum (London, England) 5:189-192.

Ray A, Zoidl G, Weickert S, Wahle P, Dermietzel R (2005) Site-specific and developmental expression of pannexin1 in the mouse nervous system. The European journal of neuroscience 21:3277-3290.

Reaume AG, de Sousa PA, Kulkarni S, Langille BL, Zhu D, Davies TC, Juneja SC, Kidder GM, Rossant J (1995) Cardiac malformation in neonatal mice lacking connexin43. Science 267:1831-1834.

Renshaw S (2007) Immunohistochemistry: Scion.

Retamal MA, Alcayaga J, Bultynck G, leybaer L, Sáez PJ, Fernandez R, León LE, Saez JC (2014) Opening of pannexin and connexin based-channels increases the excitability of nodose ganglion sensory neurons. Frontiers in Cellular Neuroscience 8.

Rexed B (1952) The cytoarchitectonic organization of the spinal cord in the cat. J Comp Neurol 96:414-495.

Rigato C, Buckinx R, Le-Corronc H, Rigo JM, Legendre P (2011) Pattern of invasion of the embryonic mouse spinal cord by microglial cells at the time of the onset of functional neuronal networks. Glia 59:675-695.

Rigato C, Swinnen N, Buckinx R, Couillin I, Mangin JM, Rigo JM, Legendre P, Le Corronc H (2012) Microglia proliferation is controlled by P2X7 receptors in a Pannexin-1-independent manner during early embryonic spinal cord invasion. The Journal of neuroscience : the official journal of the Society for Neuroscience 32:11559-11573.

Riquelme MA, Cea LA, Vega JL, Boric MP, Monyer H, Bennett MVL, Frank M, Willecke K, Sáez JC (2013) The ATP required for potentiation of skeletal muscle contraction is released via pannexin hemichannels. Neuropharmacology.

Romanov RA, Rogachevskaja OA, Bystrova MF, Jiang P, Margolskee RF, Kolesnikov SS (2007) Afferent neurotransmission mediated by hemichannels in mammalian taste cells. The EMBO journal 26:657-667.

Ruan HZ, Moules E, Burnstock G (2004) Changes in P2X3 purinoceptors in sensory ganglia of the mouse during embryonic and postnatal development. Histochemistry and cell biology 122:539-551.

Rudnicki MA, Schnegelsberg PN, Stead RH, Braun T, Arnold HH, Jaenisch R (1993) MyoD or Myf-5 is required for the formation of skeletal muscle. Cell 75:1351-1359.

Sanchez HA, Verselis VK (2014) Aberrant Cx26 Hemichannels and Keratitis-Ichthyosis-Deafness Syndrome: Insights into Syndromic Hearing Loss. Frontiers in Cellular Neuroscience 8.

Sandilos JK, Chiu YH, Chekeni FB, Armstrong AJ, Walk SF, Ravichandran KS, Bayliss DA (2012) Pannexin 1, an ATP release channel, is activated by caspase cleavage of its pore-associated C-terminal autoinhibitory region. The Journal of biological chemistry 287:11303-11311.

Sanes DH, Reh TA, Harris WA (2011) Development of the Nervous System: Elsevier Science.

Sato S, Ikeda K, Shioi G, Ochi H, Ogino H, Yajima H, Kawakami K (2010) Conserved expression of mouse Six1 in the pre-placodal region (PPR) and identification of an enhancer for the rostral PPR. Dev Biol 344:158-171.

Scemes E, Giaume C (2006) Astrocyte calcium waves: what they are and what they do. Glia 54:716-725.

Schenborn E (1995) Transcription In Vitro Using Bacteriophage RNA Polymerases. In: In Vitro Transcription and Translation Protocols, vol. 37 (Tymms, M., ed), pp 1-12: Humana Press.

Sengul G, Puchalski RB, Watson C (2012) Cytoarchitecture of the spinal cord of the postnatal (P4) mouse. Anatomical record (Hoboken, NJ : 2007) 295:837-845.

Silverman W, Locovei S, Dahl G (2008) Probenecid, a gout remedy, inhibits pannexin 1 channels. American journal of physiology Cell physiology 295:C761-767.

Simon AM, Goodenough DA, Li E, Paul DL (1997) Female infertility in mice lacking connexin 37. Nature 385:525-529.

Sohl G, Maxeiner S, Willecke K (2005) Expression and functions of neuronal gap junctions. Nat Rev Neurosci 6:191-200.

Sohl G, Willecke K (2004) Gap junctions and the connexin protein family. Cardiovascular research 62:228-232.

Sosinsky GE, Boassa D, Dermietzel R, Duffy HS, Laird DW, MacVicar B, Naus CC, Penuela S, Scemes E, Spray DC, Thompson RJ, Zhao HB, Dahl G (2011) Pannexin channels are not gap junction hemichannels. Channels (Austin, Tex) 5:193-197.

Stebbings LA, Todman MG, Phillips R, Greer CE, Tam J, Phelan P, Jacobs K, Bacon JP, Davies JA (2002) Gap junctions in Drosophila: developmental expression of the entire innexin gene family. Mechanisms of Development 113:197-205.

Suyama S, Sunabori T, Kanki H, Sawamoto K, Gachet C, Koizumi S, Okano H (2012) Purinergic signaling promotes proliferation of adult mouse subventricular zone cells. J Neurosci 32:9238-9247.

Swayne LA, Sorbara CD, Bennett SA (2010) Pannexin 2 is expressed by postnatal hippocampal neural progenitors and modulates neuronal commitment. The Journal of biological chemistry 285:24977-24986.

Tang W, Ahmad S, Shestopalov VI, Lin X (2008) Pannexins are new molecular candidates for assembling gap junctions in the cochlea. Neuroreport 19:1253-1257.

Thuring RWJ, Sanders JPM, Borst P (1975) A freeze-squeeze method for recovering long DNA from agarose gels. Analytical Biochemistry 66:213-220.

Vitalis T, Mark A, Dayer A (2013) Serotonin homeostasis and serotonin receptors as actors of cortical construction: special attention to the 3A and 6 receptor subtypes. Frontiers in Cellular Neuroscience 7.

Vogt A, Hormuzdi SG, Monyer H (2005) Pannexin1 and Pannexin2 expression in the developing and mature rat brain. Molecular Brain Research 141:113-120.

Wang H, Xing Y, Mao L, Luo Y, Kang L, Meng G (2013) Pannexin-1 influences peritoneal cavity cell population but is not involved in NLRP3 inflammasome activation. Protein & cell 4:259-265.

Wang XH, Streeter M, Liu YP, Zhao HB (2009) Identification and characterization of pannexin expression in the mammalian cochlea. J Comp Neurol 512:336-346.

Watson C, Paxinos G, Puelles L (2012) The Mouse Nervous System: Elsevier Academic Press.

Wei CJ, Xu X, Lo CW (2004) Connexins and cell signaling in development and disease. Annual review of cell and developmental biology 20:811-838.

Weiss DJ, Liggitt D, Clark JG (1999) Histochemical discrimination of endogenous mammalian beta-galactosidase activity from that resulting from lac-Z gene expression. The Histochemical journal 31:231-236.

Weissman TA, Riquelme PA, Ivic L, Flint AC, Kriegstein AR (2004) Calcium waves propagate through radial glial cells and modulate proliferation in the developing neocortex. Neuron 43:647-661.

Wicki-Stordeur LE, Dzugalo AD, Swansburg RM, Suits JM, Swayne LA (2012) Pannexin 1 regulates postnatal neural stem and progenitor cell proliferation. Neural development 7:11.

Wicki-Stordeur LE, Swayne LA (2013) Panx1 regulates neural stem and progenitor cell behaviours associated with cytoskeletal dynamics and interacts with multiple cytoskeletal elements. Cell communication and signaling : CCS 11:62.

Wikstrom SO, Anniko M (1987) Early development of the stato-acoustic and facial ganglia. Acta oto-laryngologica 104:166-174.

Winterhager E (2005) Gap Junctions in Development and Disease: Springer.

Wong RC, Pera MF, Pebay A (2008) Role of gap junctions in embryonic and somatic stem cells. Stem cell reviews 4:283-292.

Wurst W, Bally-Cuif L (2001) Neural plate patterning: Upstream and downstream of the isthmic organizer. Nat Rev Neurosci 2:99-108.

Xiang Z, Bo X, Burnstock G (1998) Localization of ATP-gated P2X receptor immunoreactivity in rat sensory and sympathetic ganglia. Neuroscience letters 256:105-108.

Xu H, Yang Y, Tang X, Zhao M, Liang F, Xu P, Hou B, Xing Y, Bao X, Fan X (2013) Bergmann glia function in granule cell migration during cerebellum development. Molecular neurobiology 47:833-844.

Zappala A, Cicero D, Serapide MF, Paz C, Catania MV, Falchi M, Parenti R, Panto MR, La Delia F, Cicirata F (2006) Expression of pannexin1 in the CNS of adult mouse: cellular localization and effect of 4-aminopyridine-induced seizures. Neuroscience 141:167-178.

Zhang F, Vadakkan KI, Kim SS, Wu LJ, Shang Y, Zhuo M (2008) Selective activation of microglia in spinal cord but not higher cortical regions following nerve injury in adult mouse. Molecular pain 4:15.

Zhang X, Chen Y, Wang C, Huang L-YM (2007) Neuronal somatic ATP release triggers neuron–satellite glial cell communication in dorsal root ganglia. Proceedings of the National Academy of Sciences 104:9864-9869.

Zoidl G, Petrasch-Parwez E, Ray A, Meier C, Bunse S, Habbes HW, Dahl G, Dermietzel R (2007) Localization of the pannexin1 protein at postsynaptic sites in the cerebral cortex and hippocampus. Neuroscience 146:9-16.

8 Publications

- **Raslan, A.**; Ernst, P.; Werle, M.; Thieme, H.; Szameit, K.; Finkensieper, M.; Guntinas-Lichius, O.; Irintchev, A., Reduced cholinergic and glutamatergic synaptic input to regenerated motoneurons after facial nerve repair in rats: potential implications for recovery of motor function. Brain Structure & Function 2014

- **Raslan, A.**; Hainz N.; Beckmann, A.; Tschernig, T.; Meier, C, Pannexin-1 expression in the developing mouse nervous system: new evidence for expression in sensory ganglia. Cell and Tissue Research 2015

- Fischer, U.; Backes, C.; **Raslan, A.**; Keller, A.; Meier, C.; Meese, E., Gene amplification during differentiation of mammalian neural stem cells *in vitro* and *in vivo*. Oncotarget 2015

- Fischer, U.; Ludwig, N.; **Raslan, A.**; Meier, C.; Meese, E., Gene amplification during myogenic differentiation. Oncotarget 2016

9 Poster

Raslan A, Schäfer B., Keim A, Meier C

Pannexin1 expression in the developing mouse embryo.

29. Arbeitstagung der Anatomischen Gesellschaft. Septemper 26-28. 2012, Würzburg, Germany.

10 Danksagung